NASA TECHNICAL MEMORANDUM

NASA TM X-3019

NASA TM X-3019

EFFECTS OF REYNOLDS NUMBER AND MODEL SUPPORT ON THE SUPERSONIC AERODYNAMIC CHARACTERISTICS OF A 140°-INCLUDED-ANGLE CONE

by Charles D. Trescot, Jr., Clarence A. Brown, Jr., and Dorothy T. Howell

Langley Research Center
Hampton, Va. 23665

NATIONAL AERONAUTICS AND SPACE ADMINISTRATION • WASHINGTON, D. C. • JULY 1974

1. Report No.	2. Government Accession No.	3. Recipient's Catalog No.
NASA TM X-3019		

4. Title and Subtitle	5. Report Date
EFFECTS OF REYNOLDS NUMBER AND MODEL SUPPORT ON THE SUPERSONIC AERODYNAMIC CHARACTERISTICS OF A 140°-INCLUDED-ANGLE CONE	July 1974
	6. Performing Organization Code

7. Author(s)	8. Performing Organization Report No.
Charles D. Trescot, Jr., Clarence A. Brown, Jr., and Dorothy T. Howell	L-9383
	10. Work Unit No. 815-20-09-08
9. Performing Organization Name and Address	11. Contract or Grant No.
NASA Langley Research Center Hampton, Va. 23665	
	13. Type of Report and Period Covered
12. Sponsoring Agency Name and Address	Technical Memorandum
National Aeronautics and Space Administration Washington, D.C. 20546	14. Sponsoring Agency Code

15. Supplementary Notes

16. Abstract

An investigation has been made in the Langley Unitary Plan wind tunnel to determine the effects of Reynolds number and sting-support interference on the static aerodynamic characteristics of a 140°-included-angle cone. Base pressures and forces and moments of the model were measured at Mach numbers of 1.50, 2.00, 2.94, and 4.00 for ratios of sting diameter to model diameter that varied from 0.125 to 0.500 through an angle-of-attack range from about -4° to 13°. The Reynolds number, based on model diameter (12.192 cm (4.80 in.)), was varied from 1.61×10^5 to 4.15×10^5.

17. Key Words (Suggested by Author(s))	18. Distribution Statement
Blunt body Cones Reynolds number effects Sting effects Stability	Unclassified – Unlimited STAR Category 01

19. Security Classif. (of this report)	20. Security Classif. (of this page)	21. No. of Pages	22. Price*
Unclassified	Unclassified	72	$3.75

*For sale by the National Technical Information Service, Springfield, Virginia 22151

EFFECTS OF REYNOLDS NUMBER AND MODEL SUPPORT ON THE SUPERSONIC AERODYNMAIC CHARACTERISTICS OF A 140°-INCLUDED-ANGLE CONE

By Charles D. Trescot, Jr., Clarence A. Brown, Jr., and Dorothy T. Howell
Langley Research Center

SUMMARY

An investigation has been made in the Langley Unitary Plan wind tunnel to determine the effects of Reynolds number and sting-support interference on the static aerodynamic characteristics of a 140°-included-angle cone. Base pressures and forces and moments of the model were measured at Mach numbers of 1.50, 2.00, 2.94, and 4.00 and at ratios of sting diameter to model diameter that varied from 0.125 to 0.500 through an angle-of-attack range from about -4° to 13°. The Reynolds number, based on model diameter, was varied from 1.61×10^5 to 4.15×10^5.

The results of the investigation indicated that, for all sting diameters tested, variation in test Reynolds number had little or no effect on the static aerodynamic characteristics of the cone. The main effect of sting diameter occurred at Mach numbers of 1.50 and 2.00 where an increase in sting diameter decreased the base-pressure coefficients and increased the axial-force coefficients. There were no appreciable effects on base-pressure coefficient or axial-force coefficient due to increasing the ratio of sting diameter to model diameter at Mach numbers of 2.94 and 4.00.

INTRODUCTION

A number of experimental investigations (refs. 1 to 26) have been made to obtain data on decelerator-shaped models in support of the Viking mission as well as for landing missions on other planets. The simultaneous determination of the static stability and axial-force characteristics for decelerator-shaped models requires precise instrumentation inasmuch as extremely small normal-force and pitching-moment values occur in combination with large axial-force values. Accurate measurement of the small normal-force and pitching-moment values can be impaired when tests are made at low Reynolds numbers with the resulting low dynamic pressures. In the past, when differences in experimental results have occurred on similar decelerator-shaped models tested in different facilities, these differences have been attributed to such factors as Reynolds number and sting-support interference effects.

The National Aeronautics and Space Administration, therefore, has made an investigation to determine the effects of Reynolds number and sting-support interference on the static aerodynamic characteristics of a decelerator-shaped model. The tests were made in the Langley Unitary Plan wind tunnel at Mach numbers of 1.50, 2.00, 2.94, and 4.00 through an angle-of-attack range from about -4° to 13° on a 140°-included-angle cone. The ratios of sting diameter to model diameter were varied from 0.125 to 0.500 and the Reynolds number, based on model diameter, was varied from 1.61×10^5 to 4.15×10^5.

SYMBOLS

The longitudinal characteristics of the model are referred to the body-axis system. The moment reference center is located at the base of the model on the geometric center line (fig. 1). Values are given in both SI and U.S. Customary Units. The measurements and calculations were made in the U.S. Customary Units.

C_A axial-force coefficient, $\frac{\text{Axial force}}{qS}$

C_m pitching-moment coefficient, $\frac{\text{Pitching moment}}{qSD}$

C_N normal-force coefficient, $\frac{\text{Normal force}}{qS}$

C_p base-pressure coefficient, $\frac{\text{Base pressure - Free-stream pressure}}{q}$

D diameter of cone, cm (in.)

d sting diameter, cm (in.)

l sting length, cm (in.)

M free-stream Mach number

q free-stream dynamic pressure, kN/m^2 (lb/ft^2)

R Reynolds number based on D

S	reference area (base area of model), $\pi D^2/4$, m^2 (ft^2)
α	angle of attack, deg

APPARATUS AND METHODS

Model

Sketches of the model and the various sting supports utilized in the investigation are shown in figure 1 and photographs of the model are shown as figure 2. The 140°-included-angle cone was constructed of polished aluminum and had a pointed nose and a flat base. A short adapter was permanently attached to the base of the cone to house the balance, and provisions were made to shield the balance from the airstream. Provisions were also made to support the model with any one of five stings having diameters of 1.52 cm (0.6 in.), 2.54 cm (1.0 in.), 3.81 cm (1.5 in.), 5.08 cm (2.0 in.), and 6.35 cm (2.5 in.). The ratios of sting diameter to model diameter (d/D) varied from 0.125 to 0.500 with a constant ratio of sting length to model diameter (l/D) of 5.83. (See fig. 1(b).) Four base-pressure tubes were located at the centroid of area on the base annulus of the cone at 90° intervals and one tube was attached to the sting inside the balance cavity.

Tunnel

The tests were made in both the low and high Mach number test sections of the Langley Unitary Plan wind tunnel, which is a variable-pressure, continuous-flow facility (refs. 27 and 28). The sections are approximately 1.22 m (4 ft) square and 2.13 m (7 ft) long. The nozzles leading to the test sections are of the asymmetric sliding-block type; this allows continuous variation in Mach number from about 1.5 to 2.9 in the low Mach number test section and from about 2.3 to 4.7 in the high Mach number test section.

Tests

For the present tests, the free-stream Mach numbers, stagnation pressures, dynamic pressures, stagnation temperatures, and Reynolds numbers were as follows:

M	Stagnation pressure		Dynamic pressure		Stagnation temperature		R
	kN/m^2	lb/ft^2	kN/m^2	lb/ft^2	K	^oF	
1.50	13.790	288	5.916	123.55	338.7	150	2.07×10^5
	20.684	432	8.873	185.33	338.7	150	3.11
	27.579	576	11.831	247.10	338.7	150	4.15
2.00	13.790	288	4.935	103.07	338.7	150	1.74×10^5
	20.684	432	7.403	154.61	338.7	150	2.60
	27.579	576	9.870	206.15	338.7	150	3.47
2.94	20.684	432	3.729	77.89	338.7	150	1.61×10^5
	34.474	720	6.216	129.82	338.7	150	2.68
	48.263	1008	8.702	181.74	338.7	150	3.76
4.00	62.053	1296	4.577	95.59	352.6	175	2.63×10^5
	89.632	1872	6.611	138.08	352.6	175	3.80

The stagnation dewpoint was maintained sufficiently low (238.7 K (-30^o F)) to insure negligible condensation effects in the test section. The model was mounted on a six-component, internal, strain-gage balance which was sting supported in the tunnel. Generally, airplane and missile models use strain-gage balances designed with a large ratio of normal force to axial force; however, the balance used in this investigation had a large ratio of axial force to normal force. The maximum design loads of the balance were 44.482 N (10 lb) of normal force, 177.929 N (40 lb) of axial force, and 1.130 m-N (10 in-lb) of pitching moment. The tests were made through an angle-of-attack range from about -4^o to 13^o at a sideslip angle of 0^o. All of the tests were made without artificially tripping the boundary layer.

Corrections and Accuracy

The angles of attack have been corrected for sting and balance deflection due to aerodynamic loads, and for tunnel airflow misalinement. The axial-force coefficients have not been adjusted to free-stream conditions acting on the base of the model.

The estimated accuracies of the data, based on calibrations and data repeatability (1/2 percent of full-scale range), are within the following limits:

M	ΔC_N	ΔC_A	ΔC_m	ΔC_p	α, deg
1.50	±0.0032	±0.0129	±0.0007	±0.0081	±0.10
2.00	±0.0039	±0.0154	±0.0008	±0.0097	±0.10
2.94	±0.0051	±0.0204	±0.0011	±0.0045	±0.10
4.00	±0.0042	±0.0166	±0.0009	±0.0037	±0.10

PRESENTATION OF RESULTS

The results of the investigation are presented in the following figures:

DISCUSSION OF RESULTS

The effect of Reynolds number variation on the aerodynamic characteristics of a 140°-included-angle cone for various ratios of sting diameter to model diameter (0.125 to 0.500) is shown in figures 3 to 6 for the test Mach number range. At $M = 1.50$, increasing the Reynolds number from 2.07×10^5 to 4.15×10^5 (based on model diameter) showed little or no effects on the variation of normal-force, axial-force, or pitching-moment coefficients with angle of attack. Although the variations in Reynolds number had little or no effects on the pitching-moment data, the pitching-moment curves exhibited nonlinearities through the test angle-of-attack range. Three separate slopes of the pitching-moment curves are noted: $\alpha = -4^{\circ}$ to -2°, $\alpha = -2^{\circ}$ to 2°, and $\alpha = 2^{\circ}$ to 13°. (See fig. 3.) At $M = 2.00$, an increase in Reynolds number from 1.74×10^5 to 3.47×10^5 had effects on the data similar to those at $M = 1.50$. However, at this Mach number, only two different slopes of the pitching-moment curves were noted (fig. 4). At $M = 2.94$ and 4.00 (figs. 5 and 6, respectively), there is little effect on the longitudinal aerodynamic characteristics of the cone due to changes in Reynolds number from 1.6×10^5 to 3.80×10^5. At both of these Mach numbers, the pitching-moment curves generally are linear. It should also be noted that the normal-force coefficient curves are linear throughout the test angle-of-attack range for all test Mach numbers.

The effects of sting diameter on the longitudinal aerodynamic characteristics of the 140°-included-angle cone at several test Reynolds numbers for Mach numbers of 1.50, 2.00, 2.94, and 4.00 are presented in figures 7 to 10, respectively. At all test Mach numbers, these data indicate no significant effects on the normal-force or pitching-moment characteristics of the model due to increasing the ratios of sting diameter to model diameter d/D from 0.125 to 0.500. At Mach numbers of 1.50 and 2.00, there is a noticeable increase in axial-force coefficient in the low angle-of-attack range as d/D is increased. This effect usually decreases or disappears at angles of attack above about 7°. At Mach numbers of 2.94 and 4.00, there is no appreciable effect on axial-force coefficient due to an increase in d/D up to 0.417. No data were obtained for $d/D = 0.500$ at these two Mach numbers.

It should be noted that sting length can influence the axial-force values at low angles of attack. The results of reference 2 indicate that, for a sting mount similar to the $d/D = 0.208$ sting of the present study, a sizable reduction in axial-force coefficient at low angles of attack was obtained at $M = 2.30$ for a ratio of sting length to model diameter l/D of 2.0 when compared with the axial-force data for $l/D = 4.0$. This decrease in the axial-force coefficient for the shorter sting was due to an increase in the base pressure of the cone which occurred when the shock wave of the sting support interacted with the trailing shock wave of the cone. This effect, as well as the sting diameter effects of the present investigation, decreases or disappears near an angle of attack of about 7°. Experience (refs. 2 and 26) has shown that sting length has an increasing effect on axial-force

coefficient with a decrease in Mach number; therefore, an arbitrary sting length of 5.83D was used in the present investigation to minimize these effects.

The effects of the position of the base-pressure tube on the variation of base-pressure coefficient with angle of attack of the 140°-included-angle cone at several Reynolds numbers are shown in figures 11 to 14. At Mach numbers of 1.50 and 2.00 (figs. 11 and 12, respectively), these data show a higher base pressure on the top pressure tube of the cone at small positive angles of attack and on the bottom pressure tube at small negative angles of attack. This probably explains the change in slope of the pitching-moment data in this angle-of-attack region. These data indicate that there is little or no effect on base-pressure coefficient with an increase in Reynolds number. The variation in axial-force coefficient may be determined from the integrated average of these pressures at the different Reynolds numbers; however, the variation appears to be within the accuracy of the axial-force measurements inasmuch as little or no change in axial-force coefficient was noted in figures 3 to 6 due to Reynolds number variation. At the higher test Mach numbers ($M = 2.94$ and 4.00), there are essentially no effects of location of the base-pressure tube or Reynolds number variation on the base-pressure coefficients. (See figs. 13 and 14.)

The effects of the ratio of sting diameter to model diameter on the variation of base-pressure coefficient with angle of attack at various base locations for several Reynolds numbers are shown in figures 15 to 18. Inasmuch as the base-pressure coefficients for the left and right side of the cone are similar, only data for the right side have been plotted in these figures. At $M = 1.50$ and 2.00 (figs. 15 and 16, respectively), these data indicate a decrease in pressure coefficient (more negative) at all locations of the base-pressure tube as the ratio of the diameters increases at angles of attack up to about 7°. Above 7° and up to the maximum of the test, the effect of sting diameter on the base-pressure coefficient decreases. The decrease in base pressures, which occurs when the sting diameter increases, results in the increase in axial-force coefficient observed in figures 7 and 8. At $M = 2.94$ and 4.00, the effect of sting diameter on base-pressure coefficient is generally small, which corresponds to the small effect of sting diameter on axial-force coefficient noted in figures 9 and 10.

CONCLUDING REMARKS

An investigation has been conducted in the Langley Unitary Plan wind tunnel to determine the effects of Reynolds number and sting-support interference on the static aerodynamic characteristics of a 140°-included-angle cone. Base pressures and forces and moments of the model were measured at Mach numbers of 1.50, 2.00, 2.94, and 4.00 through an angle-of-attack range from about -4° to 13°. The Reynolds number, based on model diameter, was varied from 1.61×10^5 to 4.15×10^5. The ratio of sting diameter to model diameter was varied from 0.125 to 0.500.

The investigation indicated that, for all sting diameters tested, variation in test Reynolds number had little or no effect on the static aerodynamic characteristics of the cone. The main effect of sting diameter occurred at Mach numbers of 1.50 and 2.00 where an increase in sting diameter decreased the base-pressure coefficients and increased the axial-force coefficients. There were no appreciable effects on base-pressure coefficient or axial-force coefficient due to increasing the ratio of sting diameter to model diameter at Mach numbers of 2.94 and 4.00.

Langley Research Center,
National Aeronautics and Space Administration,
Hampton, Va., March 13, 1974.

REFERENCES

1. Campbell, James F.: Longitudinal Aerodynamic Characteristics of Several High-Drag Bodies at Mach Numbers From 1.50 to 4.63. NASA TN D-3915, 1967.

2. Campbell, James F.; and Howell, Dorothy T.: Supersonic Aerodynamics of Large-Angle Cones. NASA TN D-4719, 1968.

3. Stallings, Robert L., Jr.; and Tudor, Dorothy H.: Experimental Pressure Distributions on a 120^{o} Cone at Mach Numbers From 2.96 to 4.63 and Angles of Attack From 0^{o} to 20^{o}. NASA TN D-5054, 1969.

4. Campbell, James F.; and Howell, Dorothy T.: Supersonic Lifting Capabilities of Large-Angle Cones. NASA TN D-5499, 1969.

5. Campbell, James F.: Supersonic Aerodynamic Characteristics and Shock Standoff Distances for Large-Angle Cones With and Without Cylindrical Afterbodies. NASA TN D-5334, 1969.

6. Stallings, Robert L., Jr.: Experimentally Determined Local Flow Properties and Drag Coefficients for a Family of Blunt Bodies at Mach Numbers From 2.49 to 4.63. NASA TR R-274, 1967.

7. Owens, Robert V.: Aerodynamic Characteristics of Spherically Blunted Cones at Mach Numbers From 0.5 to 5.0. NASA TN D-3088, 1965.

8. Nichols, James O.; and Nierengarten, Edward A.: Aerodynamic Characteristics of Blunt Bodies. Tech. Rep. No. 32-677 (Contract NAS 7-100), Jet Propulsion Lab., California Inst. Technol., Nov. 19, 1964.

9. Walker, Billy; and Weaver, Robert W.: Static Aerodynamic Characteristics of Blunted Cones in the Mach-Number Range From 2.2 to 9.5. Tech. Rep. 32-1213 (Contract No. NAS 7-100), Jet Propulsion Lab., California Inst. Technol., Dec. 1, 1967.

10. Kurtz, Donald W.: Detailed Pressure Distribution on a Blunted 60-deg Half-Angle Cone at Mach Numbers of 6.08 and 9.46. Tech. Mem. 33-404 (Contract No. NAS 7-100), Jet Propulsion Lab., California Inst. Technol., Sept. 1, 1968.

11. Boison, J. Christopher; and Curtiss, Howard A.: An Experimental Investigation of Blunt Body Stagnation Point Velocity Gradient. ARS J., vol. 29, no. 2, Feb. 1959, pp. 130-135.

12. Davenport, Edwin E.: Static Longitudinal Aerodynamic Characteristics of Some Supersonic Decelerator Models at Mach Numbers of 2.30 and 4.63. NASA TN D-5219, 1969.

13. Deveikis, William D.; and Sawyer, James Wayne: Aerodynamic Characteristics of Tension Shell Shapes at Mach 3.0. NASA TN D-3633, 1966.

14. Harris, Charles D.: Transonic Aerodynamic Investigation of Tension Shell and Blunted 100° Conical Shapes for Unmanned Entry Vehicles. NASA TN D-3700, 1966.

15. Marte, Jack E.; and Weaver, Robert W.: Low Subsonic Dynamic-Stability Investigation of Several Planetary-Entry Configurations in a Vertical Wind Tunnel (Part I). Tech. Rep. No. 32-743 (Contract No. NAS 7-100), Jet Propulsion Lab., California Inst. Technol., May 1, 1965.

16. Bendura, Richard J.: Low Subsonic Static and Dynamic Stability Characteristics of Two Blunt 120° Cone Configurations. NASA TN D-3853, 1967.

17. Inouye, Mamoru; Marvin, Joseph G.; and Sinclair, A. Richard: Comparison of Experimental and Theoretical Shock Shapes and Pressure Distributions on Flat-Faced Cylinders at Mach 10.5. NASA TN D-4397, 1968.

18. Henning, Allen B.; and Lundstrom, Reginald R. (With appendix A by James C. Young): Flight Test of an Erectable Spacecraft Used for Decelerator Testing at Simulated Mars Entry Conditions. NASA TN D-6910, 1972.

19. McShera, John T., Jr.: Wind-Tunnel Pressure Measurements in the Wake of a Cone-Cylinder Model at Mach Numbers of 2.30 and 4.65. NASA TN D-2928, 1965.

20. Campbell, James F.; and Grow, Josephine W.: Experimental Flow Properties in the Wake of a 120° Cone at Mach Number 2.20. NASA TN D-5365, 1969.

21. Brown, Clarence A., Jr.; Campbell, James F.; and Tudor, Dorothy H.: Experimental Wake Survey Behind a 120°-Included-Angle Cone at Angles of Attack of 0° and 5°, Mach Numbers From 1.60 to 3.95, and Longitudinal Stations Varying From 1.0 to 8.39 Body Diameters. NASA TM X-2139, 1971.

22. Brown, Clarence A., Jr.; Campbell, James F.; and Tudor, Dorothy H: Experimental Wake Survey Behind Viking '75 Entry Vehicle at Angles of Attack of 0° and 5°, Mach Numbers From 1.60 to 3.95, and Longitudinal Stations From 1.0 to 8.39 Body Diameters. NASA TM X-2312, 1971.

23. Brown, Clarence A., Jr.; and Campbell, James F.: Experimental Wake Survey Behind a 140°-Included-Angle Cone at Angles of Attack of 0° and 5°, Mach Numbers From 1.60 to 3.95, and Longitudinal Stations Varying From 1.0 to 8.39 Body Diameters. NASA TM X-2409, 1971.

24. Brown, Clarence A., Jr.; and Campbell, James F.: Evaluation of Flow Properties Behind 120°- and 140°-Included-Angle Cones and a Viking '75 Entry Vehicle at Mach Numbers From 1.60 to 3.95. NASA TN D-7089, 1973.

25. Brown, Clarence A., Jr.; Trescot, Charles D., Jr.; and Richardson, Celia S.: Experimental Aerodynamic Characteristics of 120°-Included-Angle Cone With Attached and Separated 20°-Included-Angle Cone at Mach Numbers of 2.36 and 2.70. NASA TM X-2603, 1972.

26. Perkins, Edward W.: Experimental Investigation of the Effects of Support Interference on the Drag of Bodies of Revolution at a Mach Number of 1.5. NACA TN 2292, 1951.

27. Anon.: Manual for Users of the Unitary Plan Wind Tunnel Facilities of the National Advisory Committee for Aeronautics. NACA, 1956.

28. Schaefer, William T., Jr.: Characteristics of Major Active Wind Tunnels at the Langley Research Center. NASA TM X-1130, 1965.

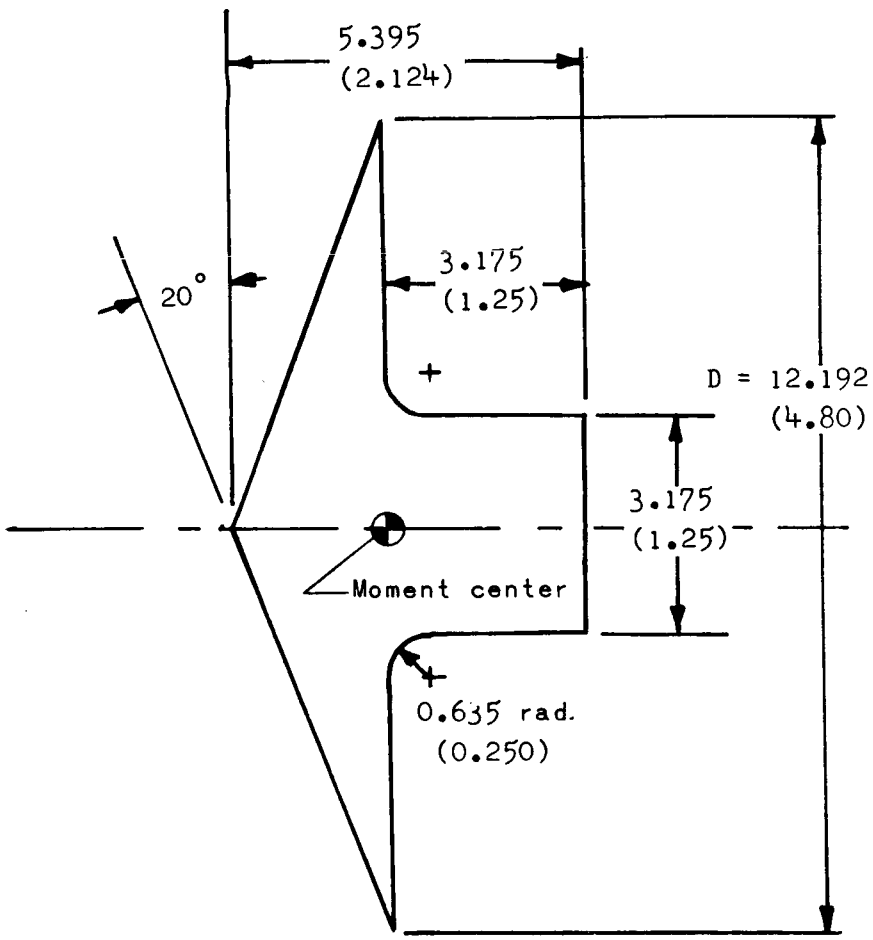

(a) Sketch of model.

Figure 1.- Sketches of model, sting supports, and pressure-orifice locations. All dimensions are in cm (in.).

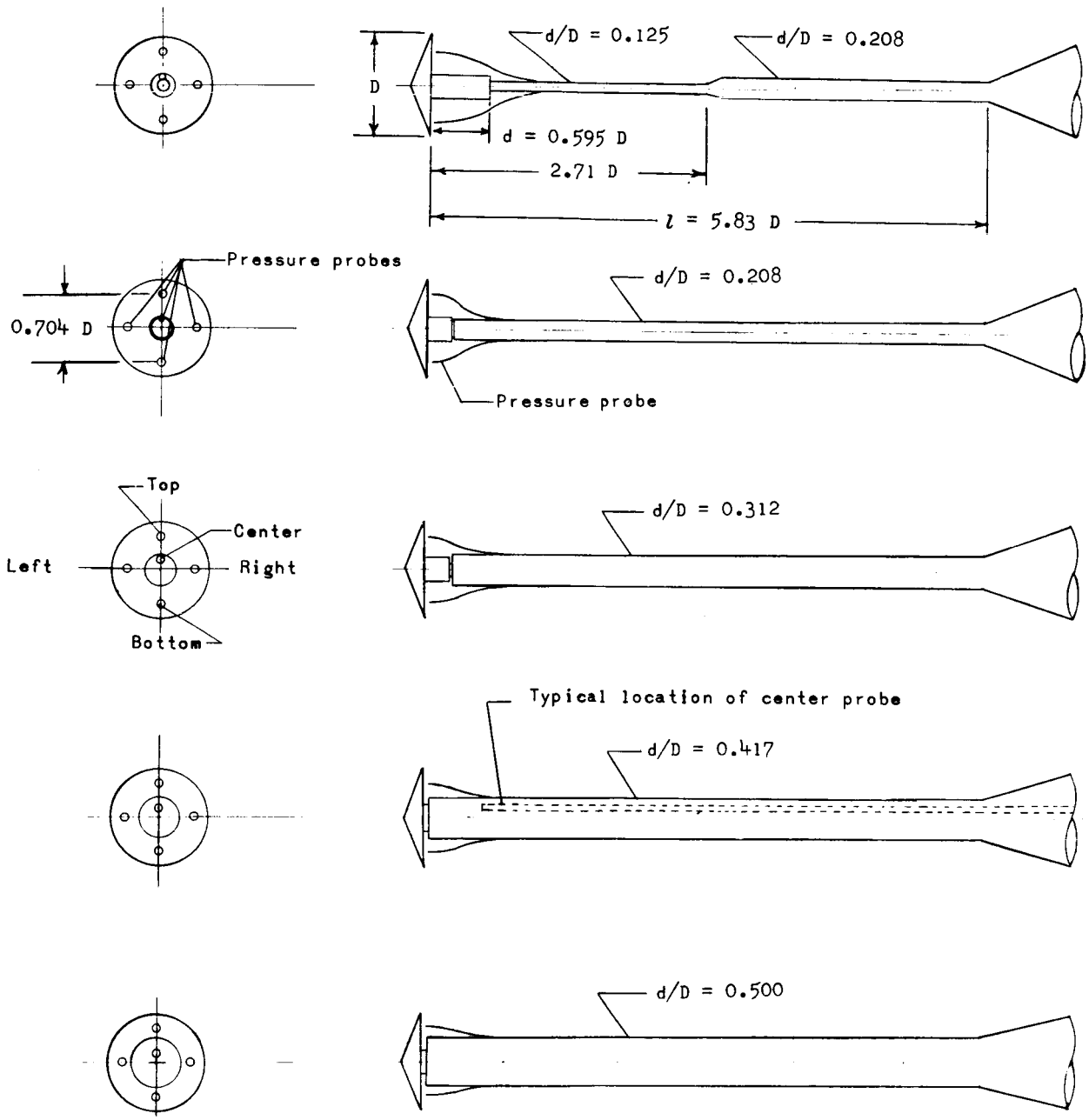

(b) Sketch of sting supports and locations of pressure orifices.

Figure 1.- Concluded.

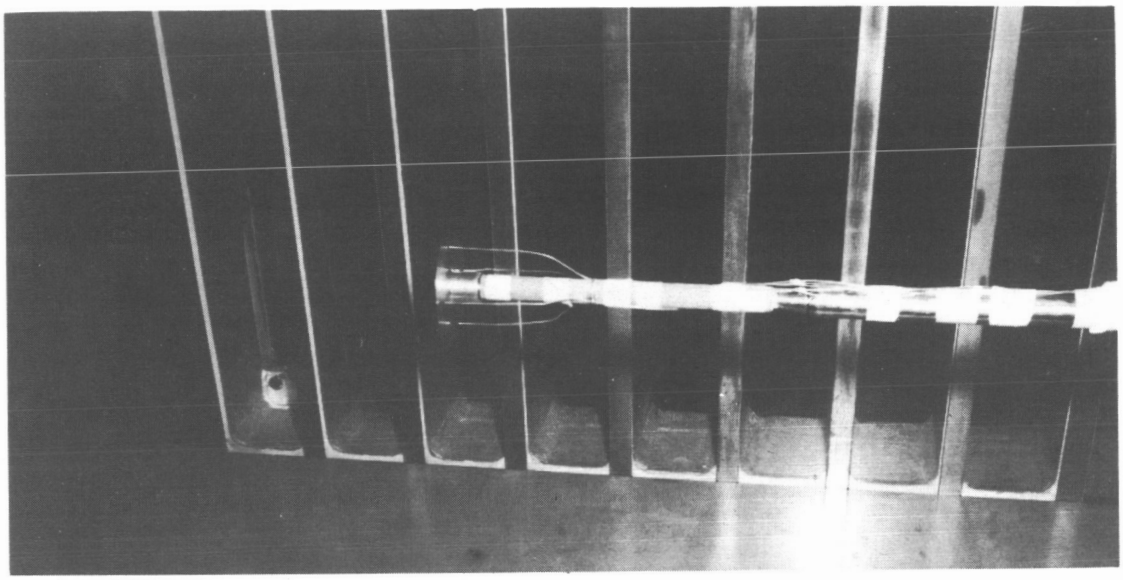

(a) d/D = 0.208.

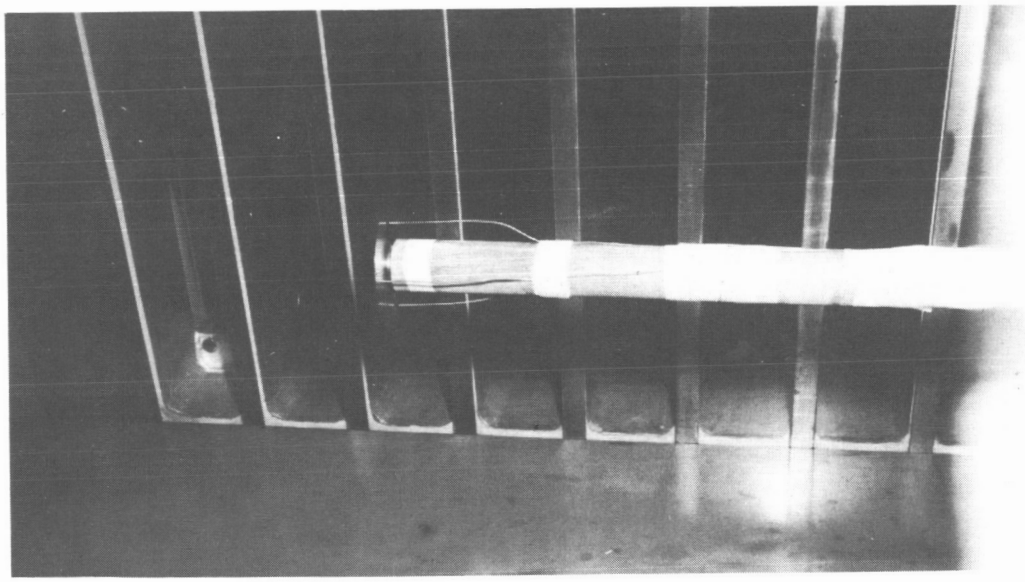

(b) d/D = 0.417.

Figure 2.- Photographs of model. L-74-1067

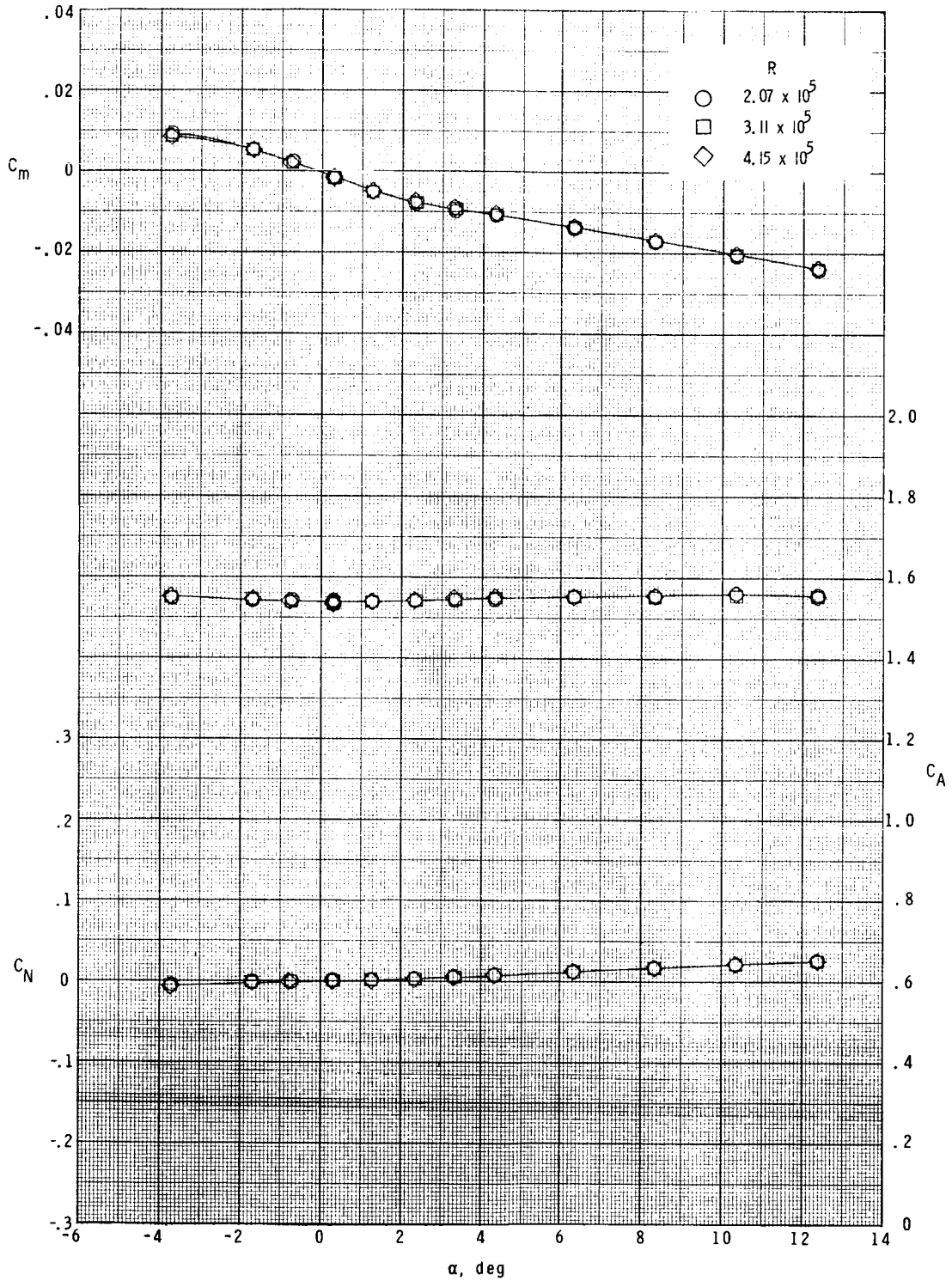

(a) d/D = 0.125.

Figure 3.- Effect of Reynolds number on the longitudinal aerodynamic characteristics of the model for various ratios of sting diameter to model diameter at M = 1.50.

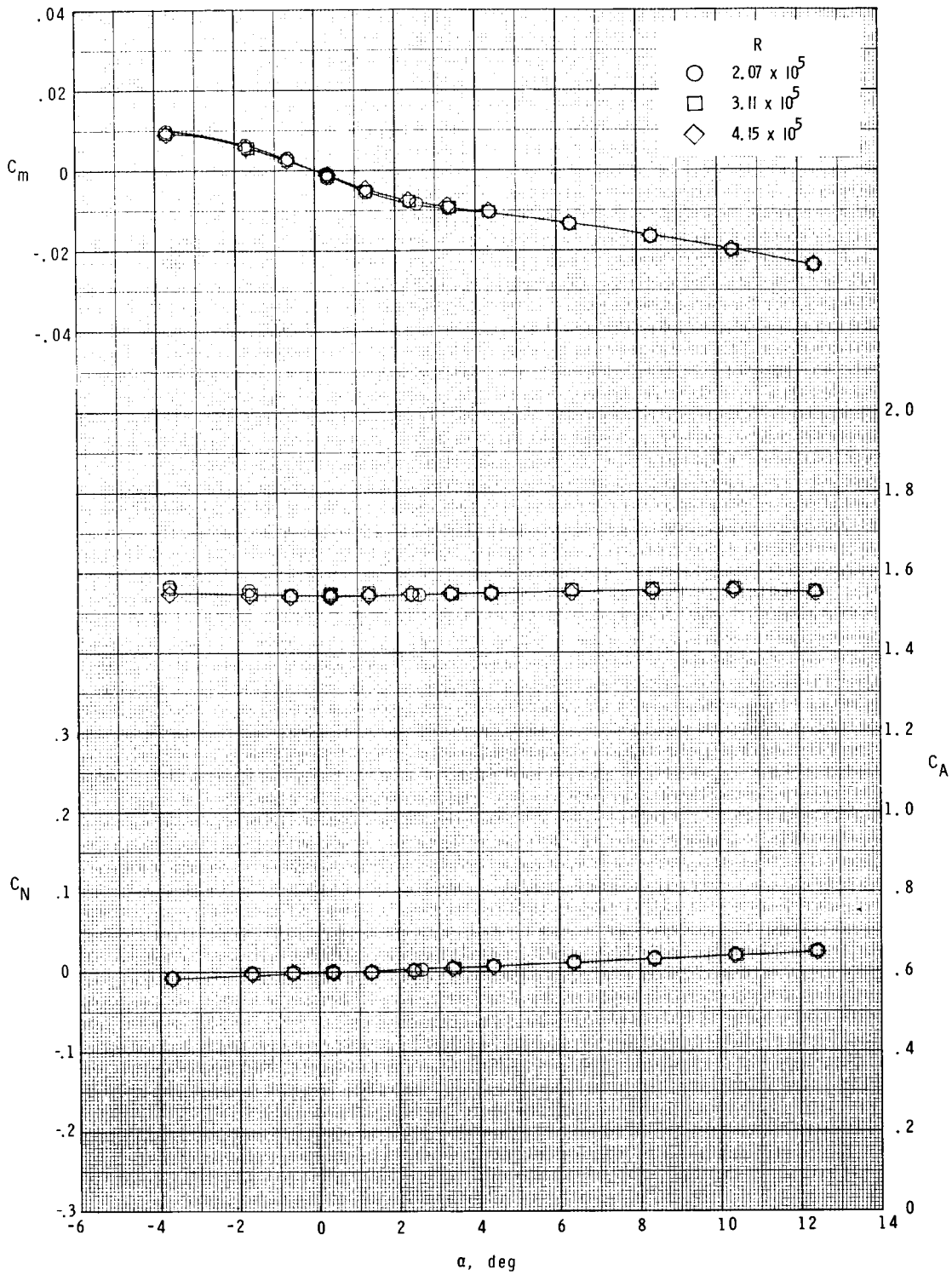

(b) d/D = 0.208.

Figure 3.- Continued.

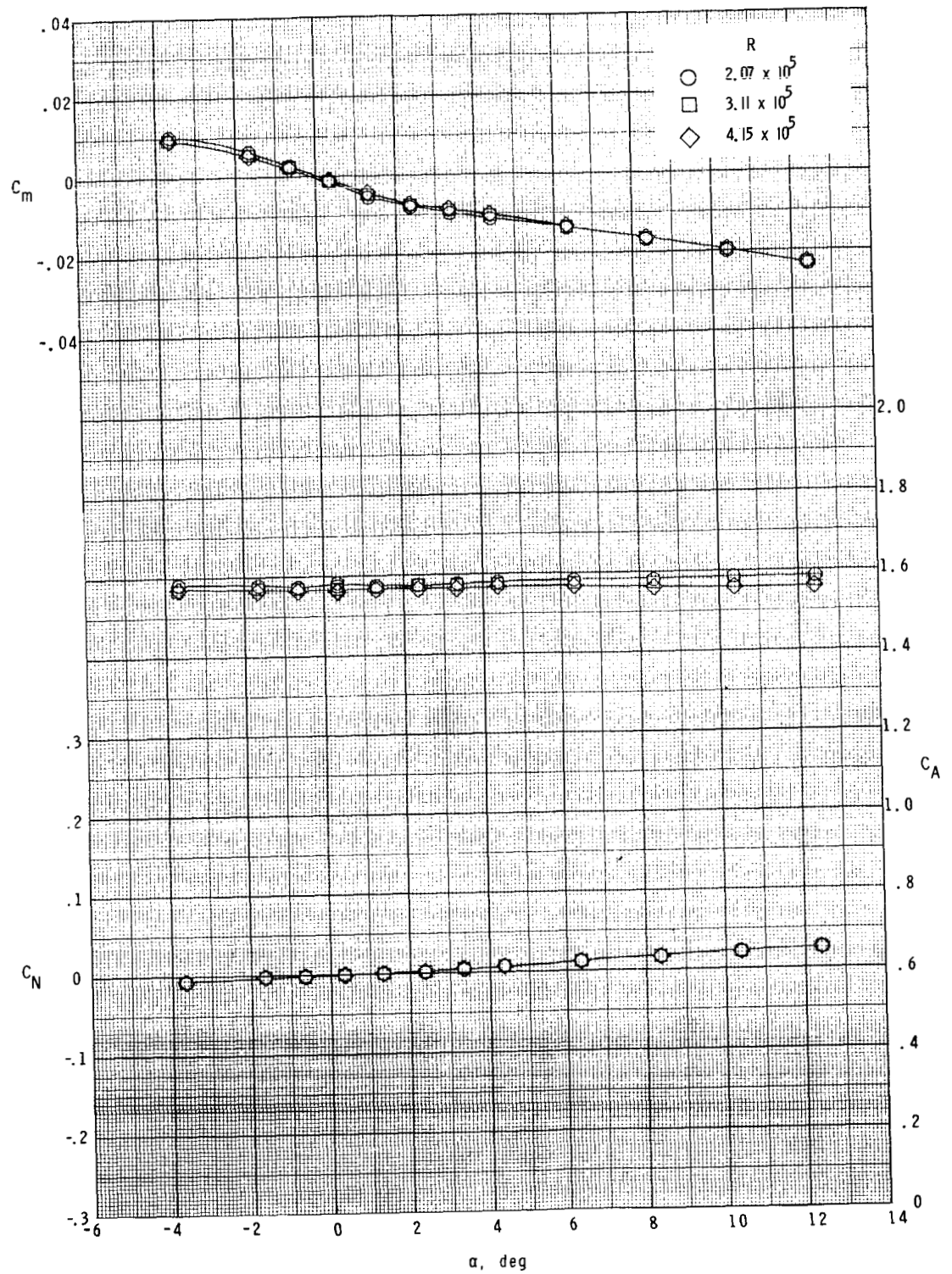

(c) d/D = 0.312.

Figure 3.- Continued.

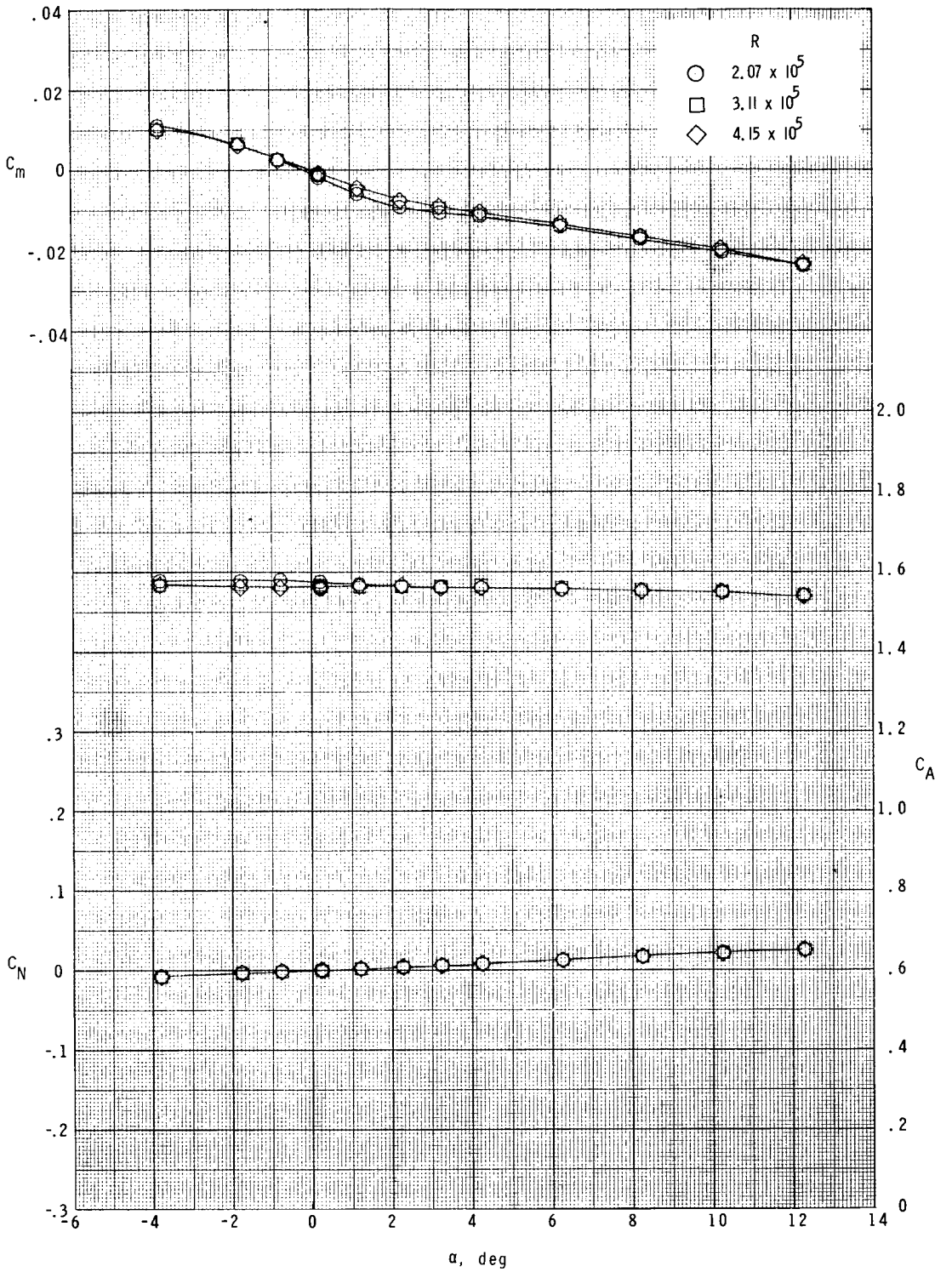

(d) d/D = 0.417.

Figure 3.- Continued.

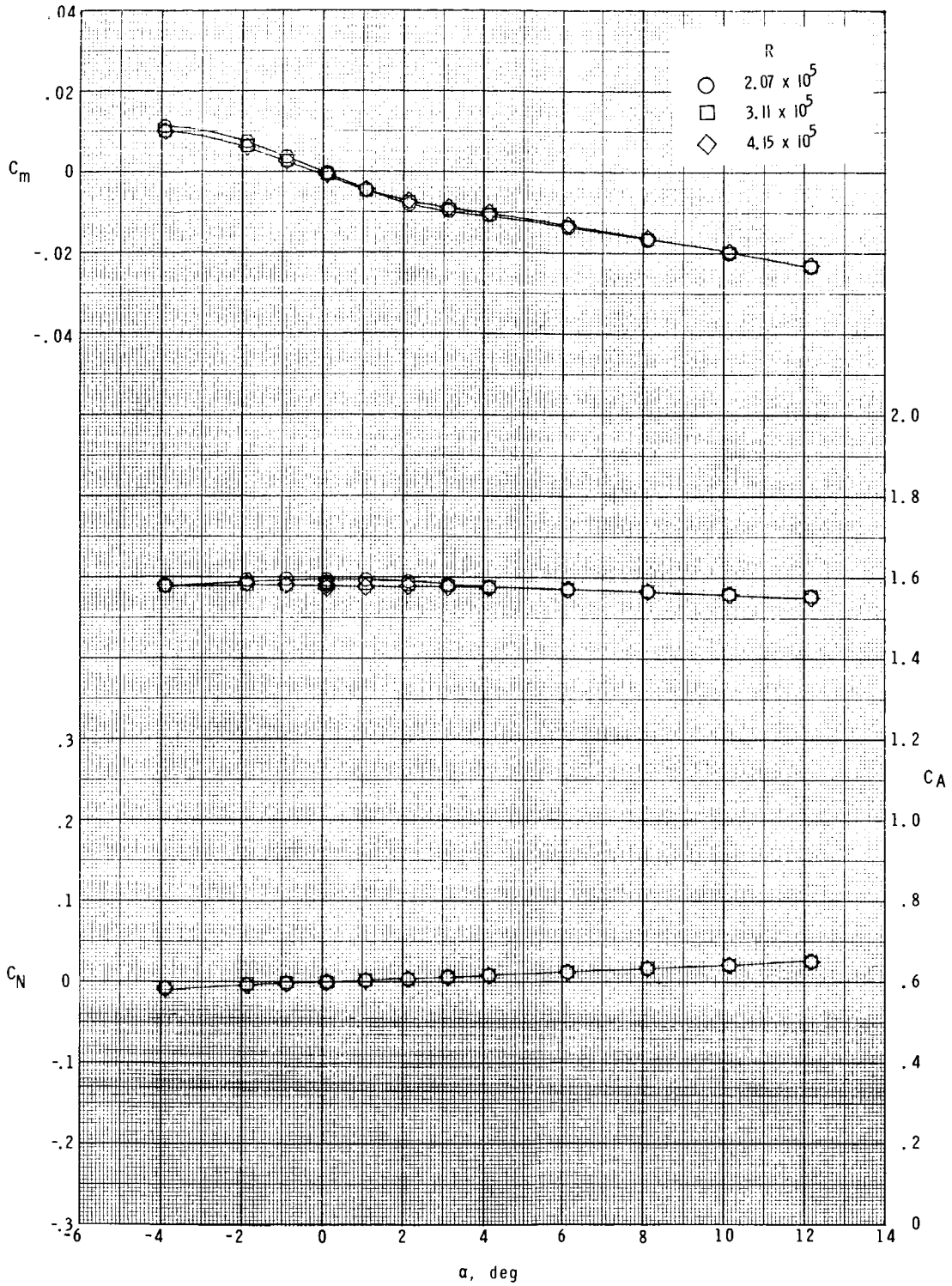

(e) d/D = 0.500.

Figure 3.- Concluded.

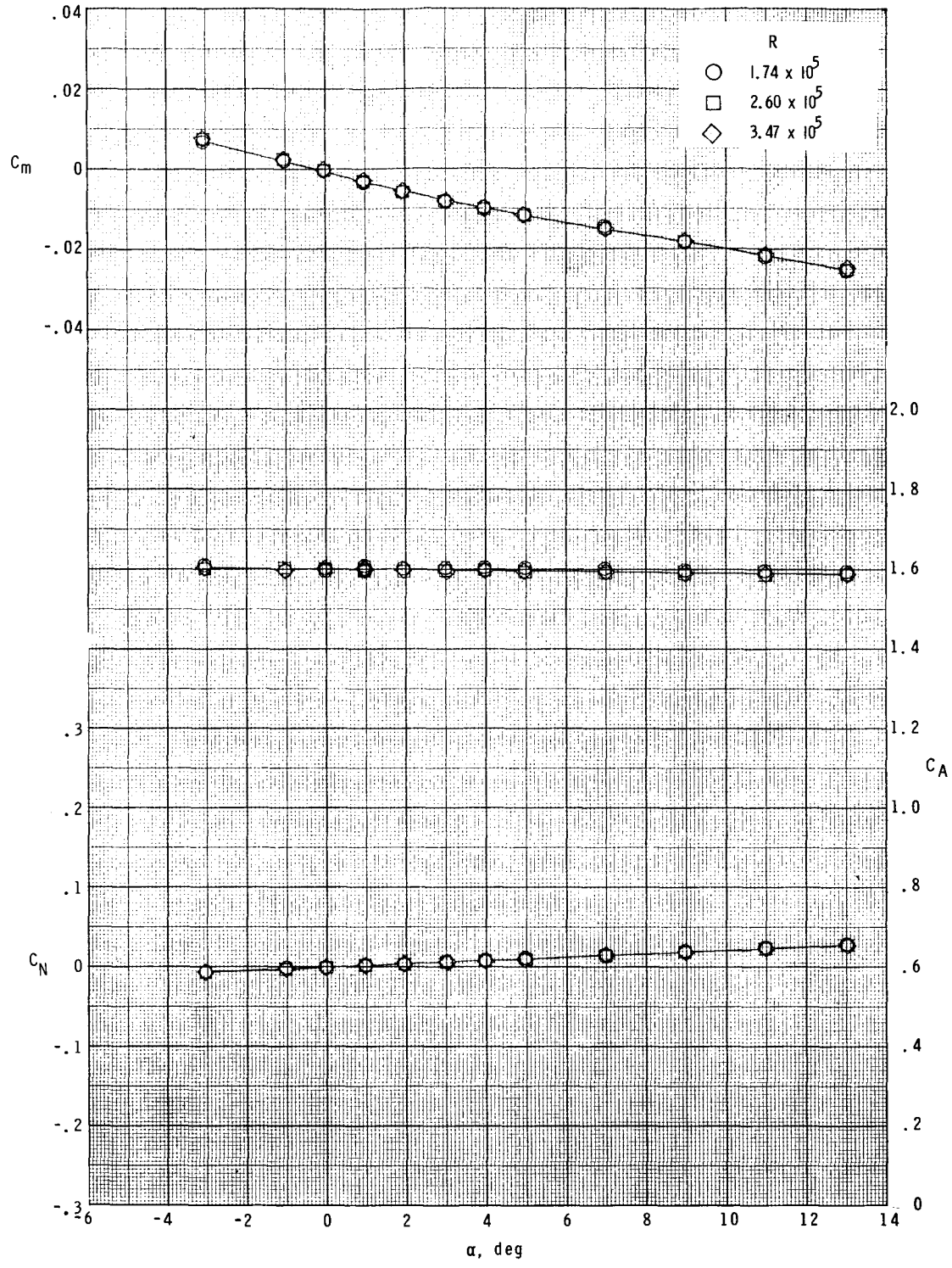

(a) d/D = 0.125.

Figure 4.- Effect of Reynolds number on the longitudinal aerodynamic characteristics of the model for various ratios of sting diameter to model diameter at M = 2.00.

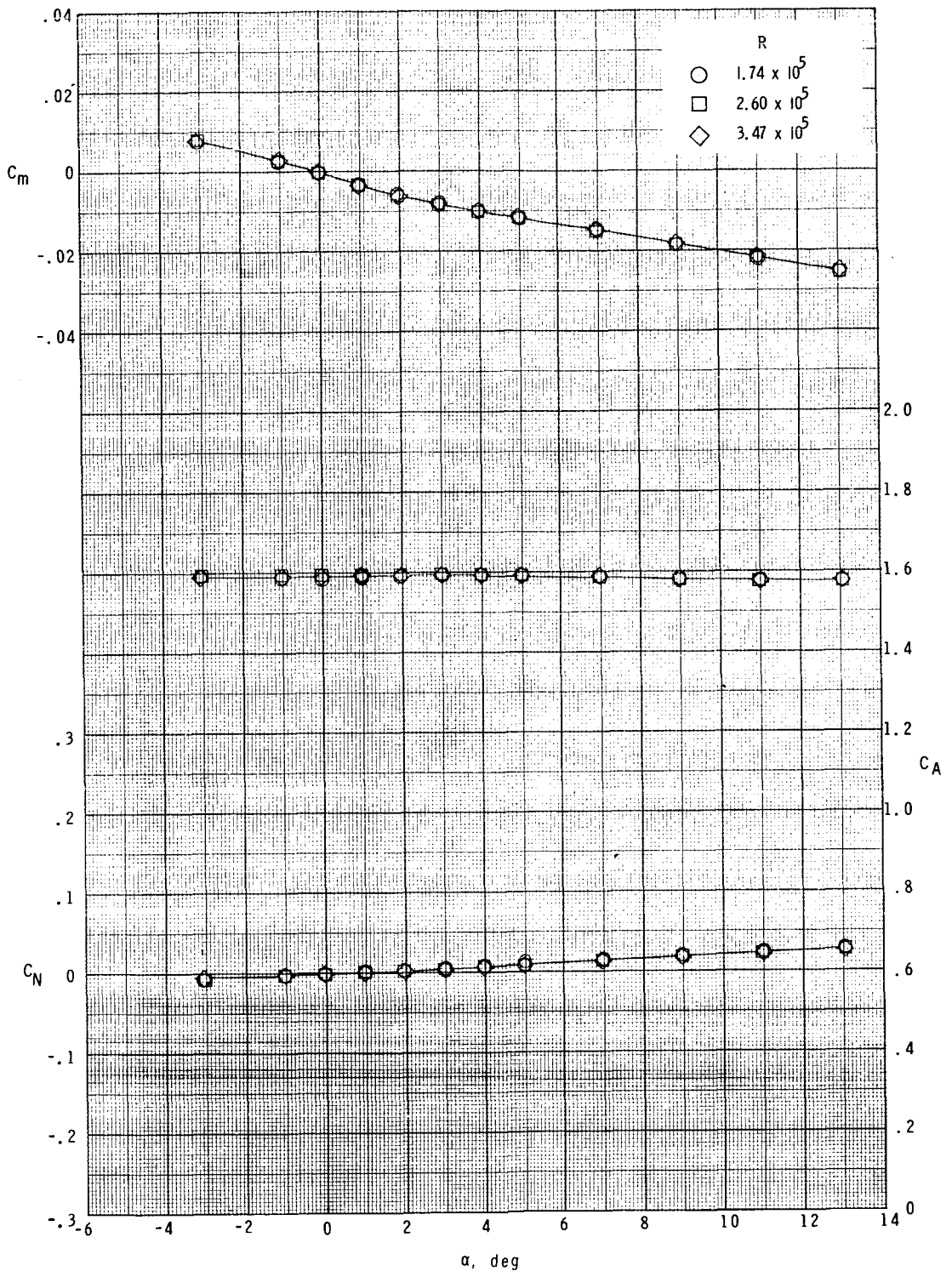

(b) d/D = 0.208.

Figure 4.- Continued.

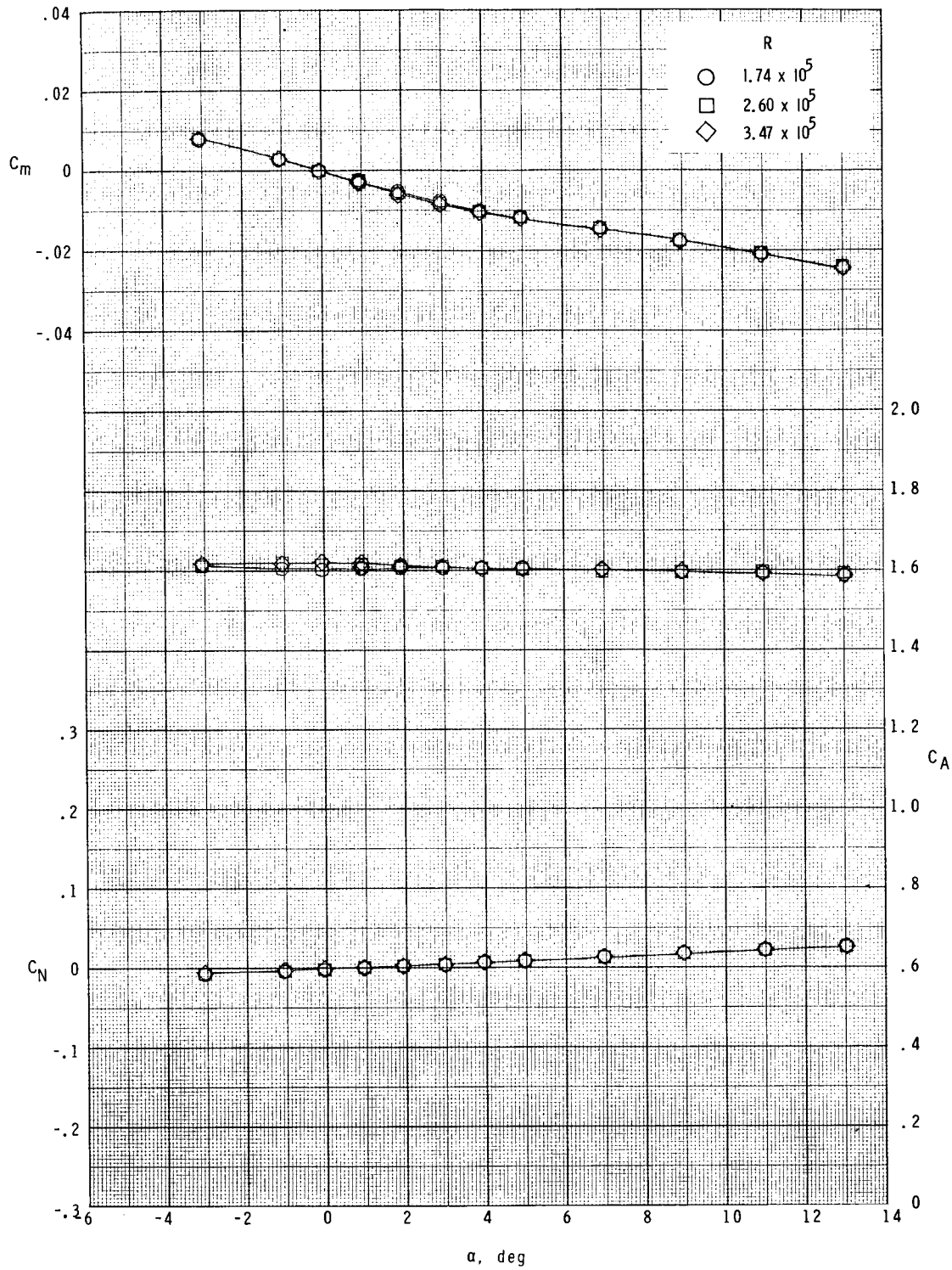

(c) d/D = 0.312.

Figure 4.- Continued.

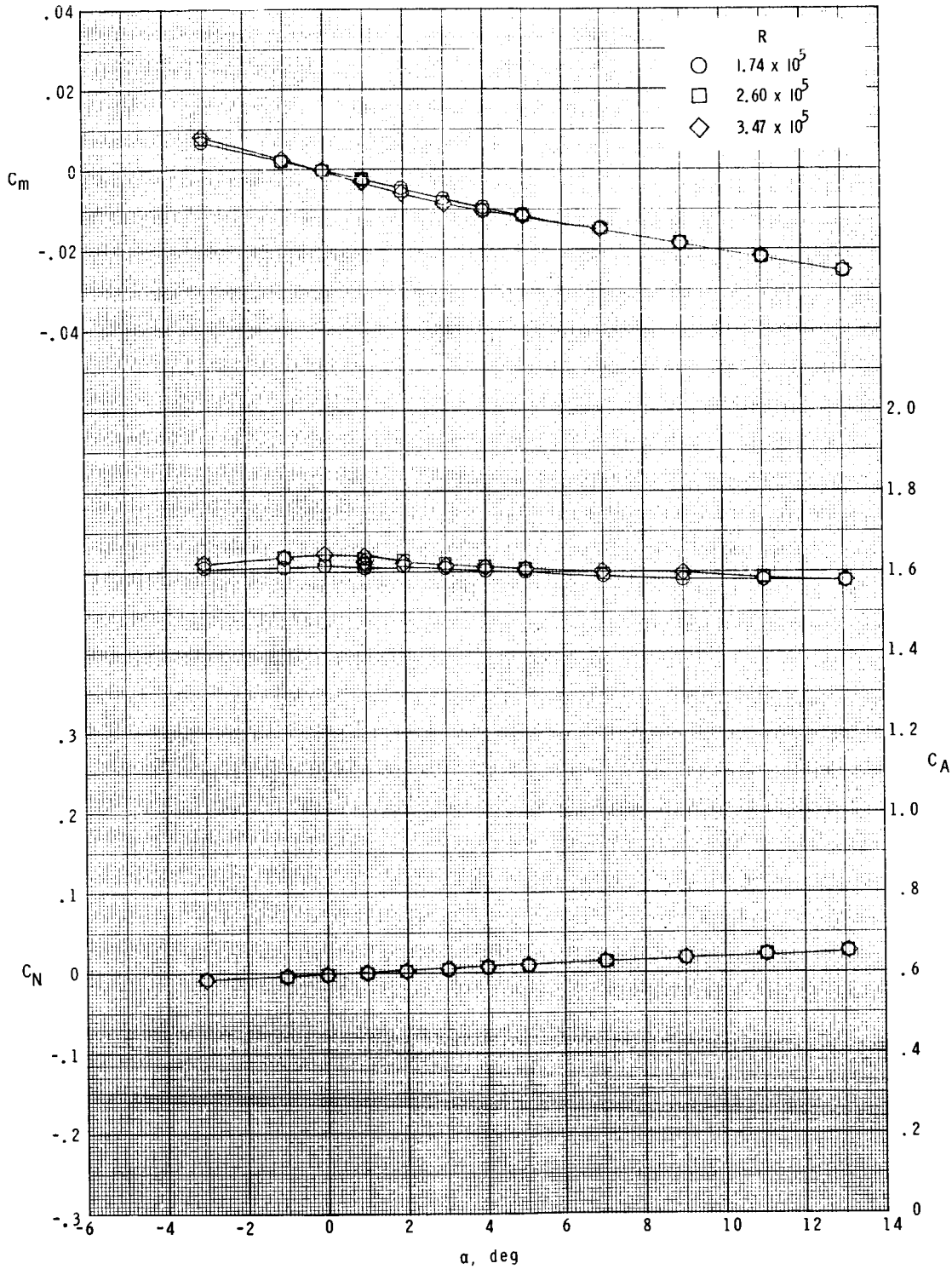

(d) d/D = 0.417.

Figure 4.- Continued.

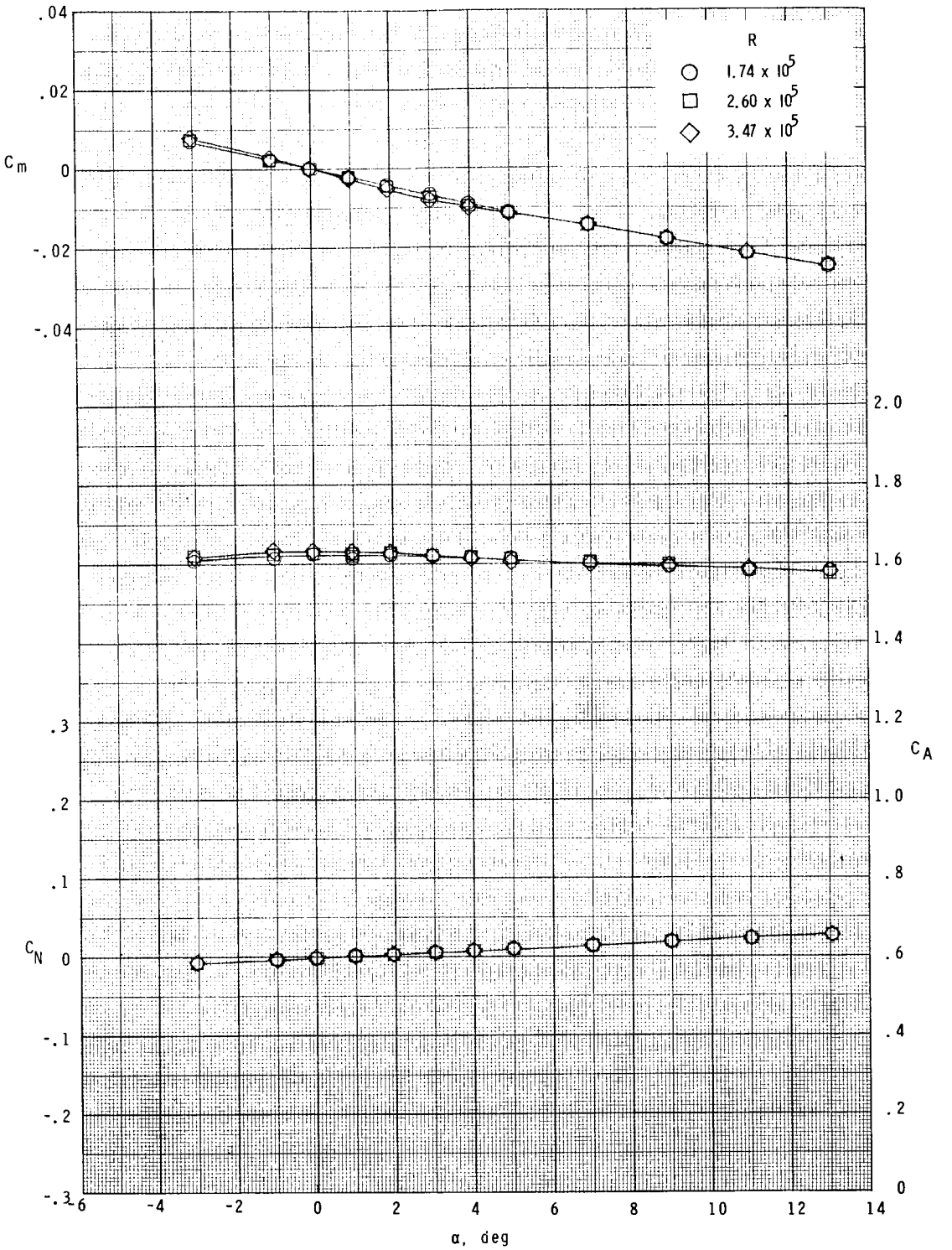

(e) d/D = 0.500.

Figure 4.- Concluded.

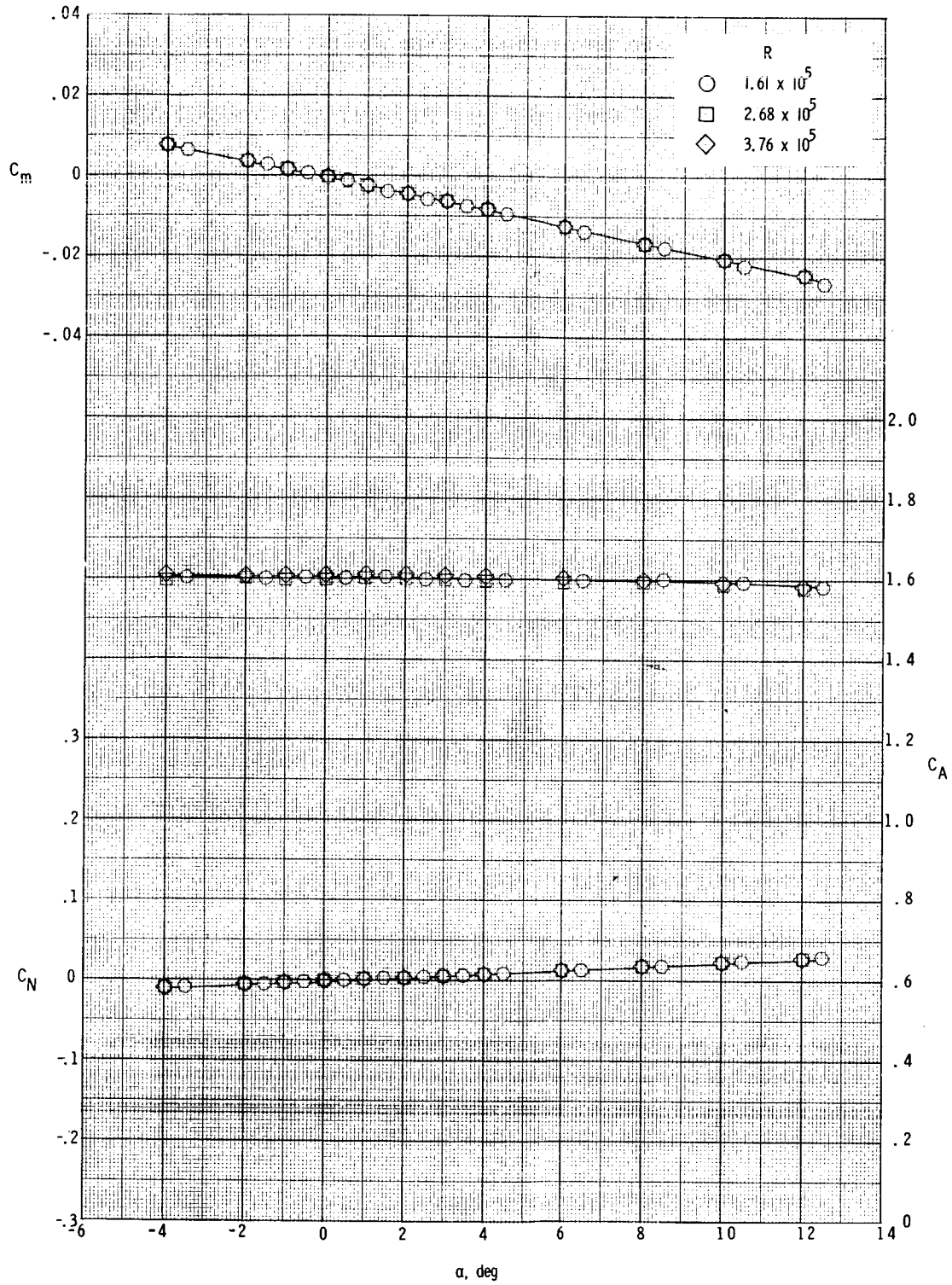

(a) d/D = 0.125.

Figure 5.- Effect of Reynolds number on the longitudinal aerodynamic characteristics of the model for various ratios of sting diameter to model diameter at M = 2.94.

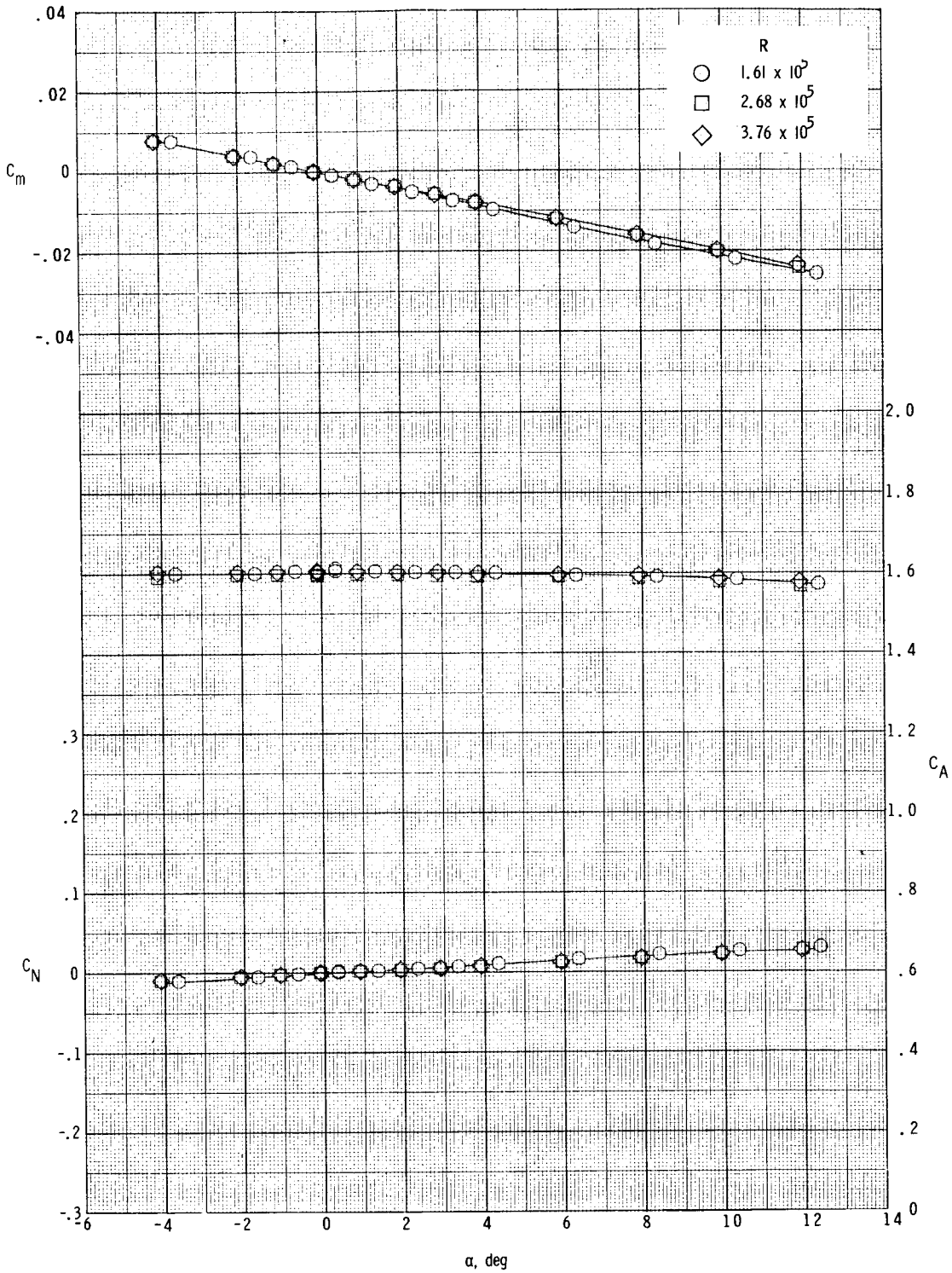

(b) d/D = 0.208.

Figure 5.- Continued.

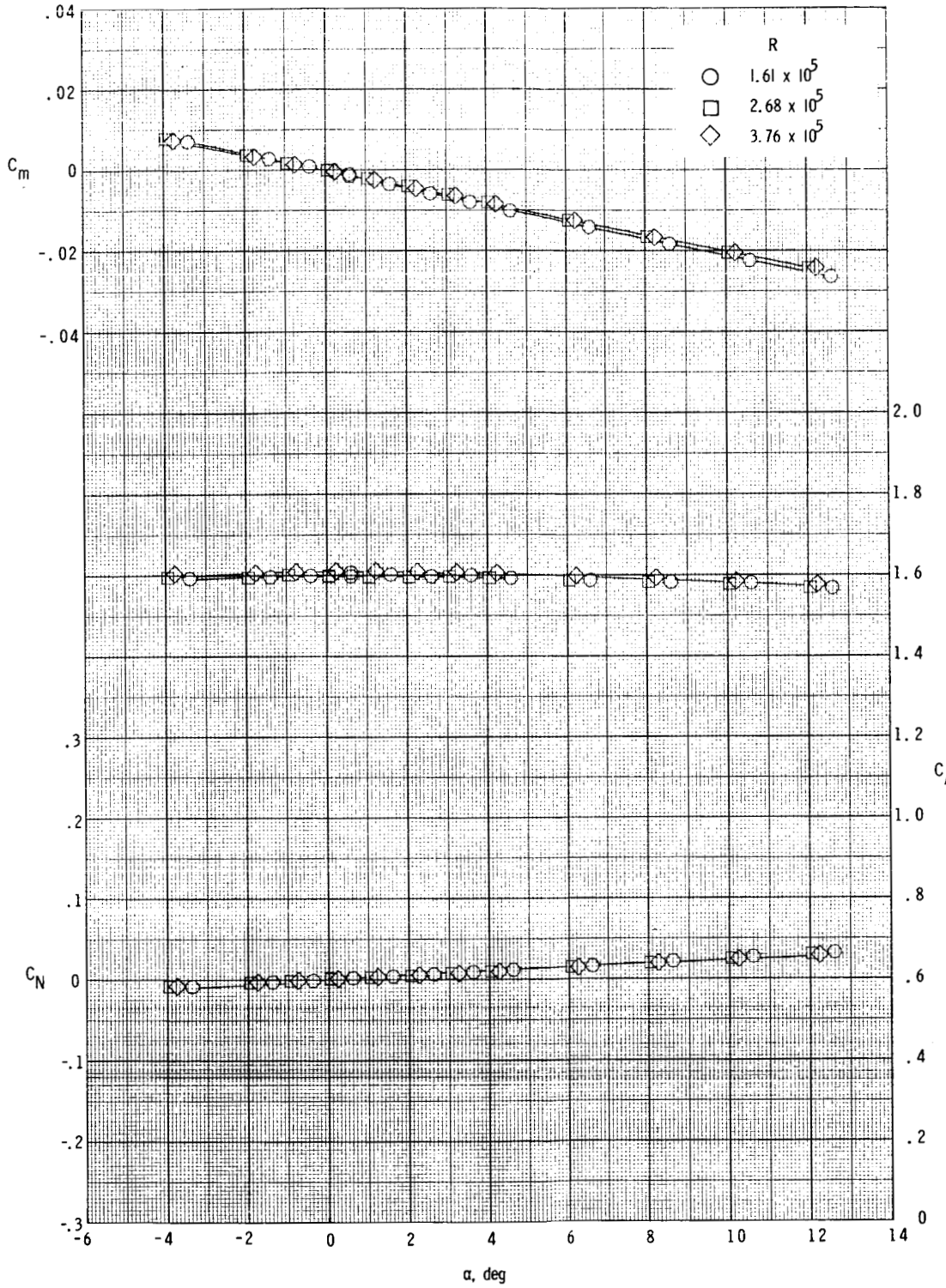

(c) d/D = 0.312.

Figure 5.- Continued.

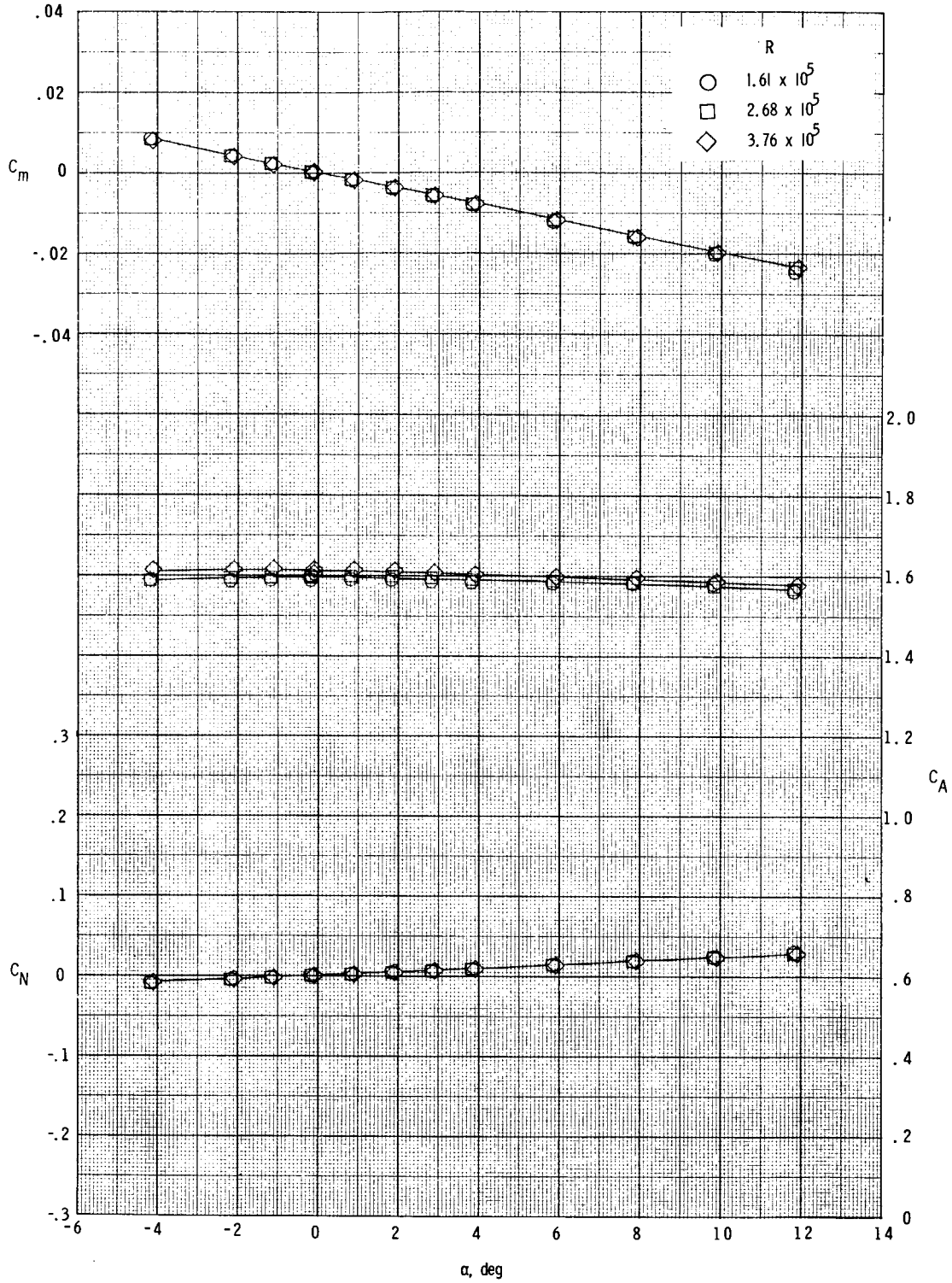

(d) d/D = 0.417.

Figure 5.- Concluded.

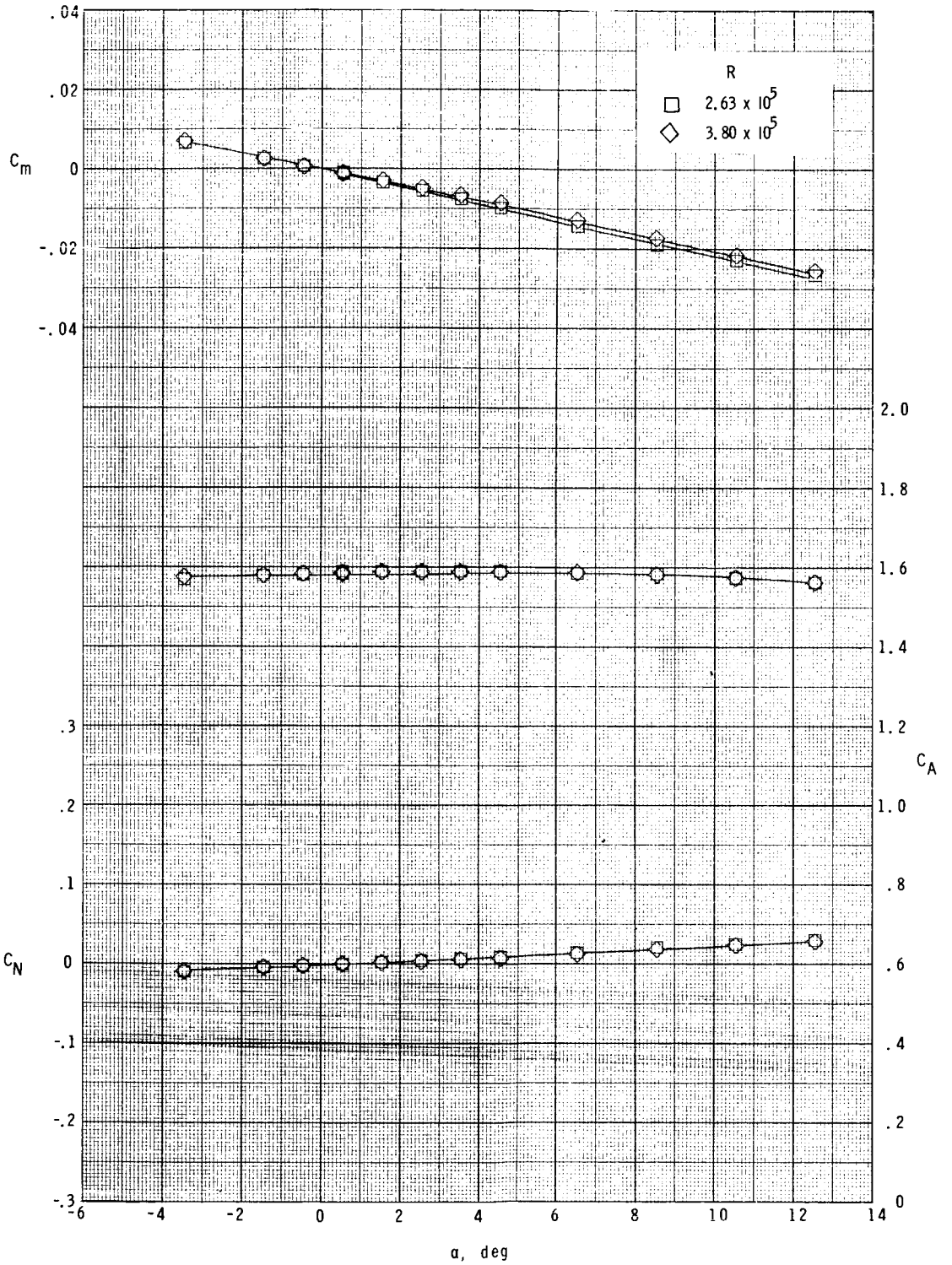

(a) d/D = 0.125.

Figure 6.- Effect of Reynolds number on the longitudinal aerodynamic characteristics of the model for various ratios of sting diameter to model diameter at M = 4.00.

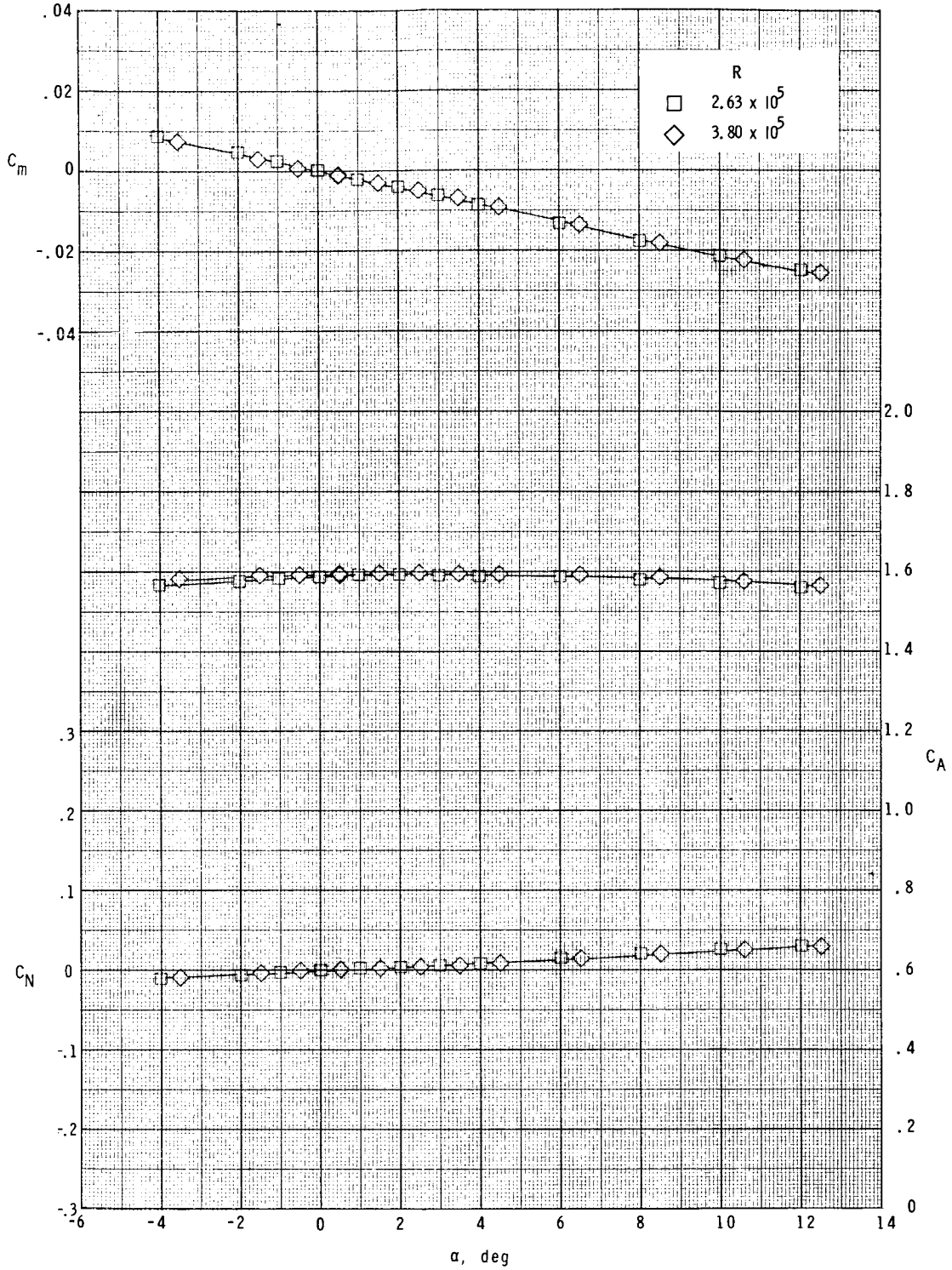

(b) d/D = 0.208.

Figure 6.- Continued.

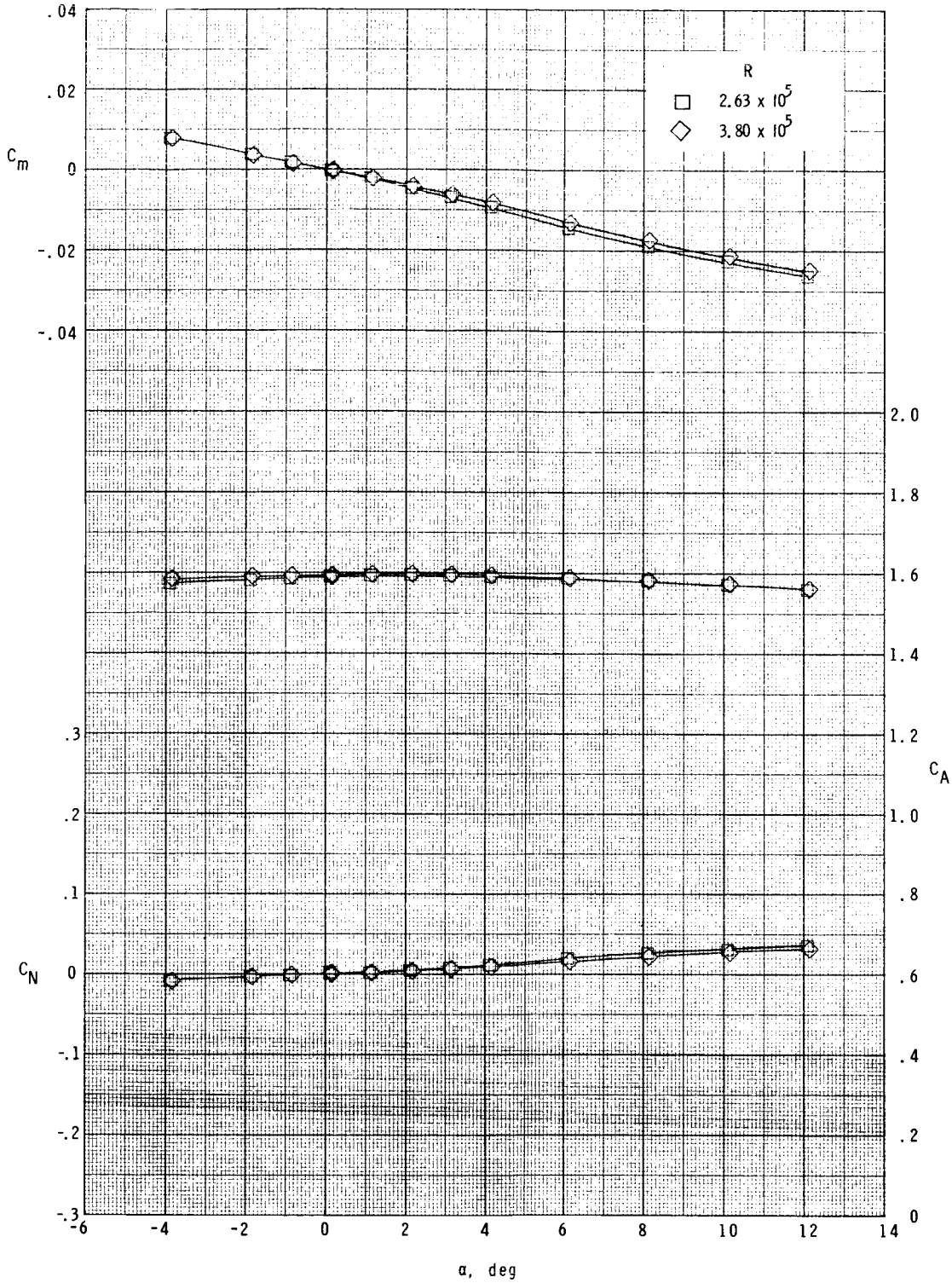

(c) d/D = 0.312.

Figure 6.- Continued.

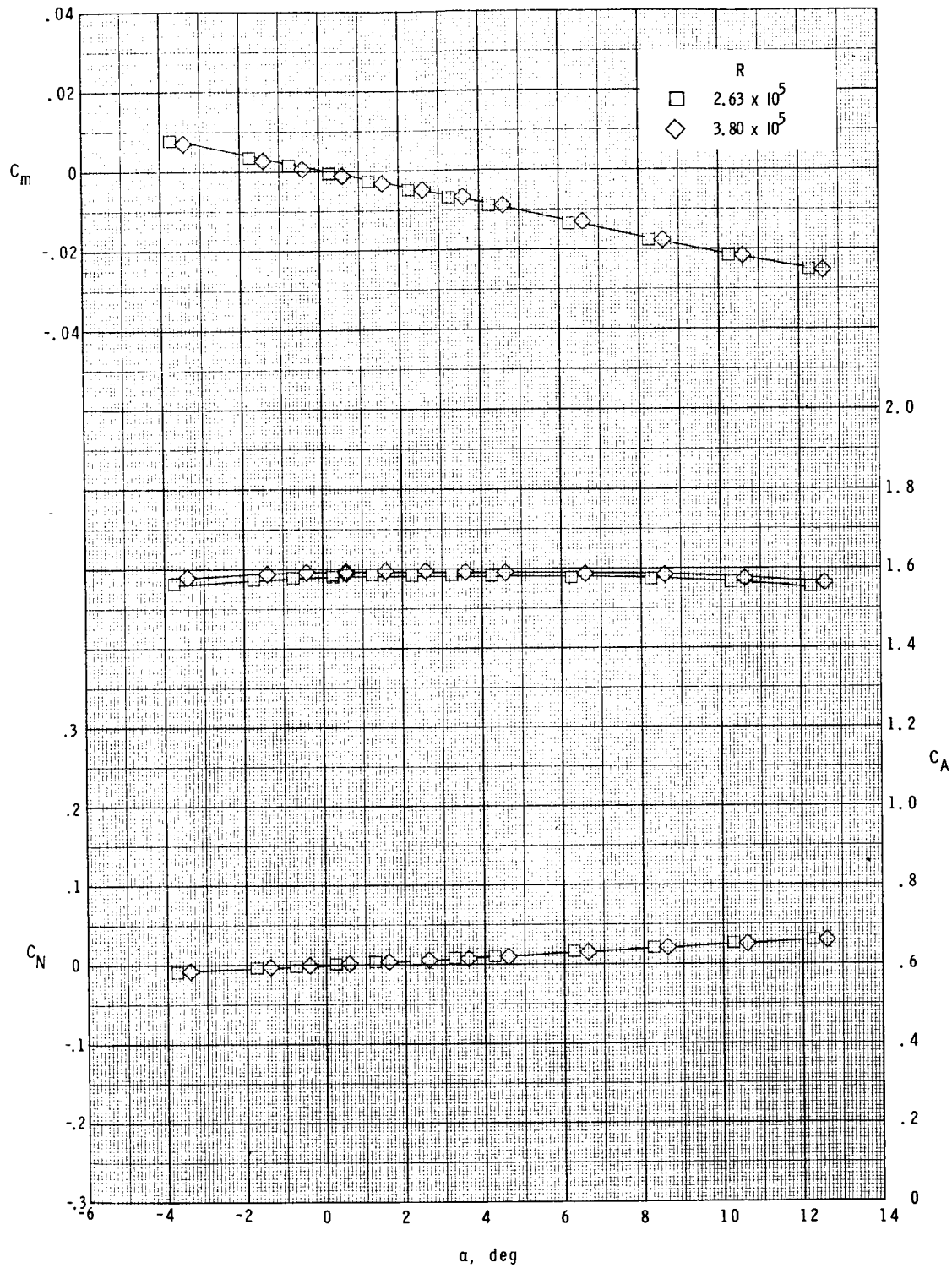

(d) d/D = 0.417.

Figure 6.- Concluded.

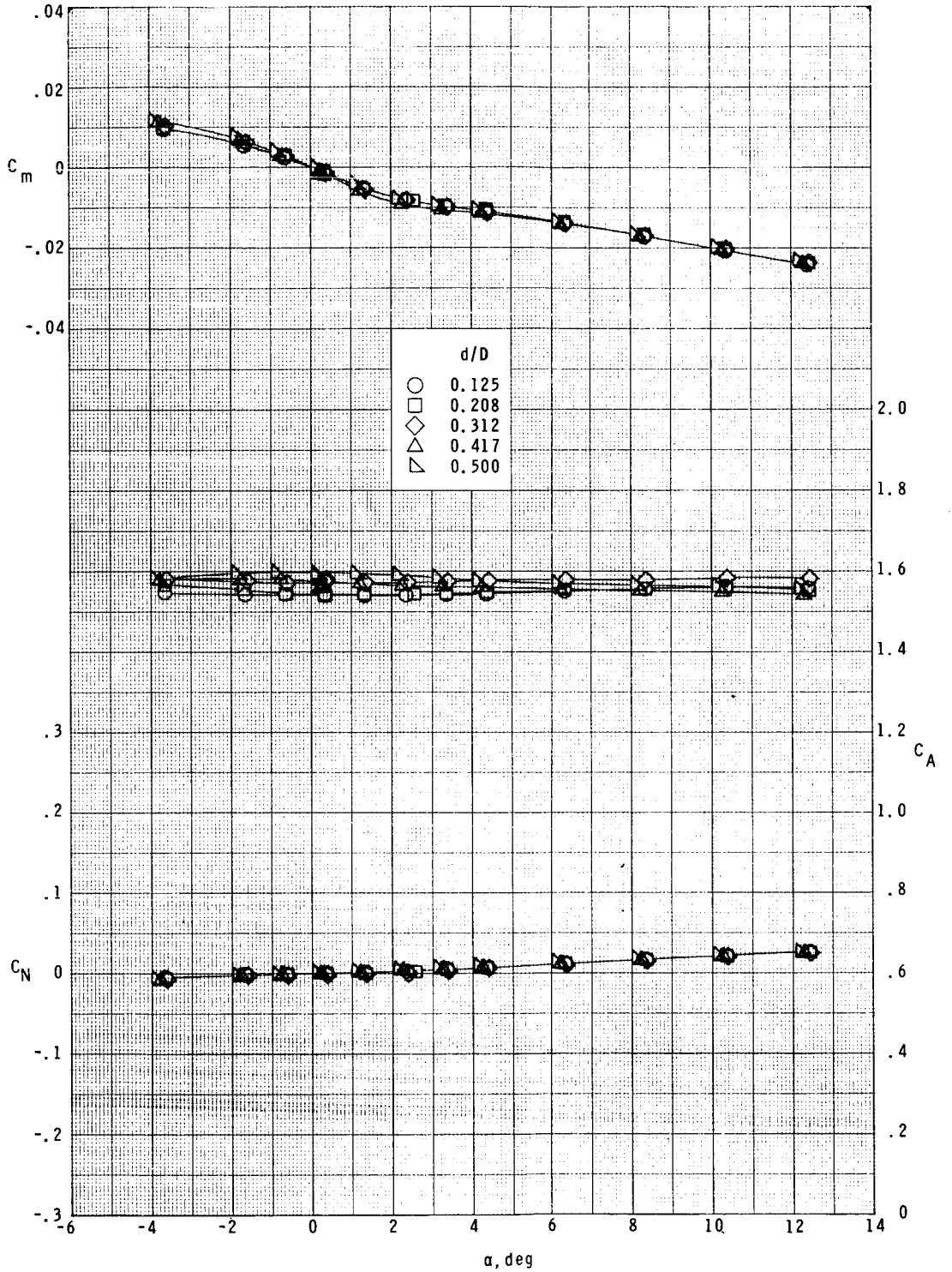

(a) $R = 2.07 \times 10^5$.

Figure 7.- Effect of sting diameter on the longitudinal aerodynamic characteristics of the model for three Reynolds numbers at M = 1.50.

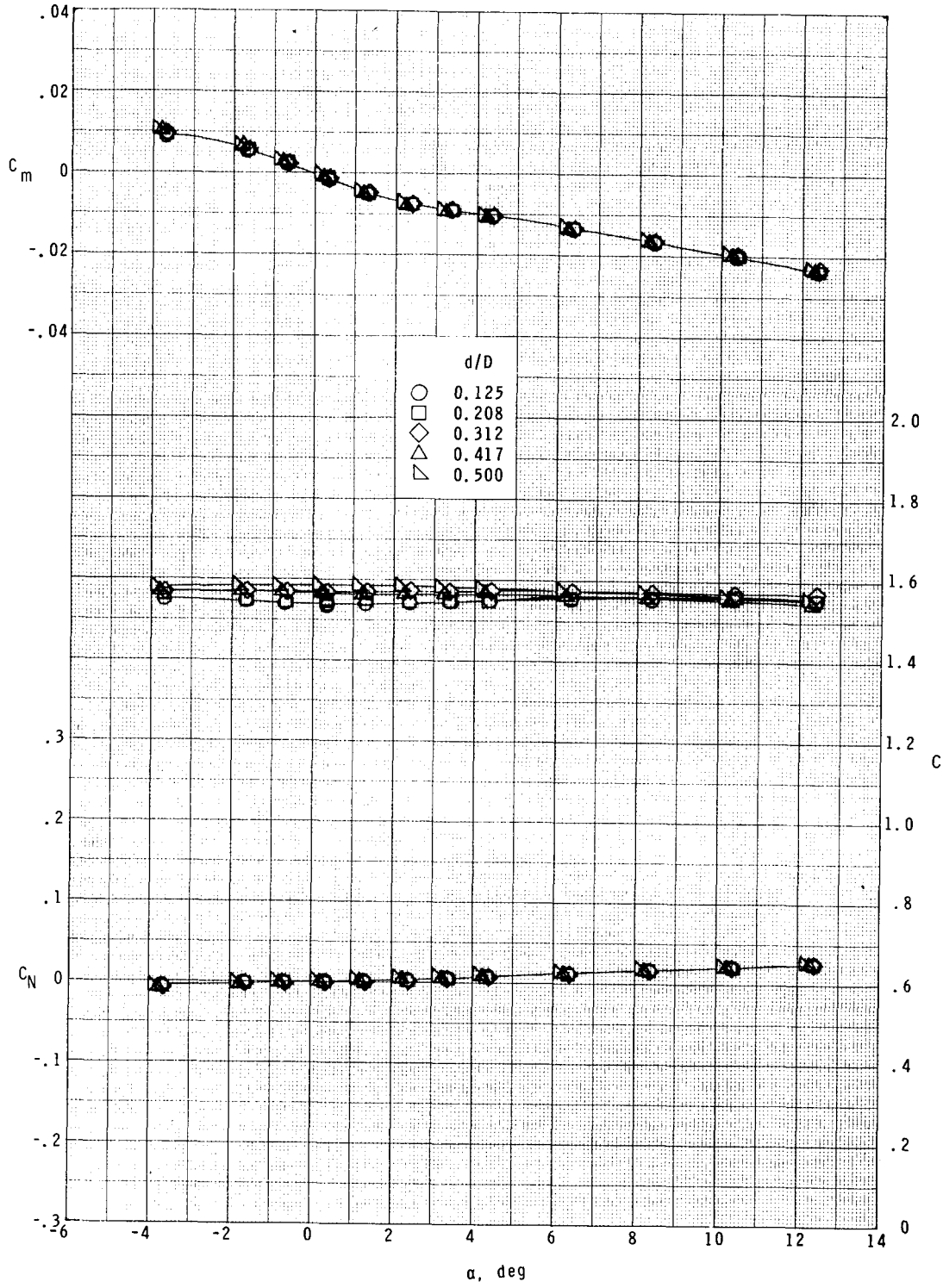

(b) $R = 3.11 \times 10^5$.

Figure 7.- Continued.

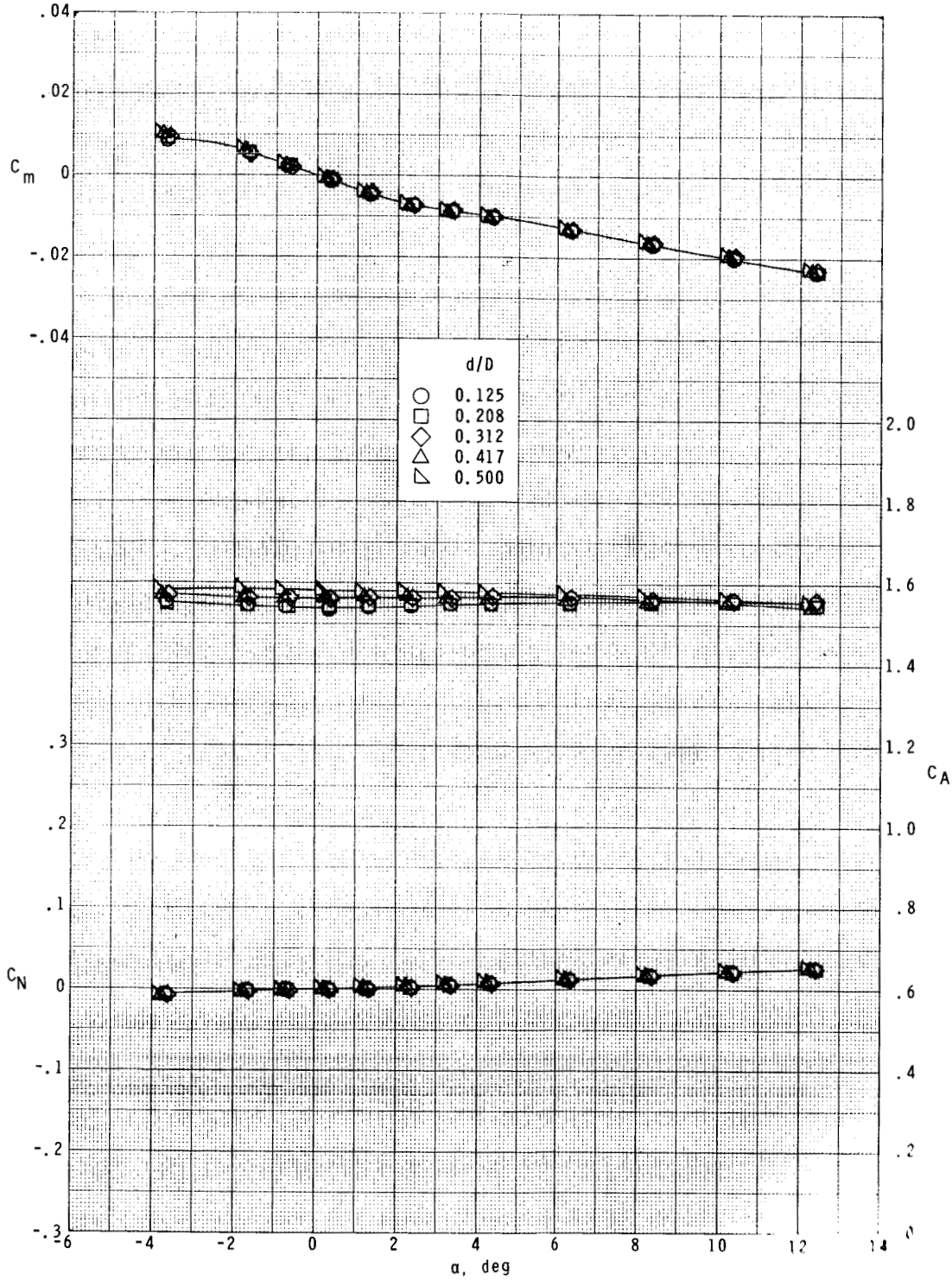

(c) $R = 4.15 \times 10^5$.

Figure 7.- Concluded.

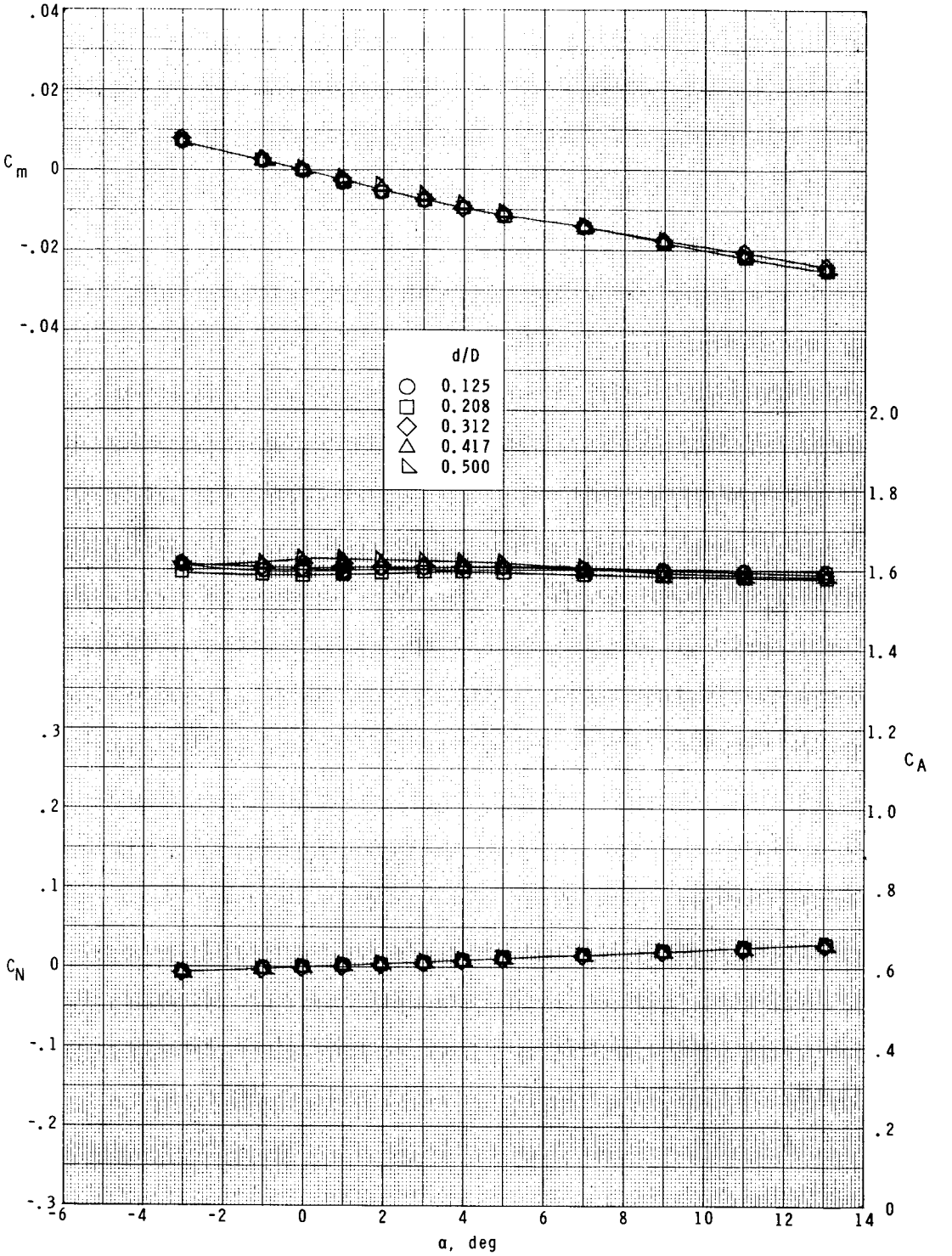

(a) $R = 1.74 \times 10^5$.

Figure 8.- Effect of sting diameter on the longitudinal aerodynamic characteristics of the model for three Reynolds numbers at M = 2.00.

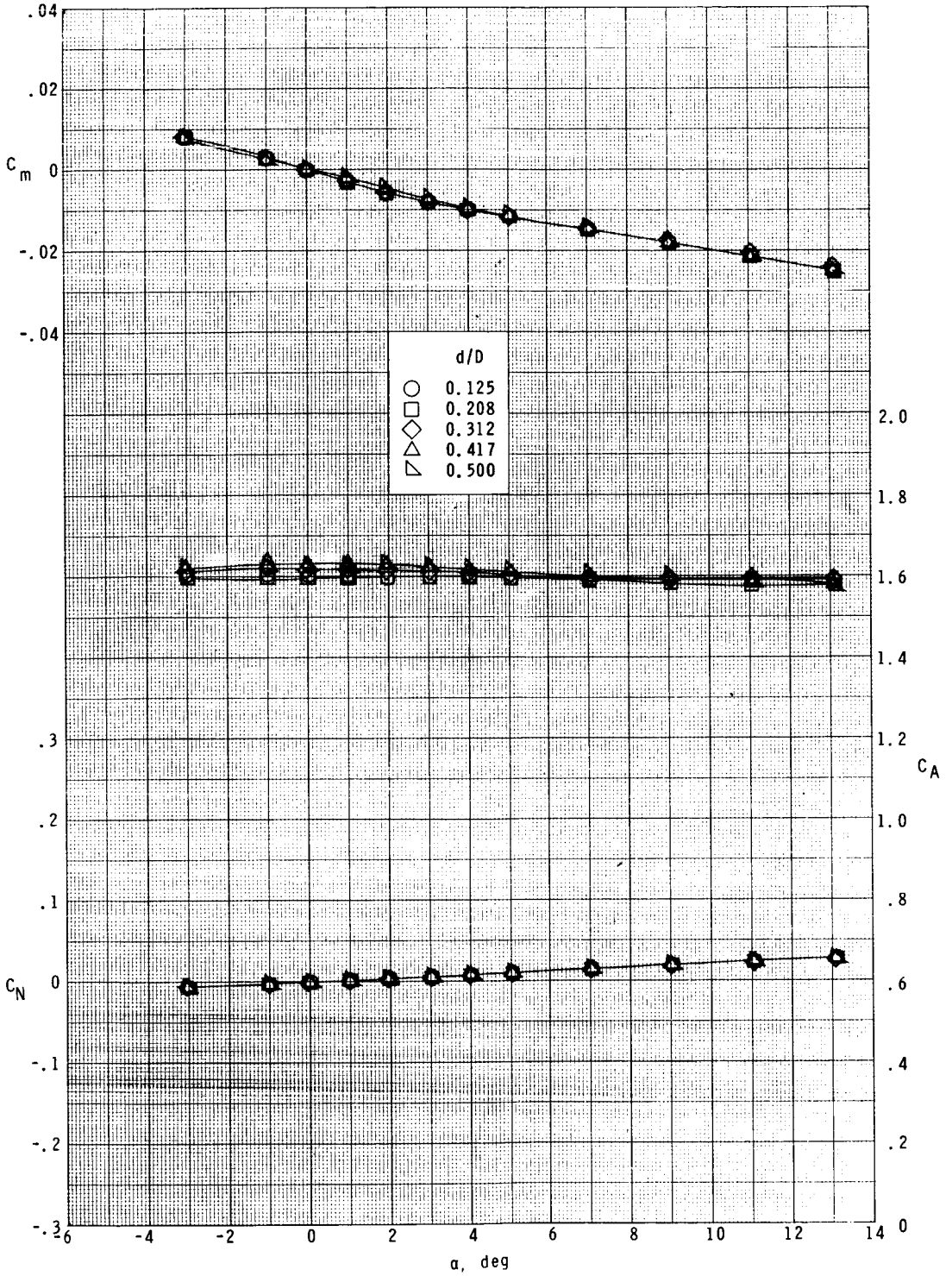

(b) $R = 2.60 \times 10^5$.

Figure 8.- Continued.

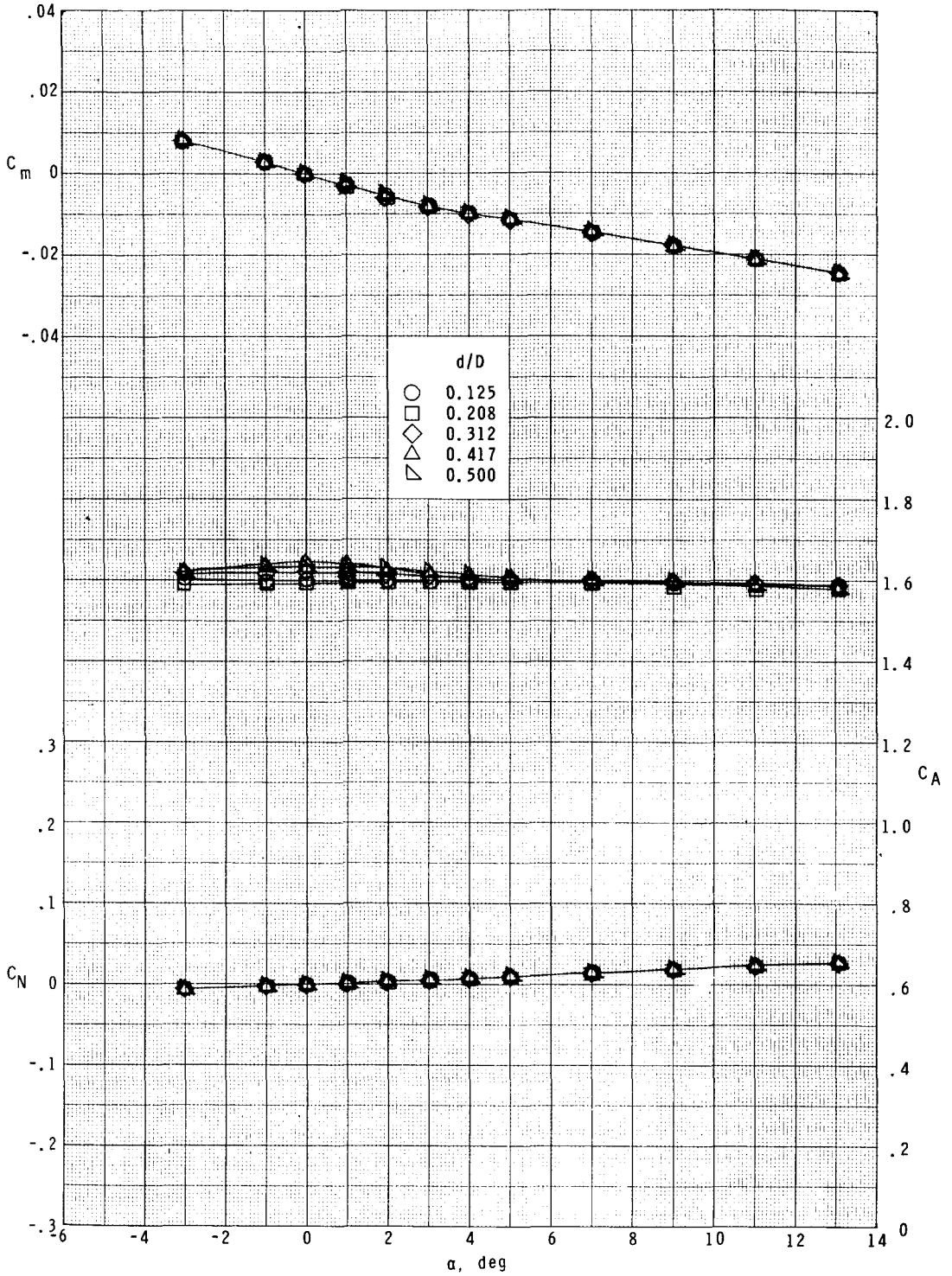

(c) $R = 3.47 \times 10^5$.

Figure 8.- Concluded.

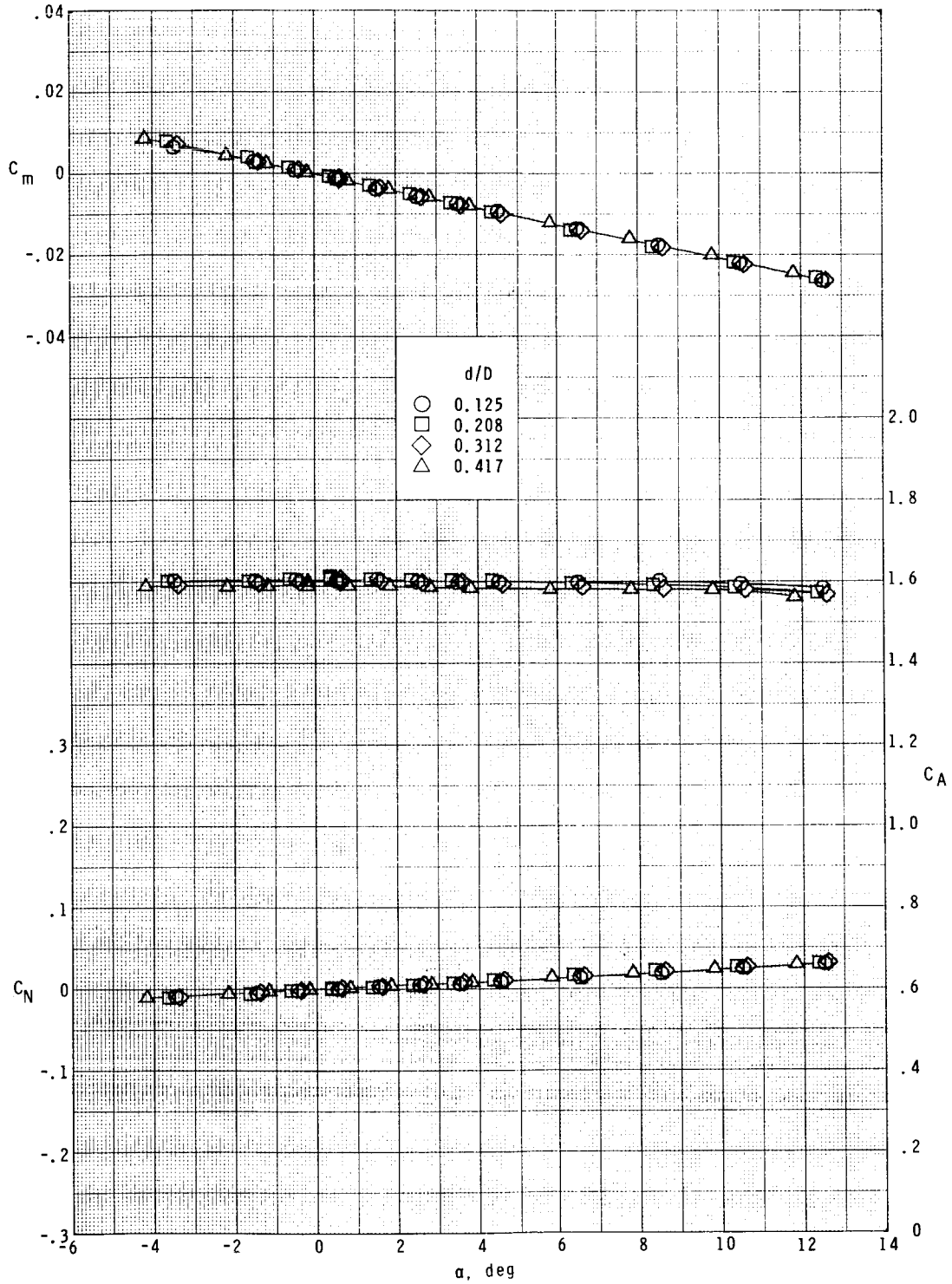

(a) $R = 1.61 \times 10^5$.

Figure 9.- Effect of sting diameter on the longitudinal aerodynamic characteristics of the model for three Reynolds numbers at M = 2.94.

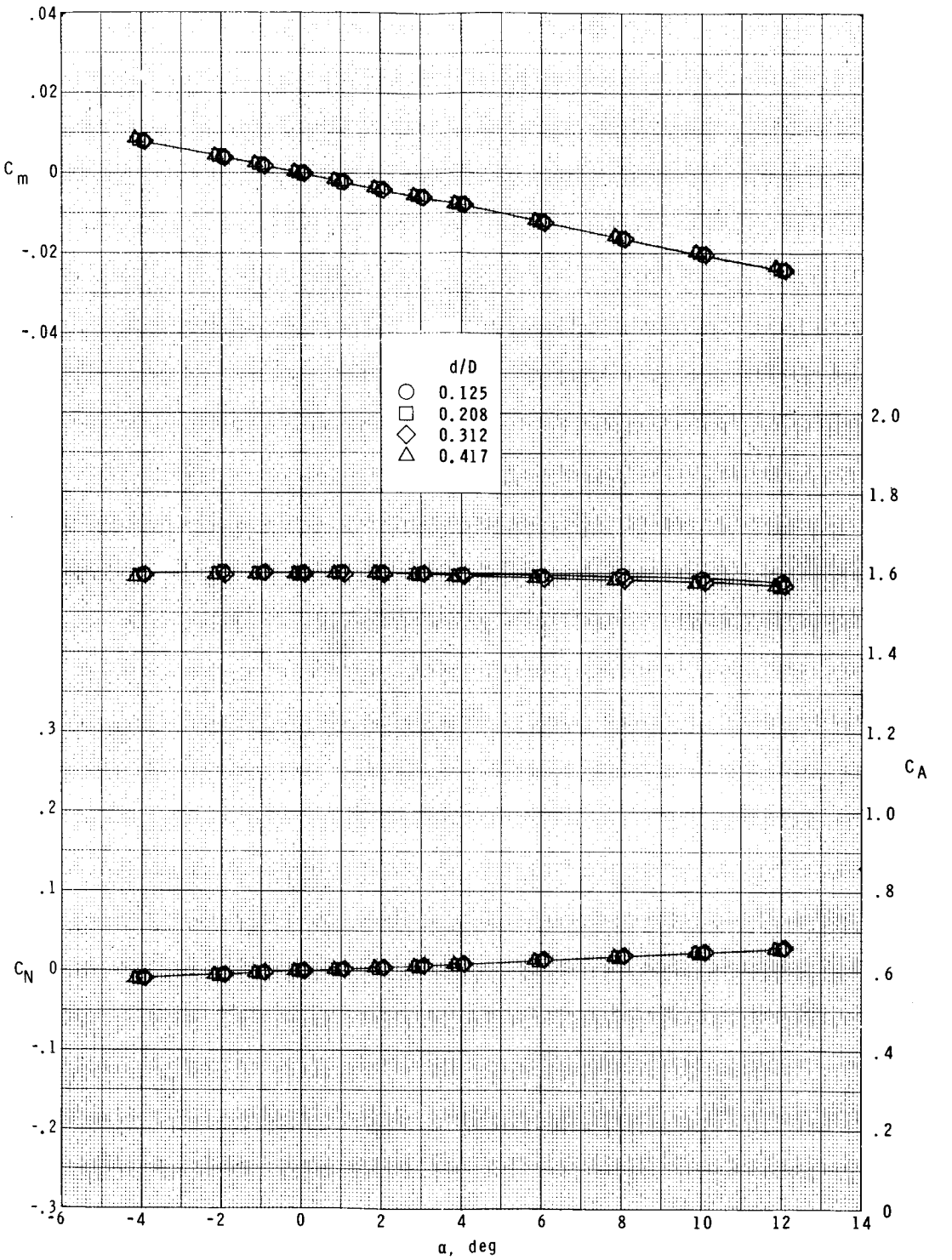

(b) $R = 2.68 \times 10^5$.

Figure 9.- Continued.

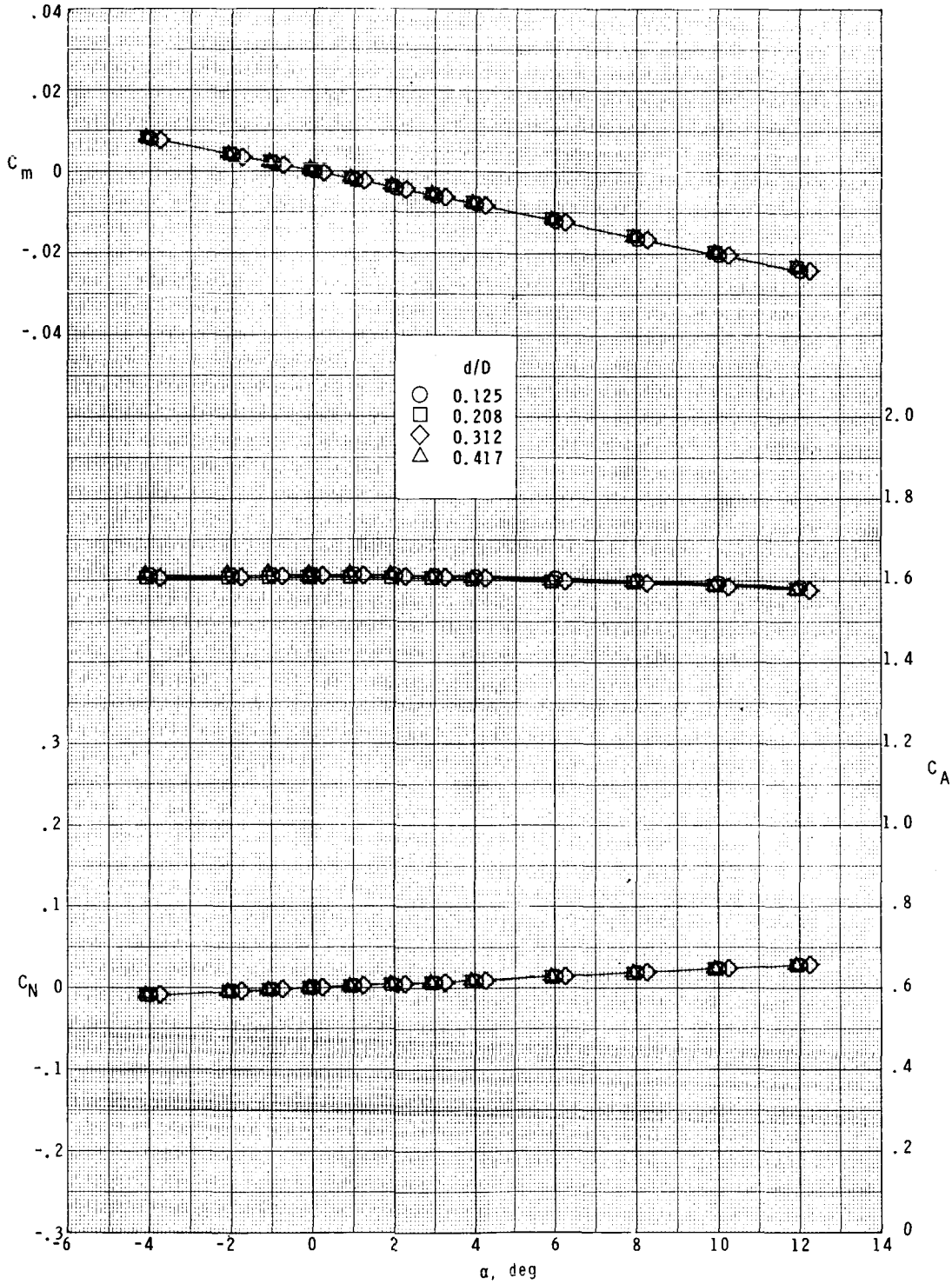

(c) $R = 3.76 \times 10^5$.

Figure 9.- Concluded.

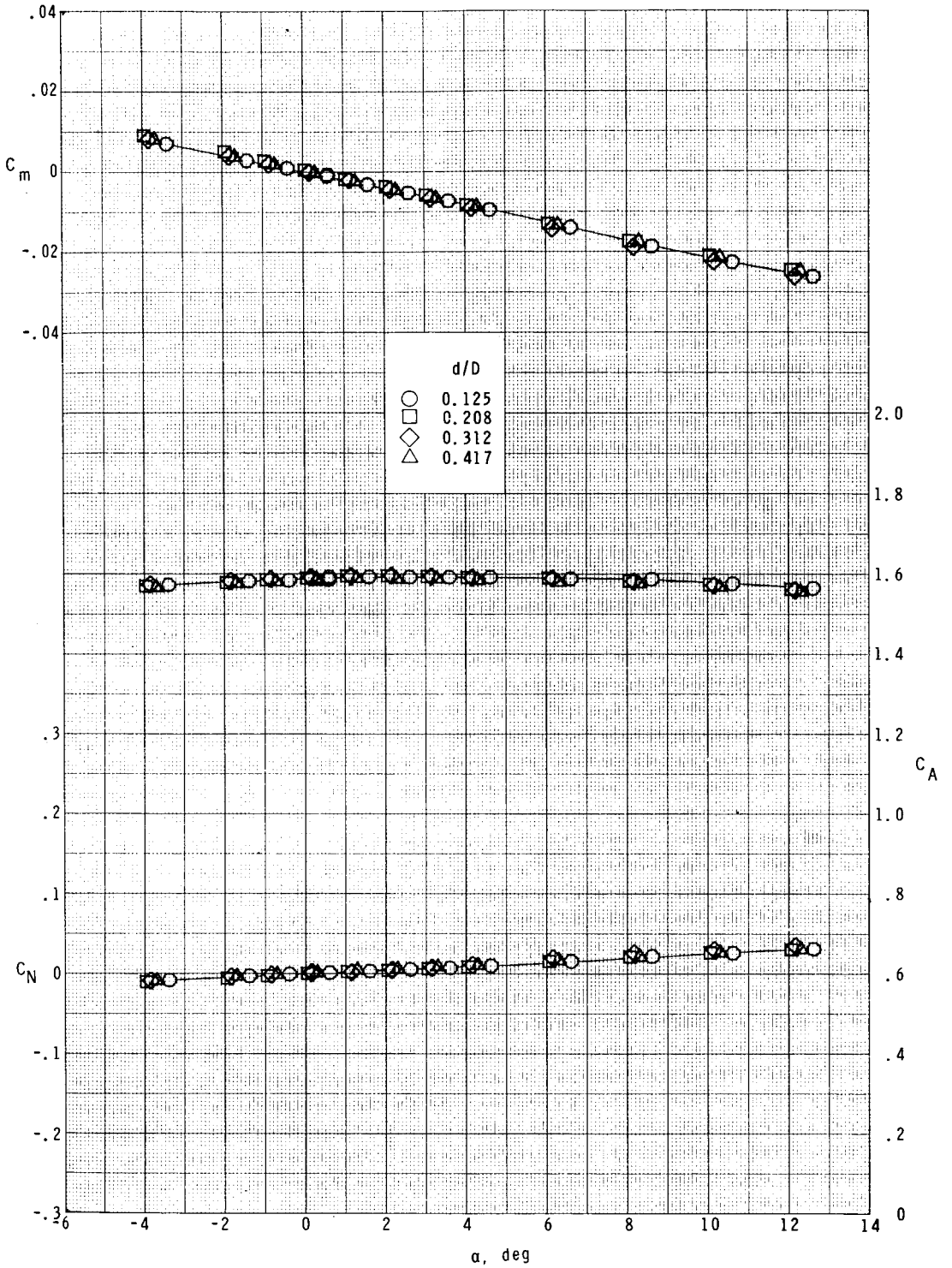

(a) $R = 2.63 \times 10^5$.

Figure 10.- Effect of sting diameter on the longitudinal aerodynamic characteristics of the model for two Reynolds numbers at M = 4.00.

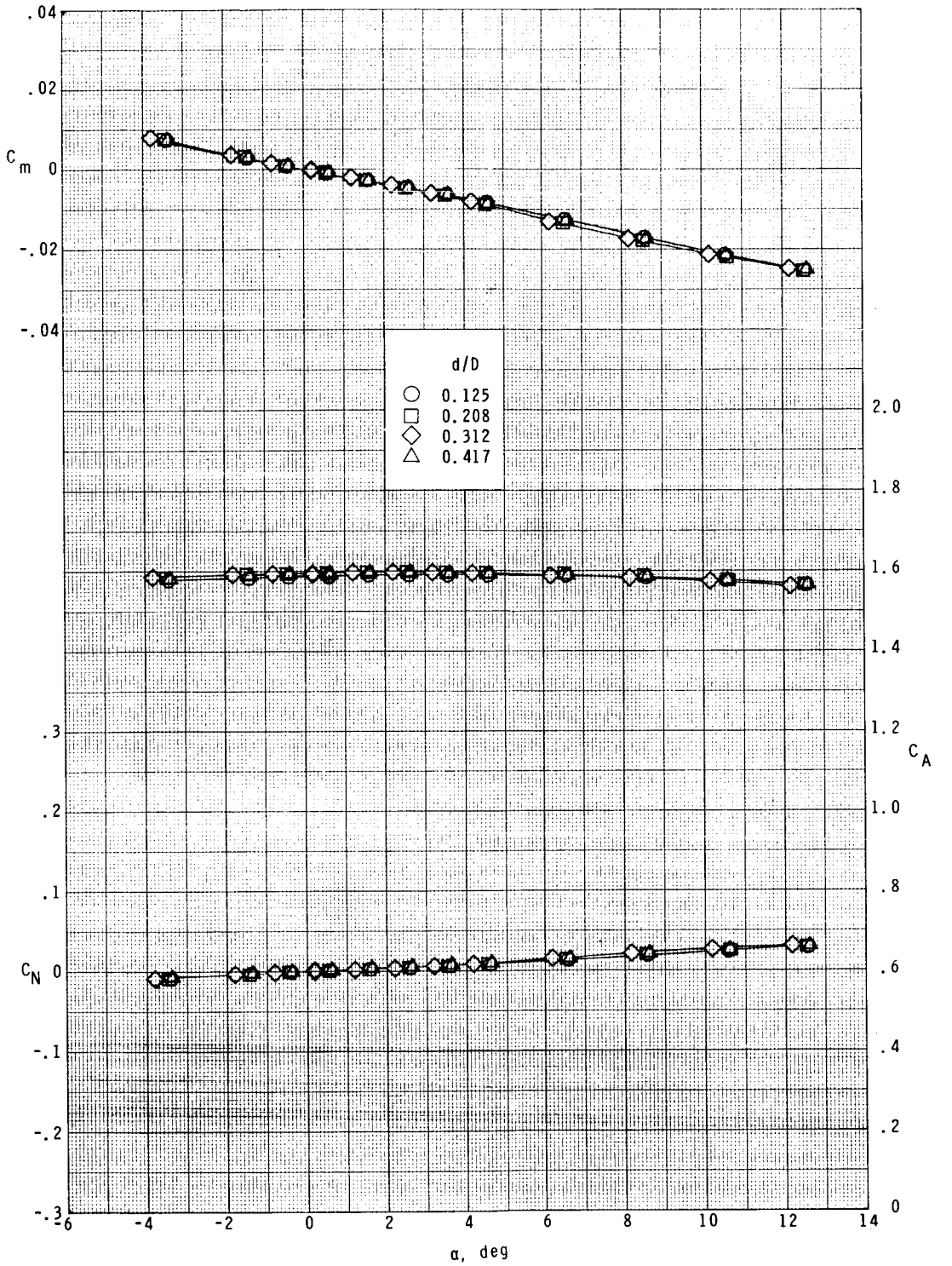

(b) $R = 3.80 \times 10^5$.

Figure 10.- Concluded.

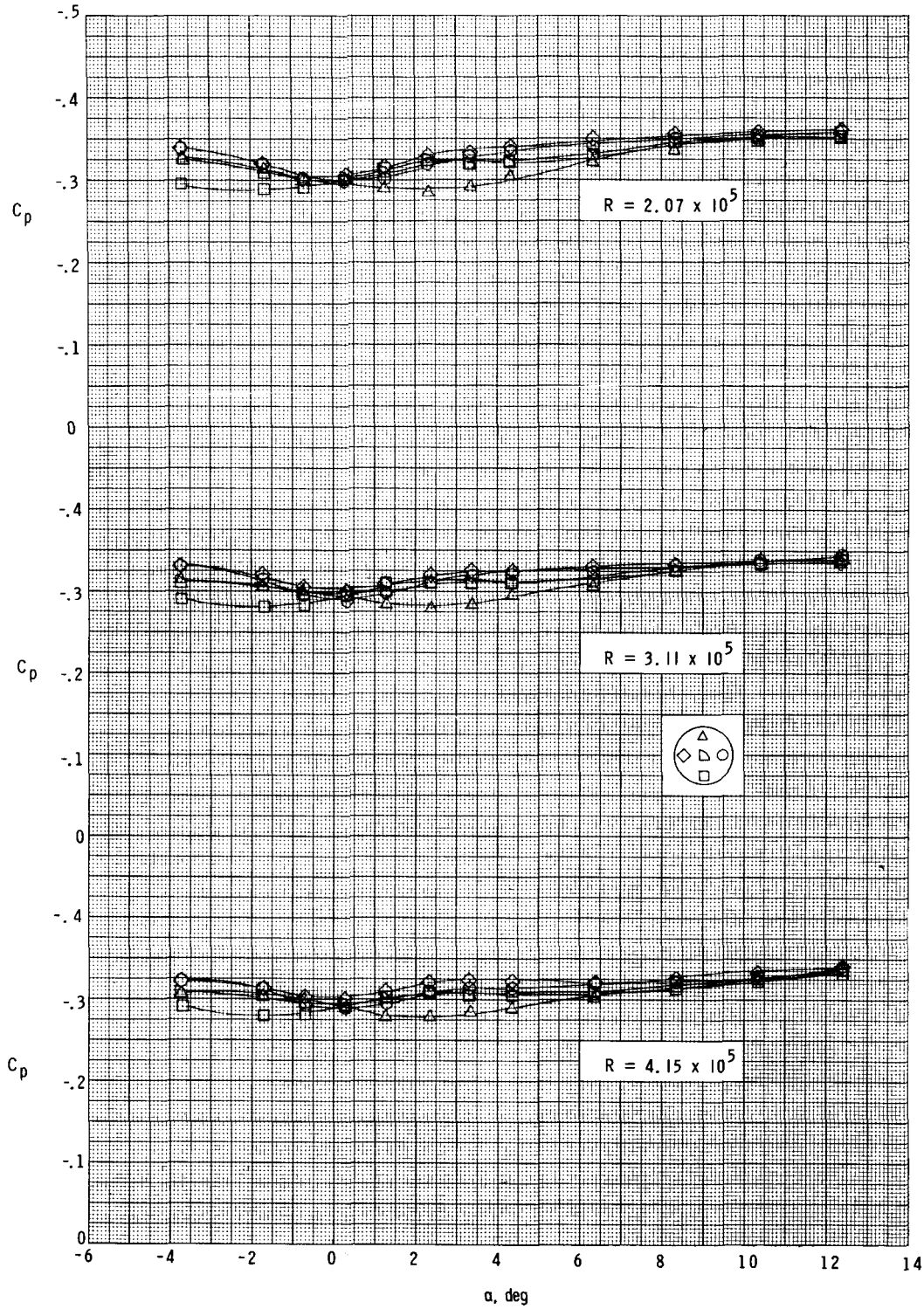

(a) d/D = 0.125.

Figure 11.- Effect of base position on the variation of base-pressure coefficient with angle of attack for various ratios of sting diameter to model diameter at M = 1.50.

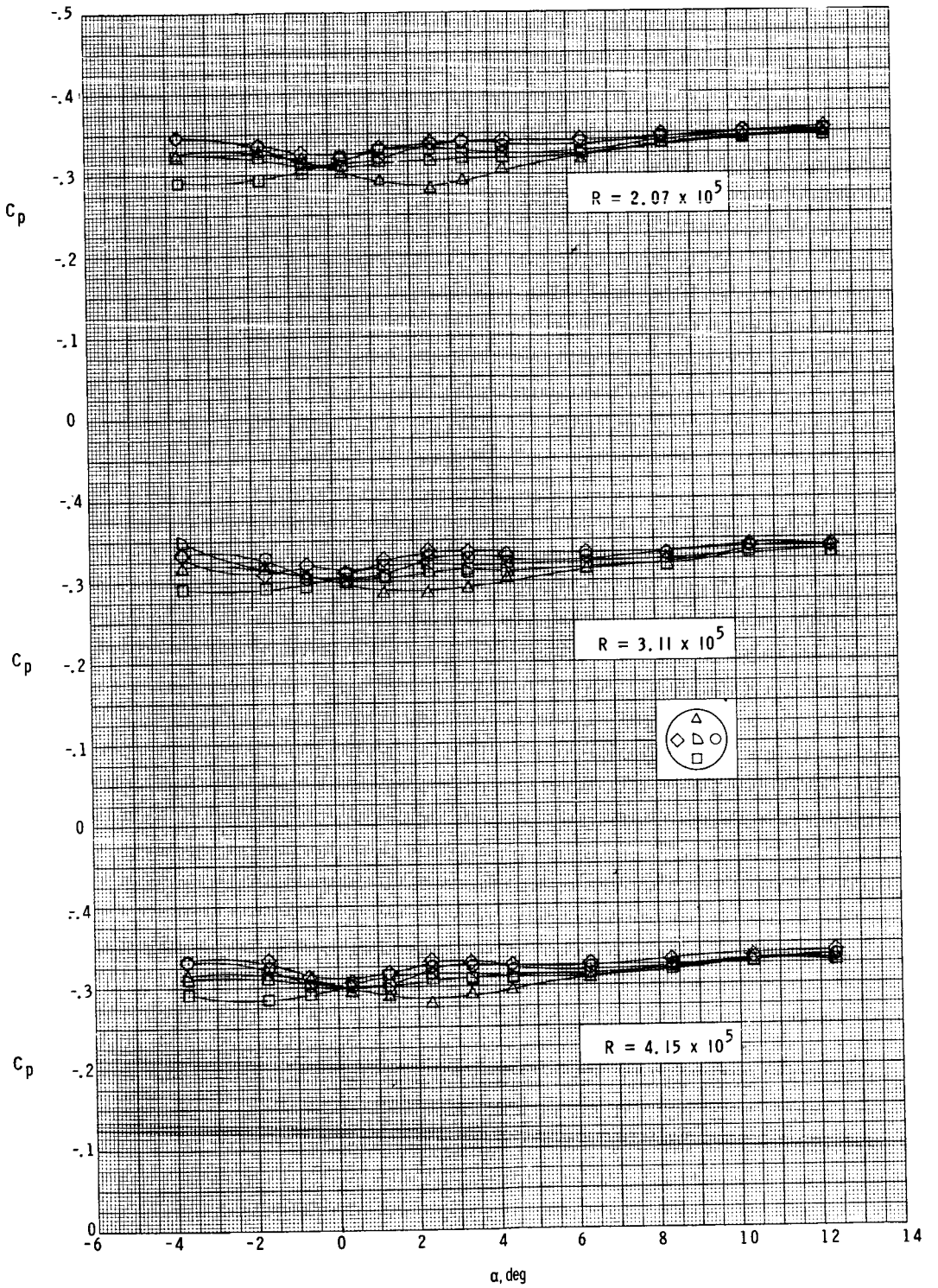

(b) d/D = 0.208.

Figure 11.- Continued.

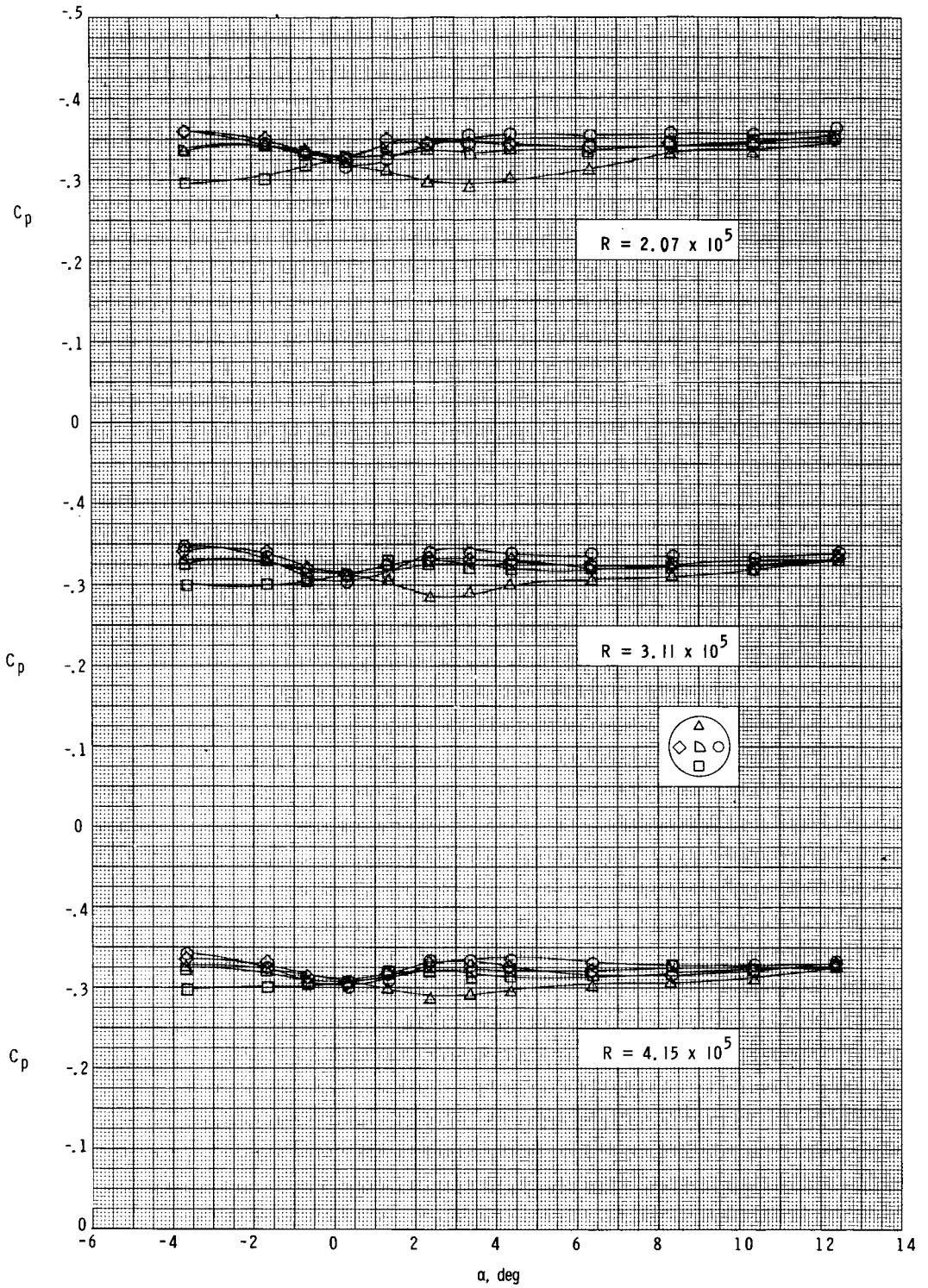

(c) d/D = 0.312.

Figure 11.- Continued.

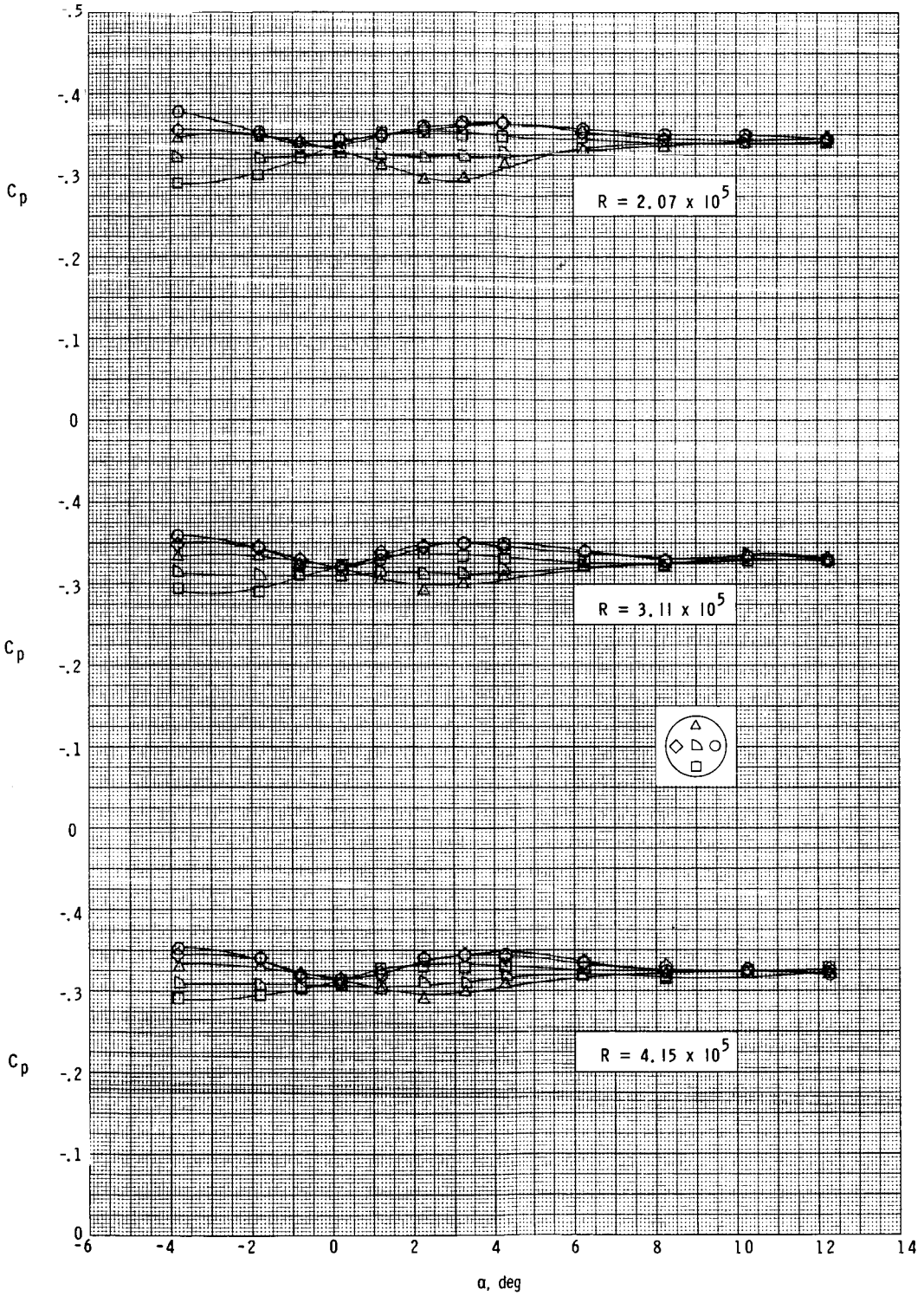

(d) d/D = 0.417.

Figure 11.- Continued.

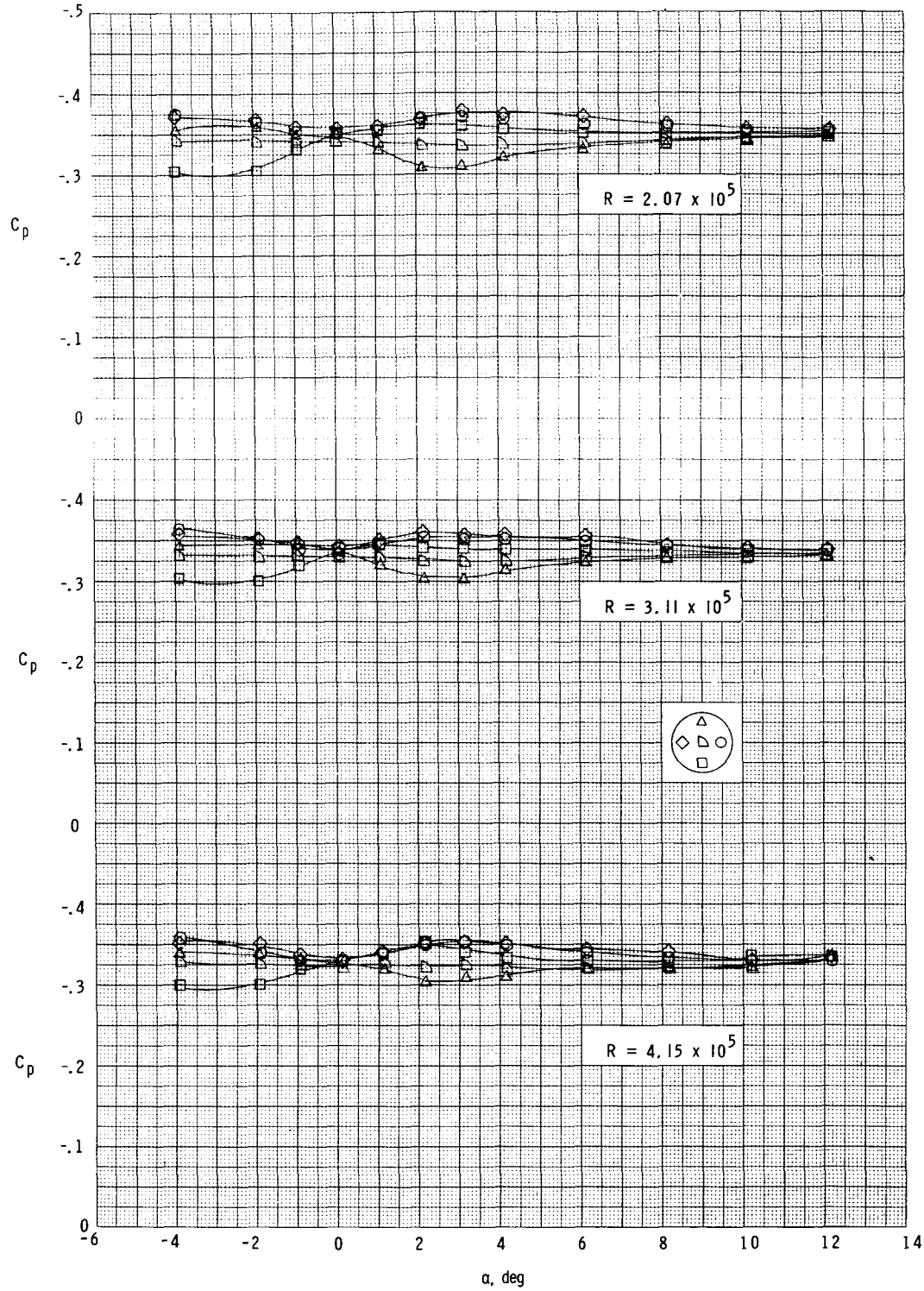

(e) d/D = 0.500.

Figure 11.- Concluded.

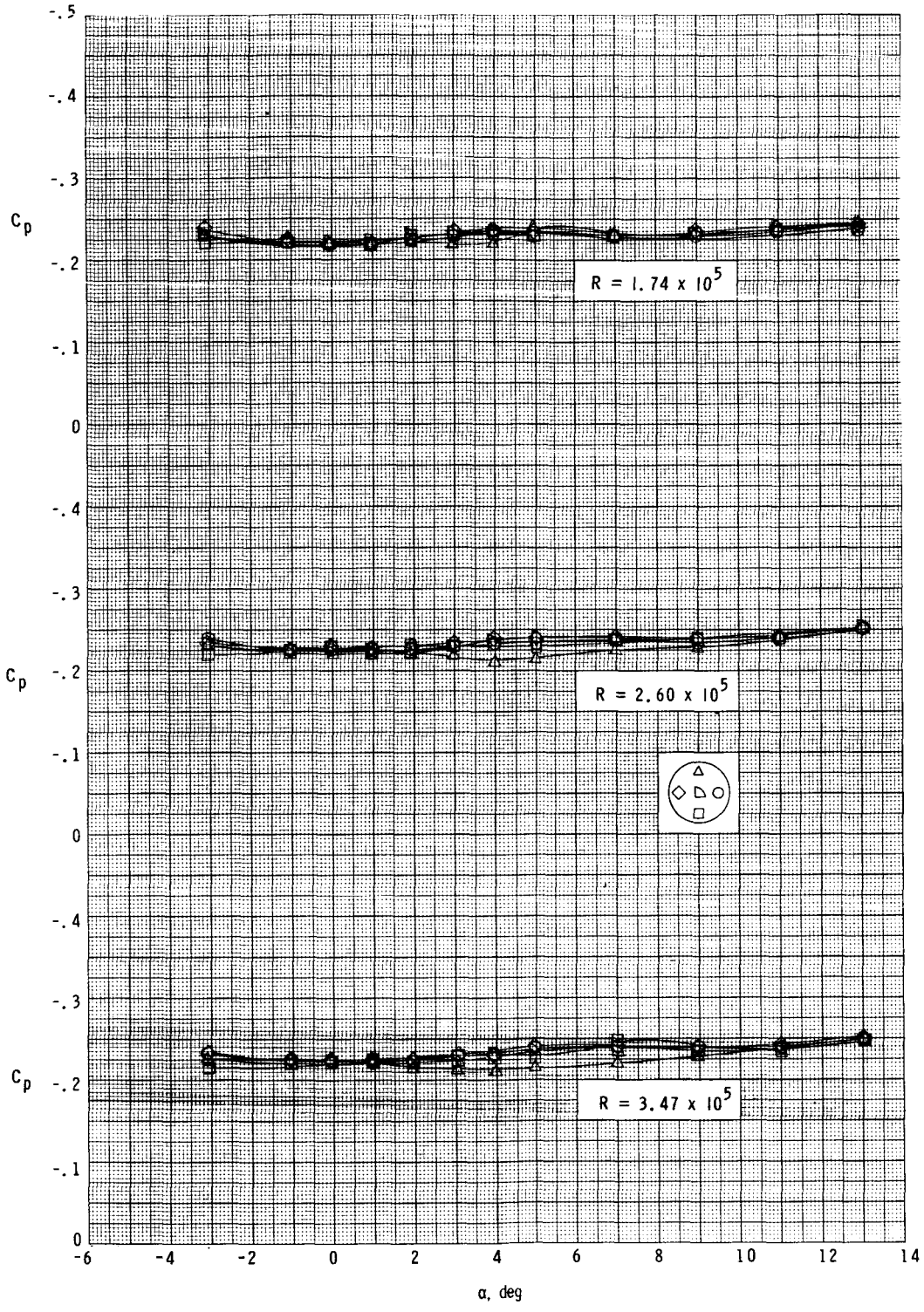

(a) d/D = 0.125.

Figure 12.- Effect of base position on the variation of base-pressure coefficient with angle of attack for various ratios of sting diameter to model diameter at M = 2.00.

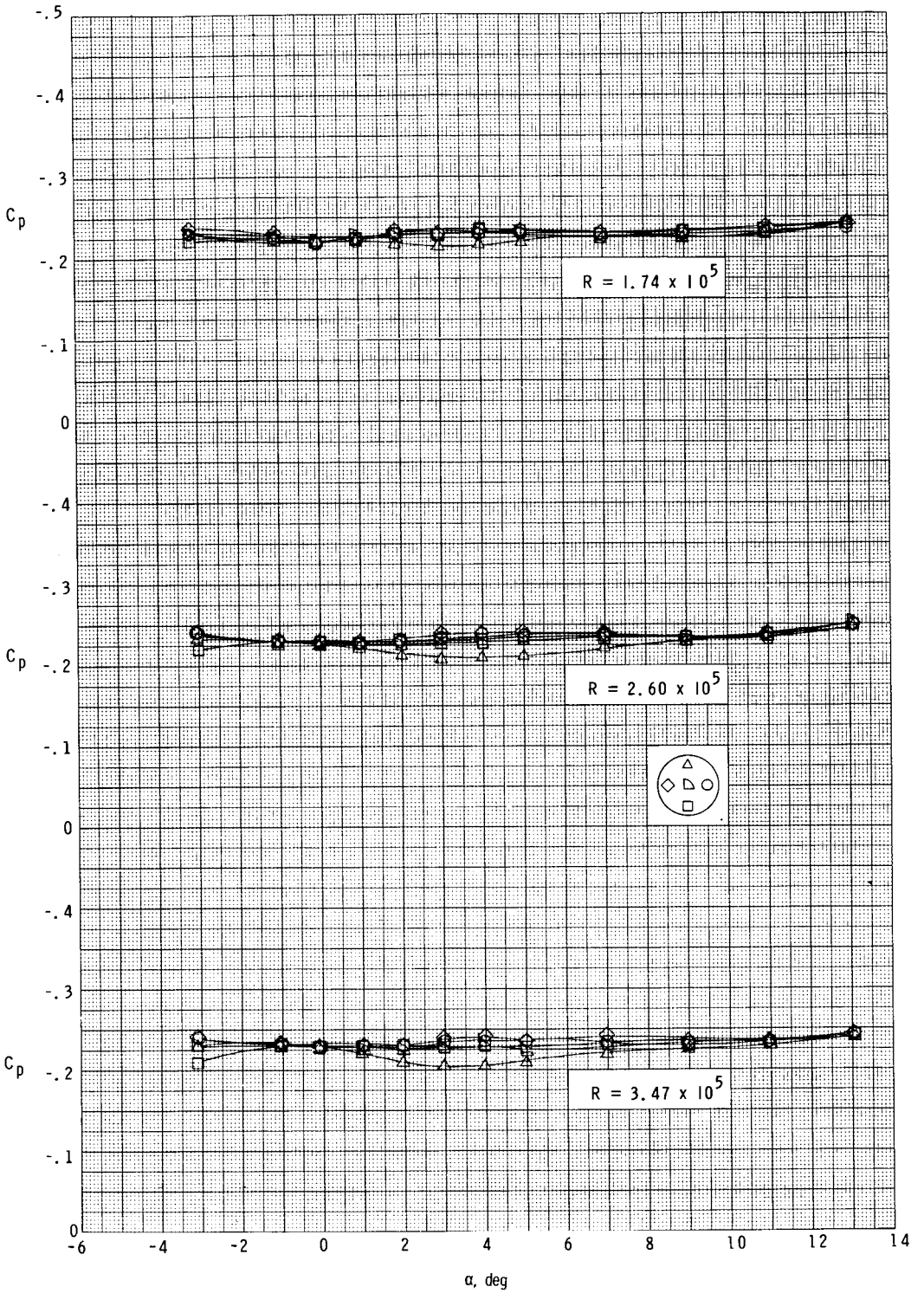

(b) d/D = 0.208.

Figure 12.- Continued.

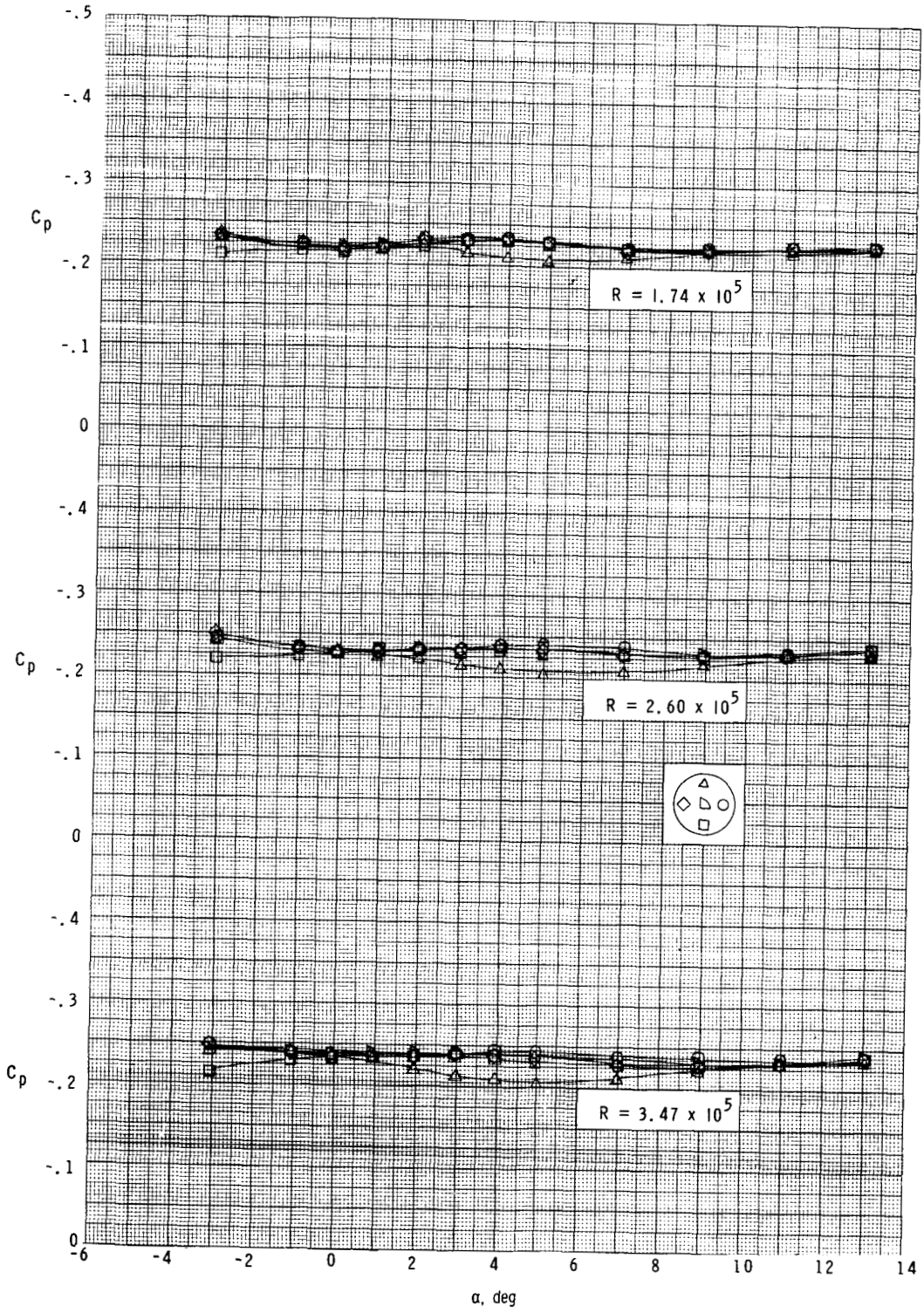

(c) d/D ≐ 0.312.

Figure 12.- Continued.

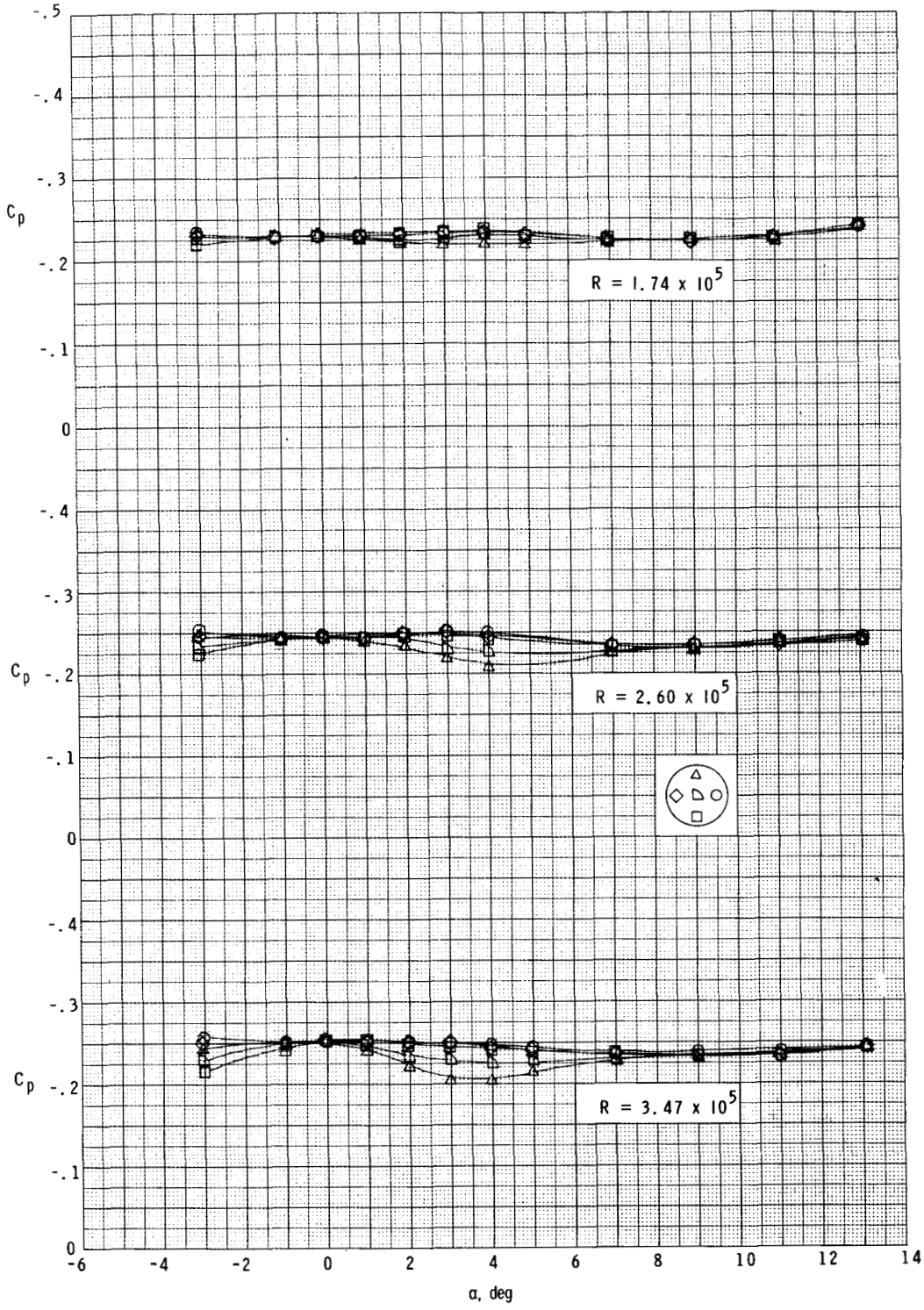

(d) d/D = 0.417.

Figure 12.- Continued.

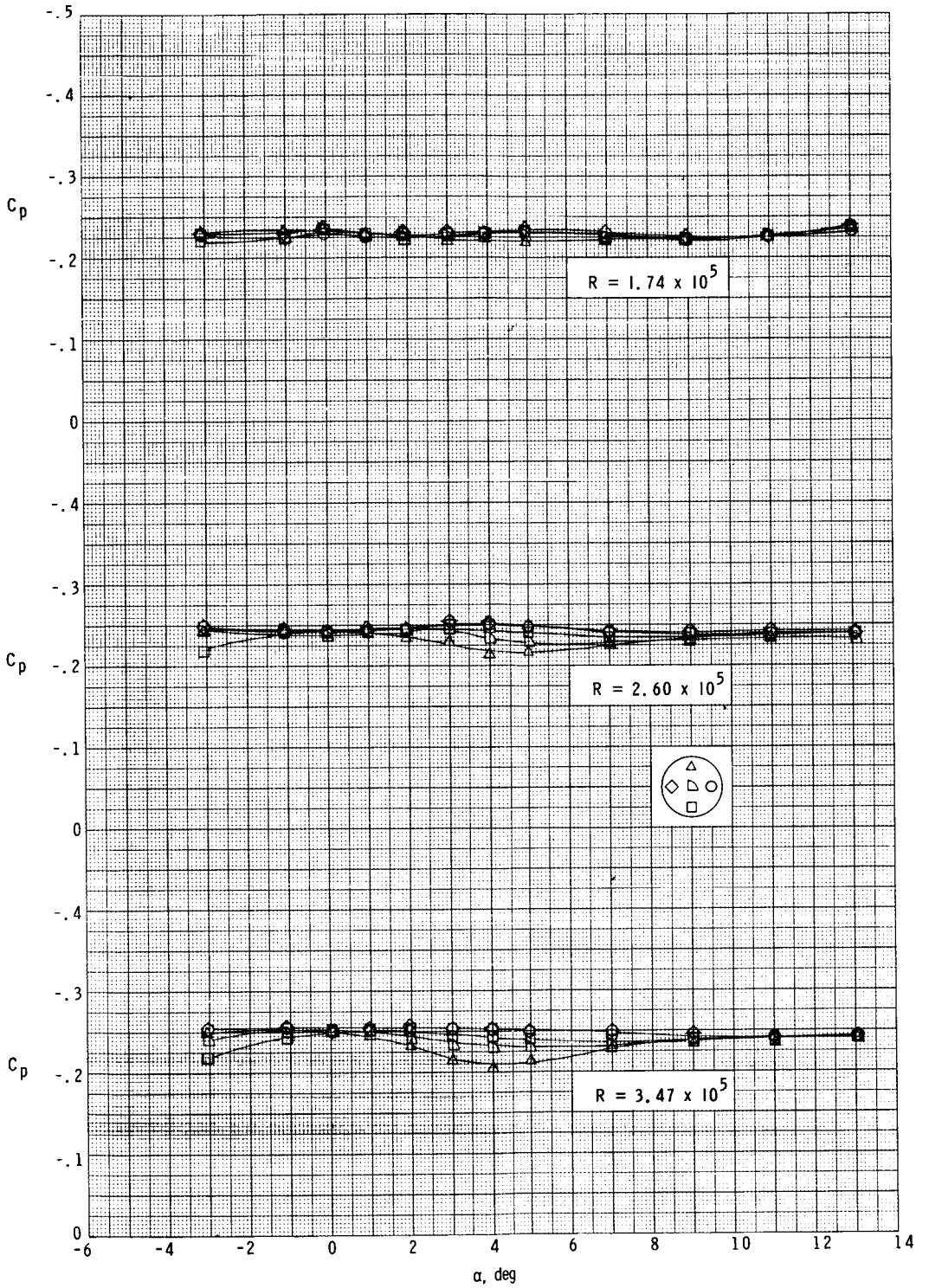

(e) d/D = 0.500.

Figure 12.- Concluded.

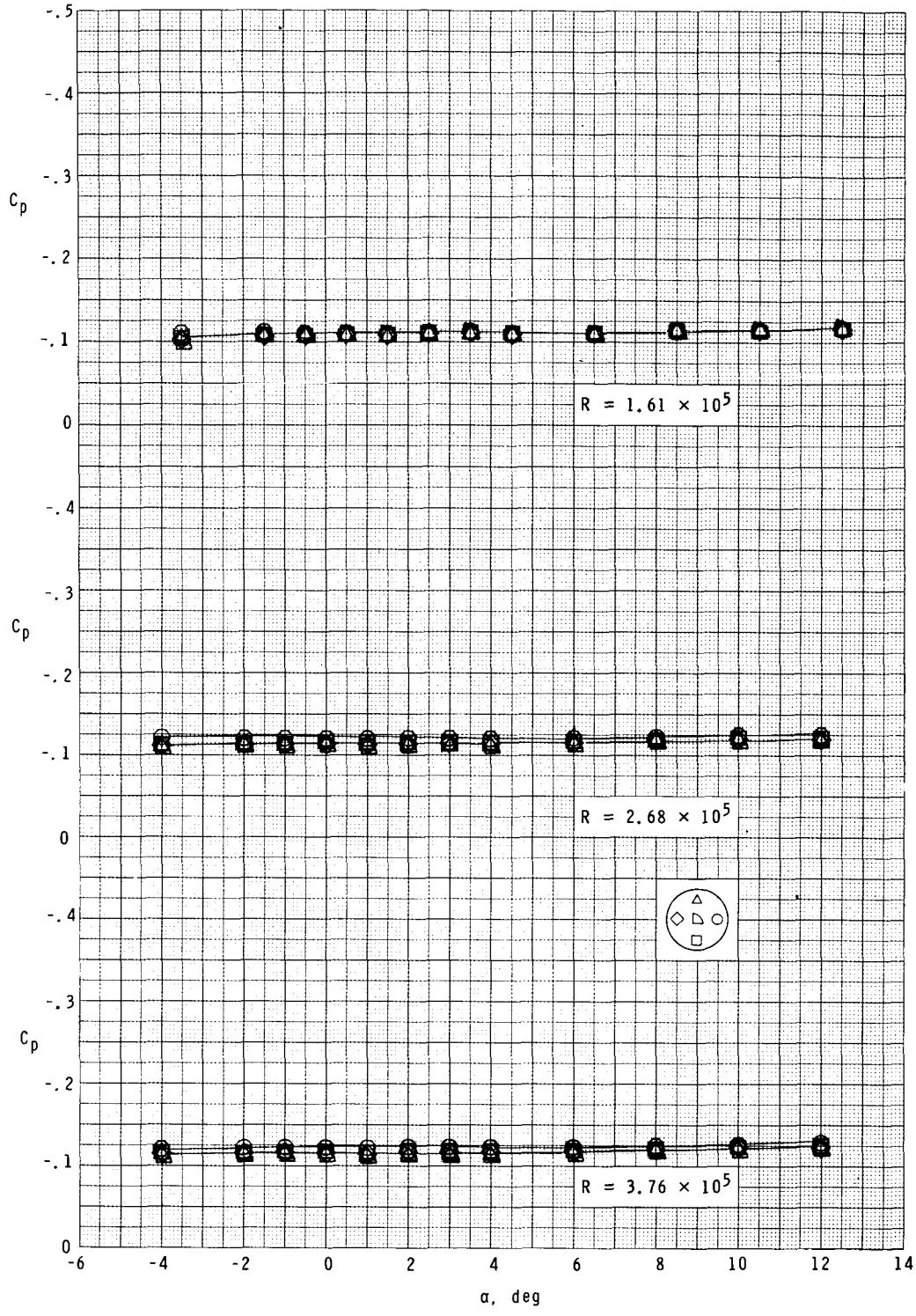

(a) d/D = 0.125.

Figure 13. - Effect of base position on the variation of base-pressure coefficient with angle of attack for various ratios of sting diameter to model diameter at M = 2.94.

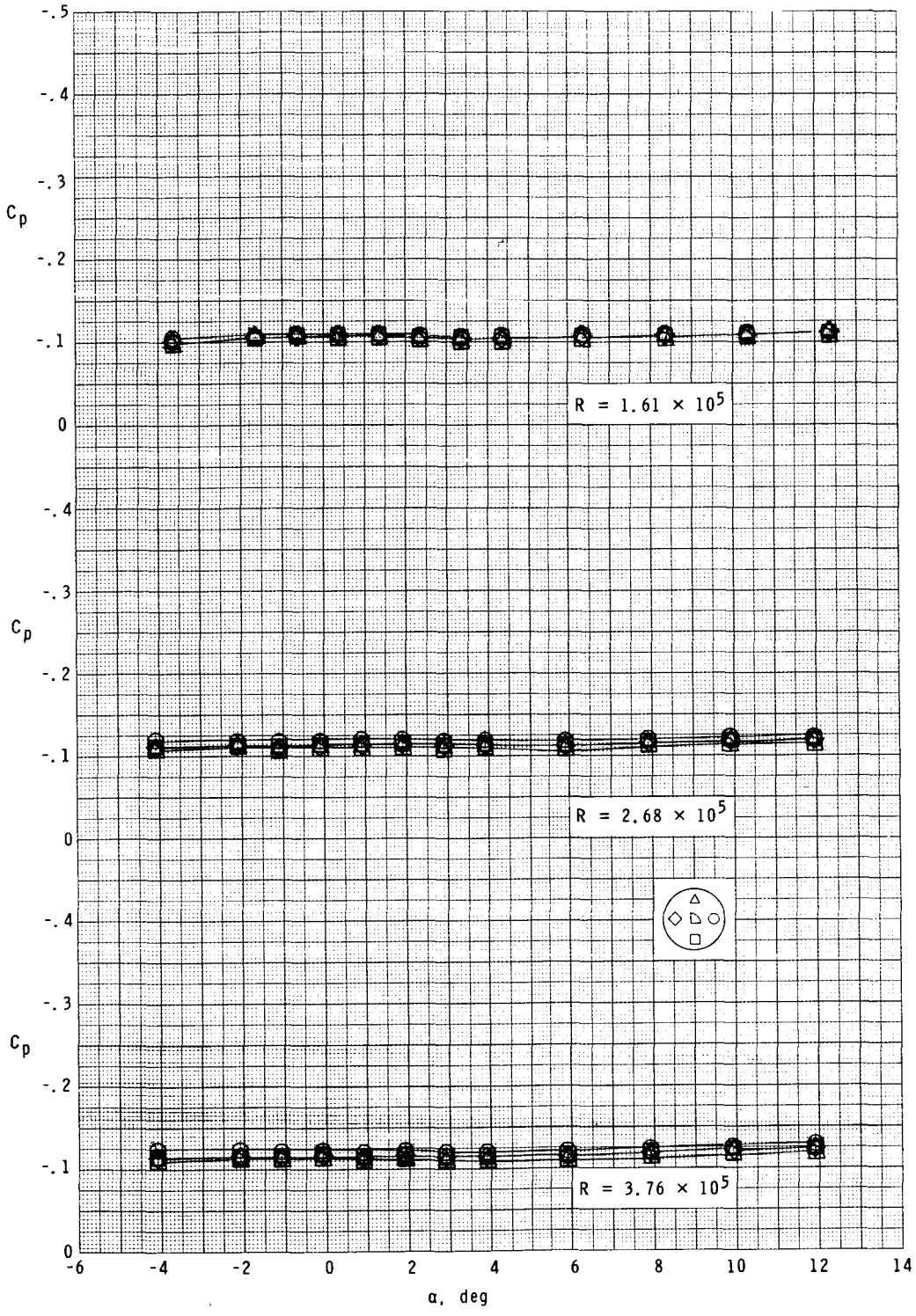

(b) d/D = 0.208.

Figure 13.- Continued.

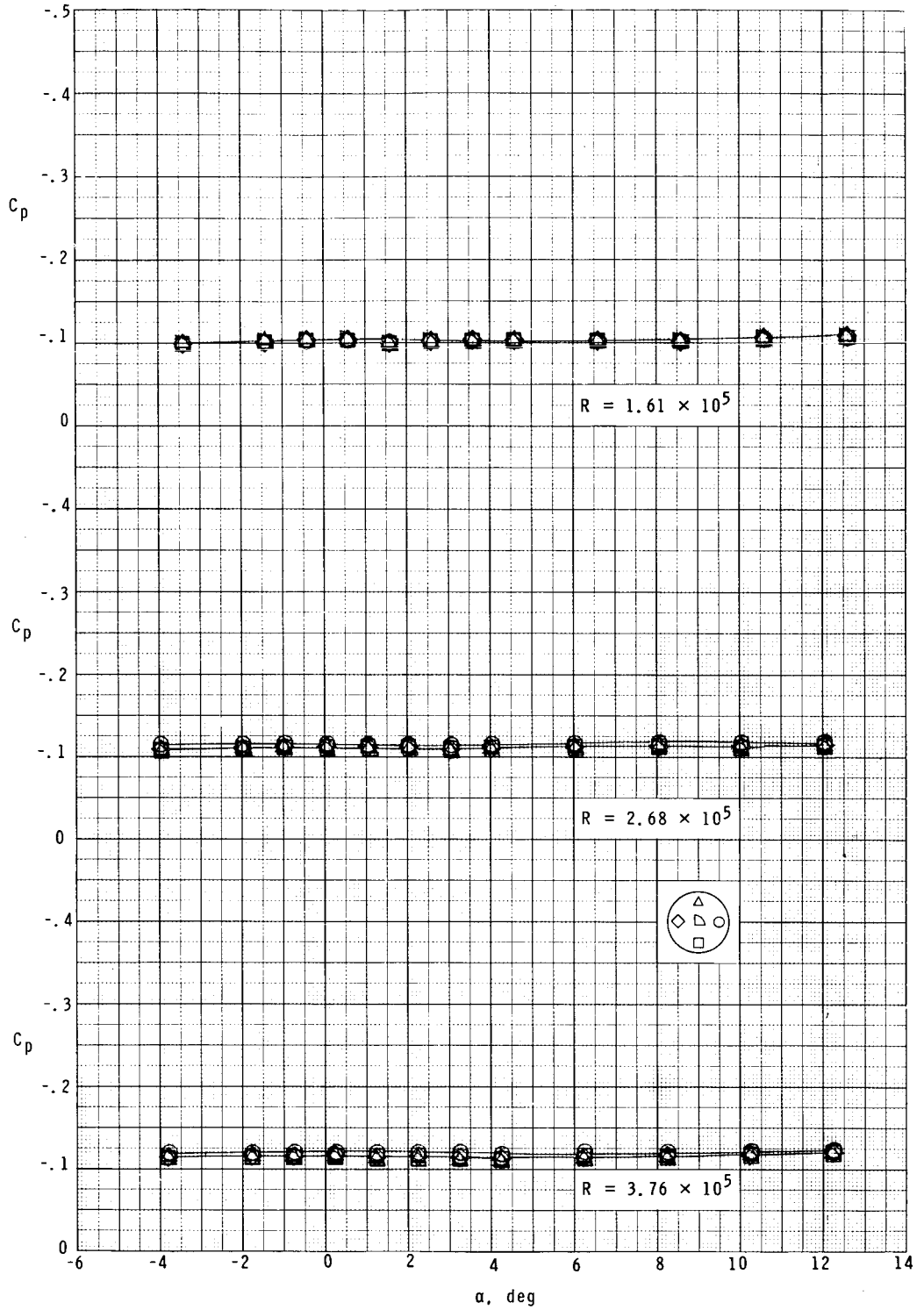

(c) d/D = 0.312.

Figure 13.- Continued.

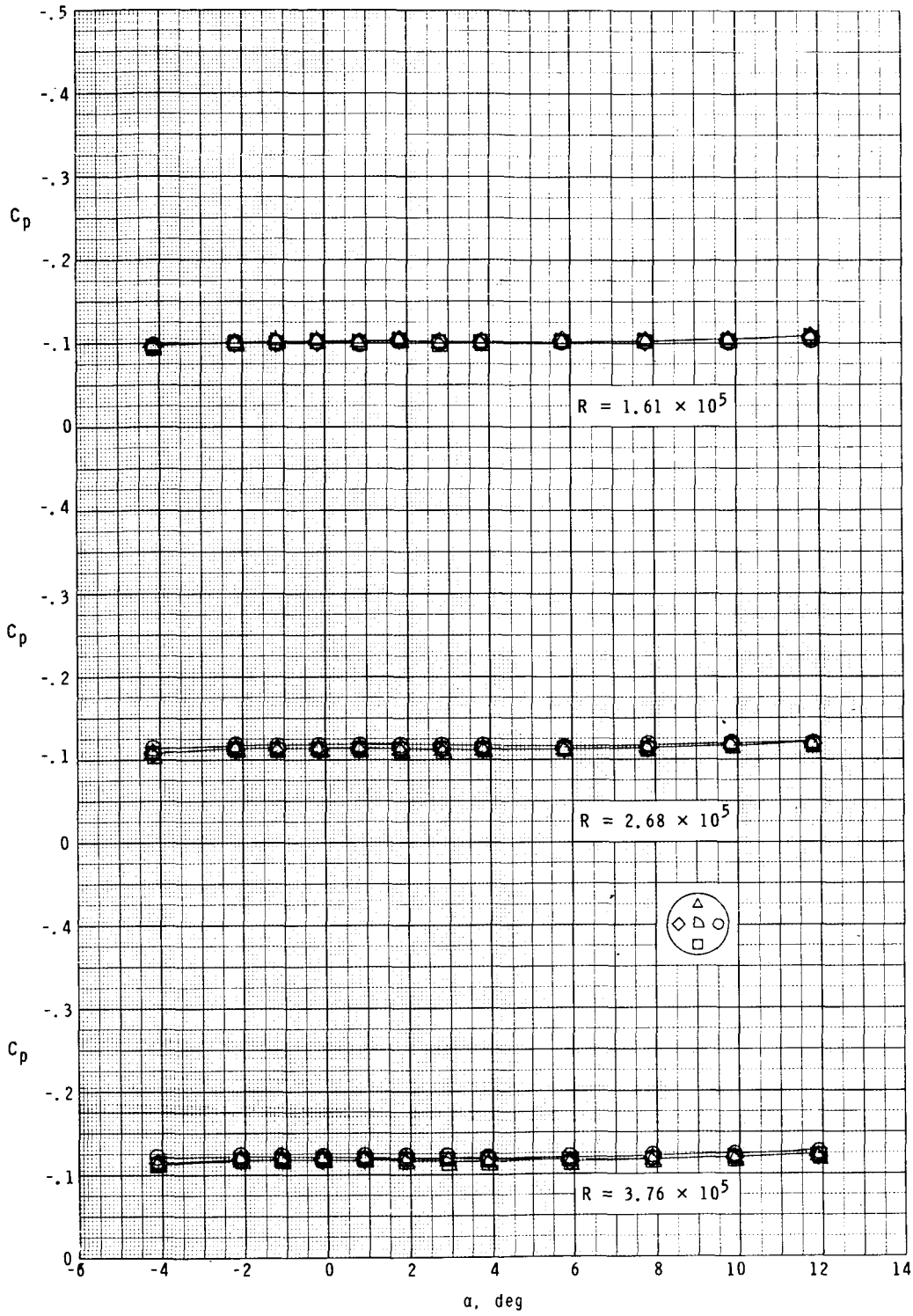

(d) d/D = 0.417.

Figure 13.- Concluded.

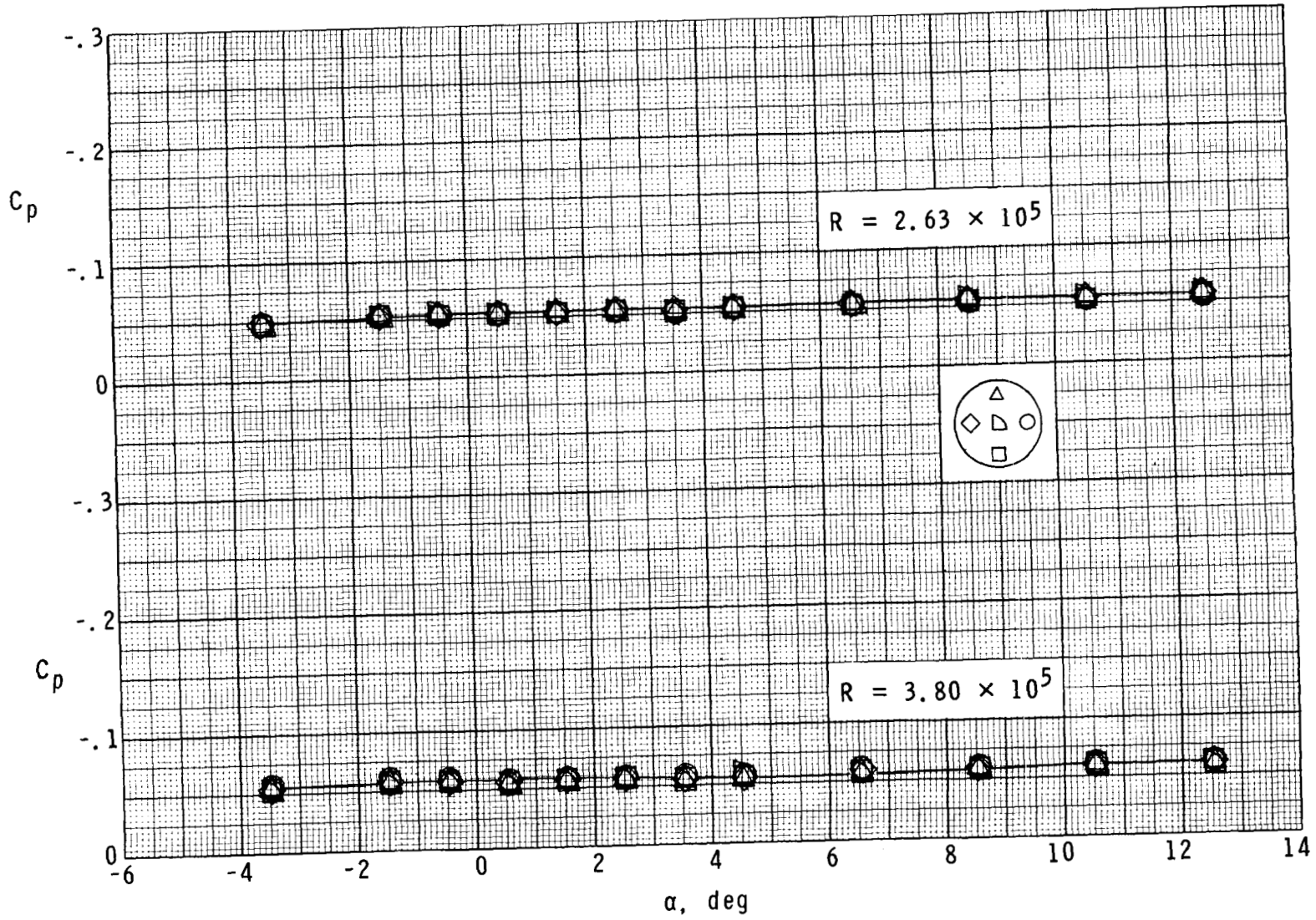

(a) d/D = 0.125.

Figure 14.- Effect of base position on the variation of base-pressure coefficient with angle of attack for various ratios of sting diameter to model diameter at M = 4.00.

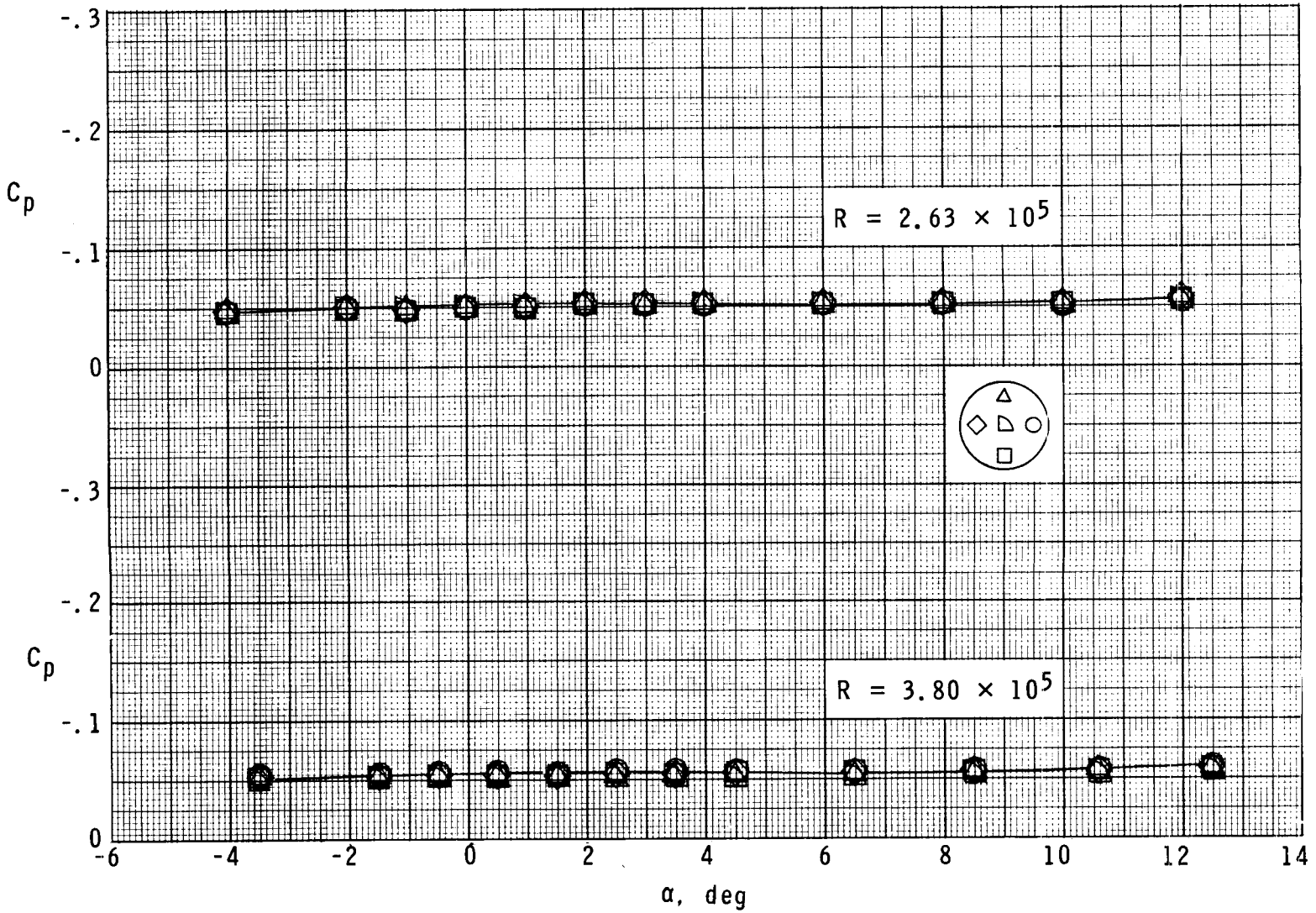

(b) d/D = 0.208.

Figure 14.- Continued.

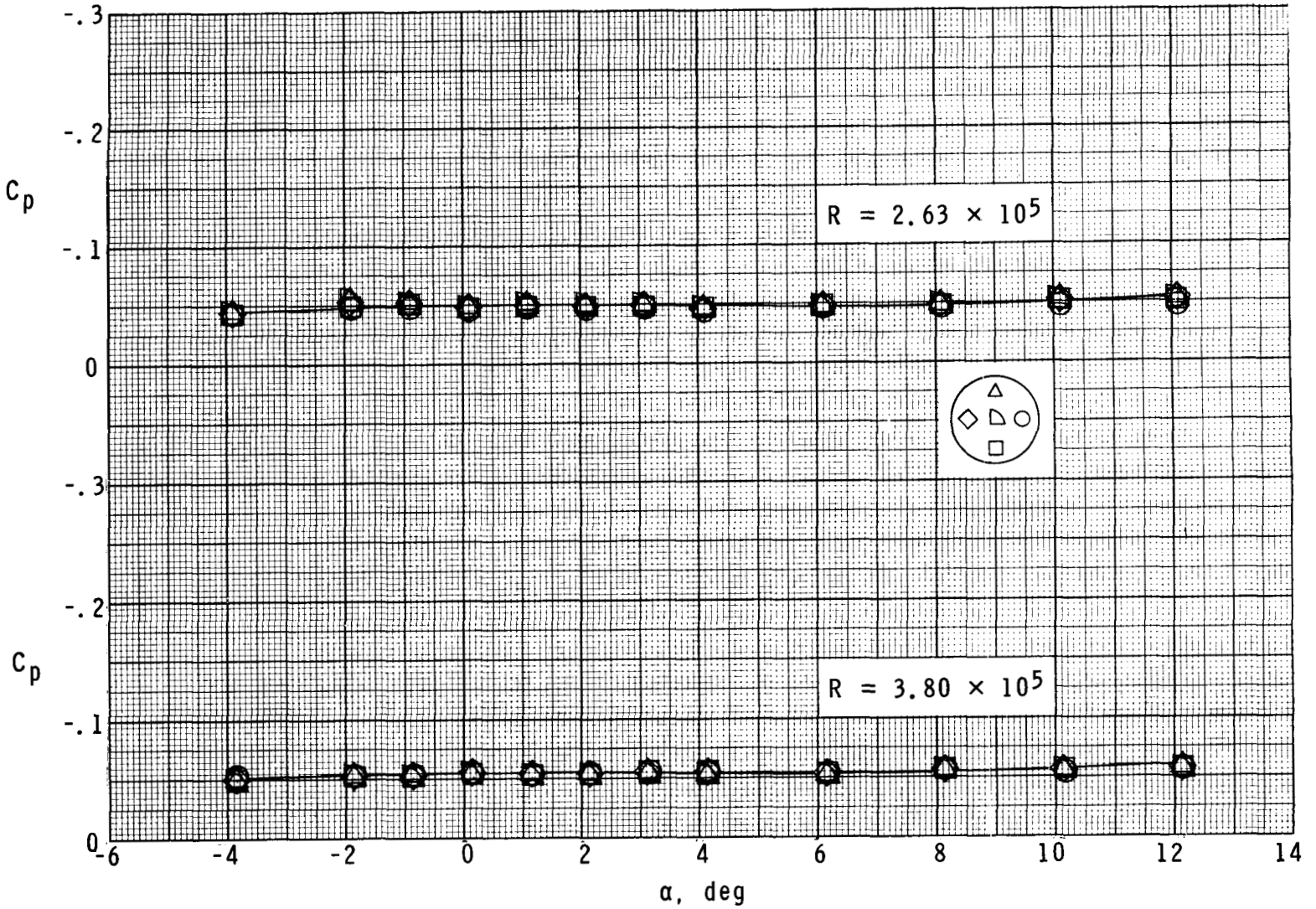

(c) d/D = 0.312.

Figure 14.- Continued.

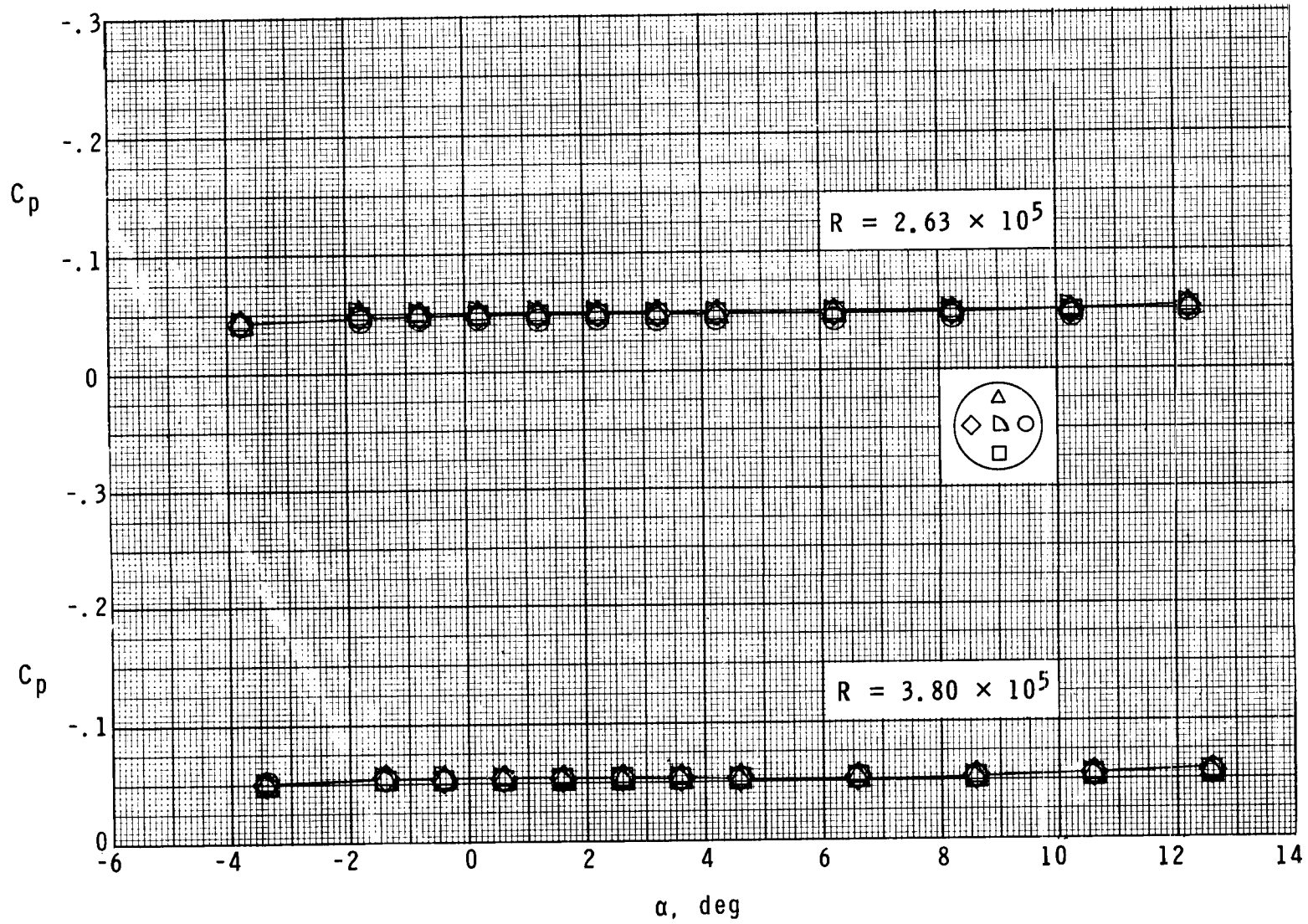

(d) d/D = 0.417.

Figure 14.- Concluded.

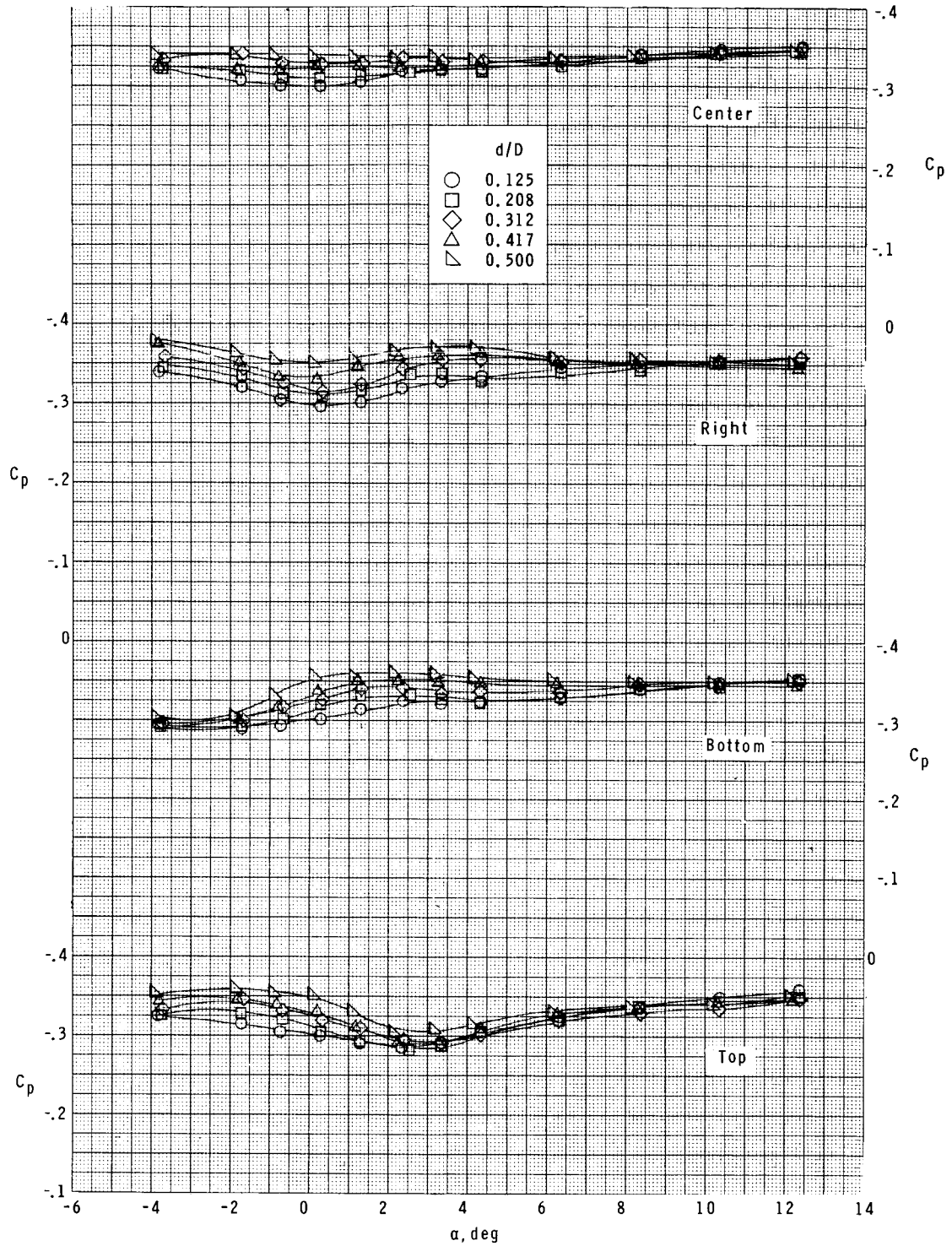

(a) $R = 2.07 \times 10^5$.

Figure 15.- Effect of sting diameter on the variation of base-pressure coefficient with angle of attack for three Reynolds numbers at M = 1.50.

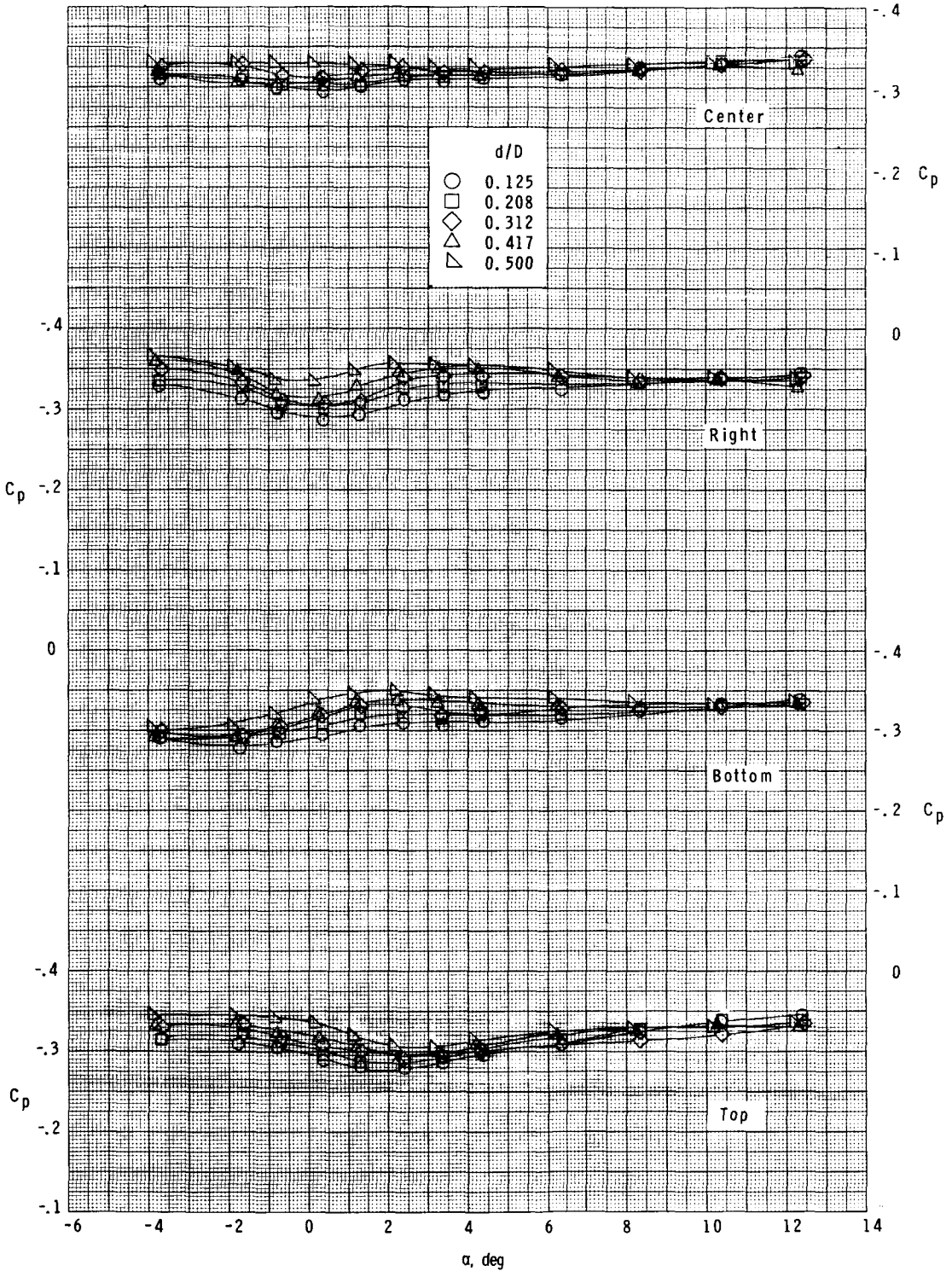

(b) $R = 3.11 \times 10^5$.

Figure 15.- Continued.

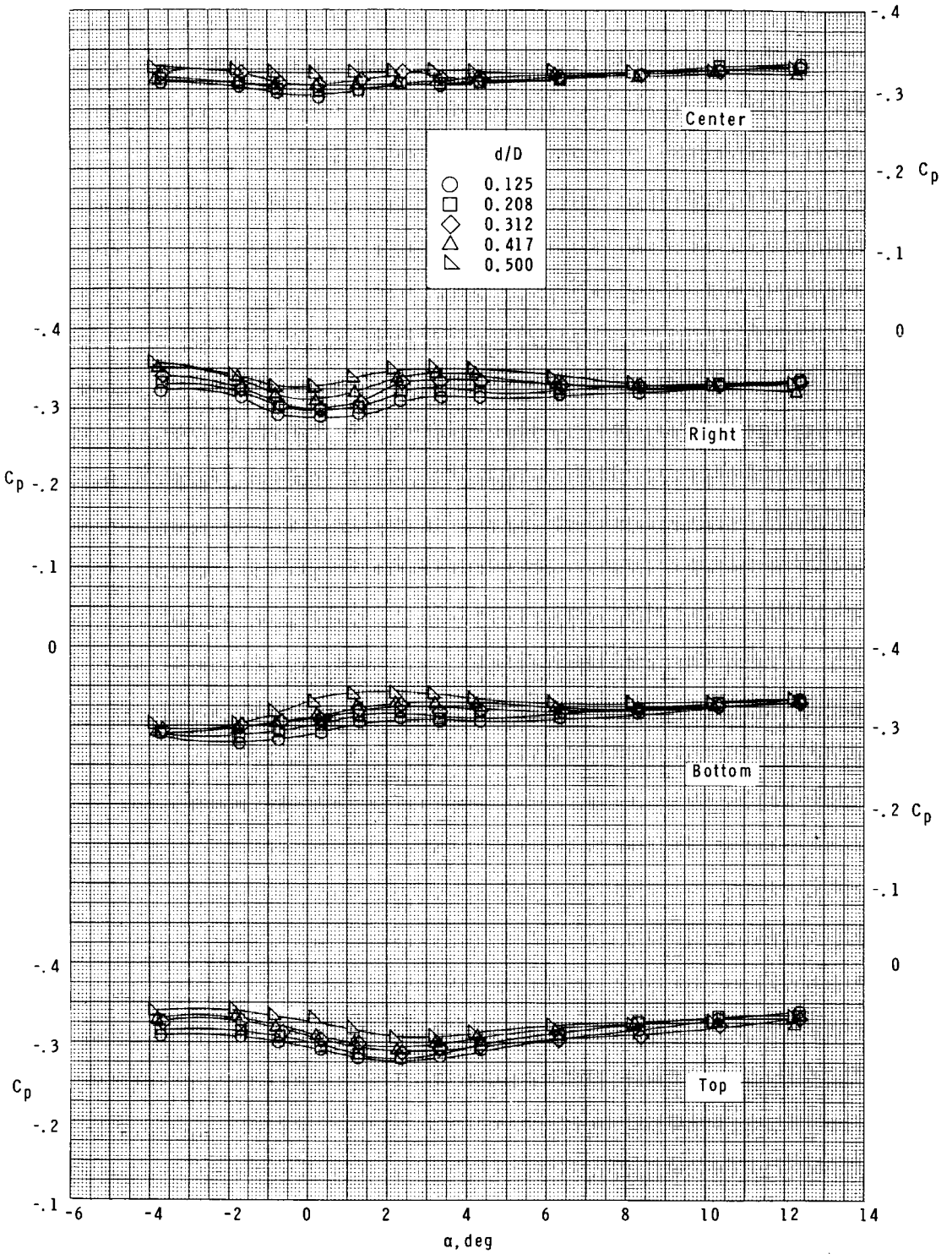

(c) $R = 4.15 \times 10^5$.

Figure 15.- Concluded.

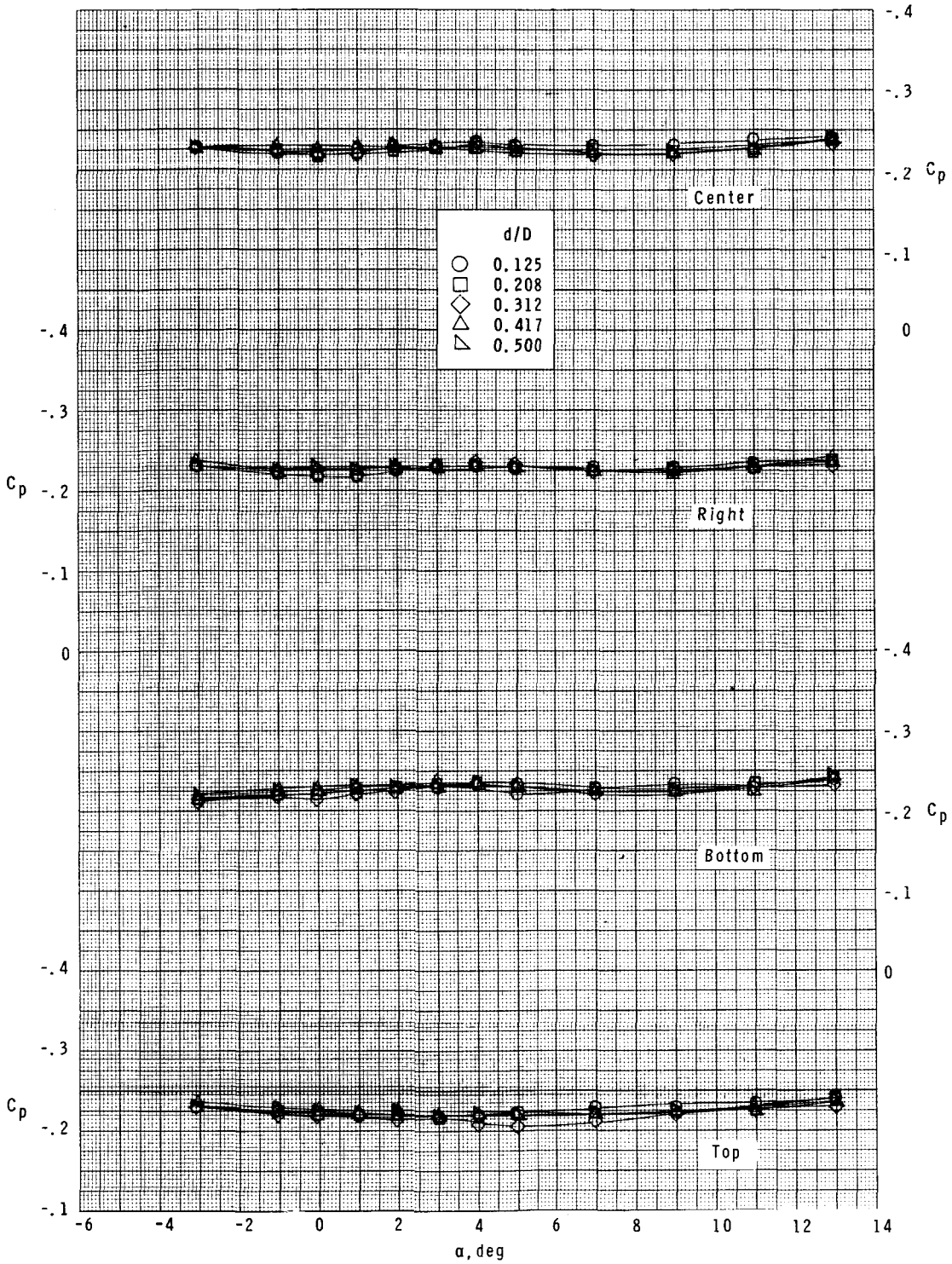

(a) $R = 1.74 \times 10^5$.

Figure 16.- Effect of sting diameter on the variation of base-pressure coefficient with angle of attack for three Reynolds numbers at M = 2.00.

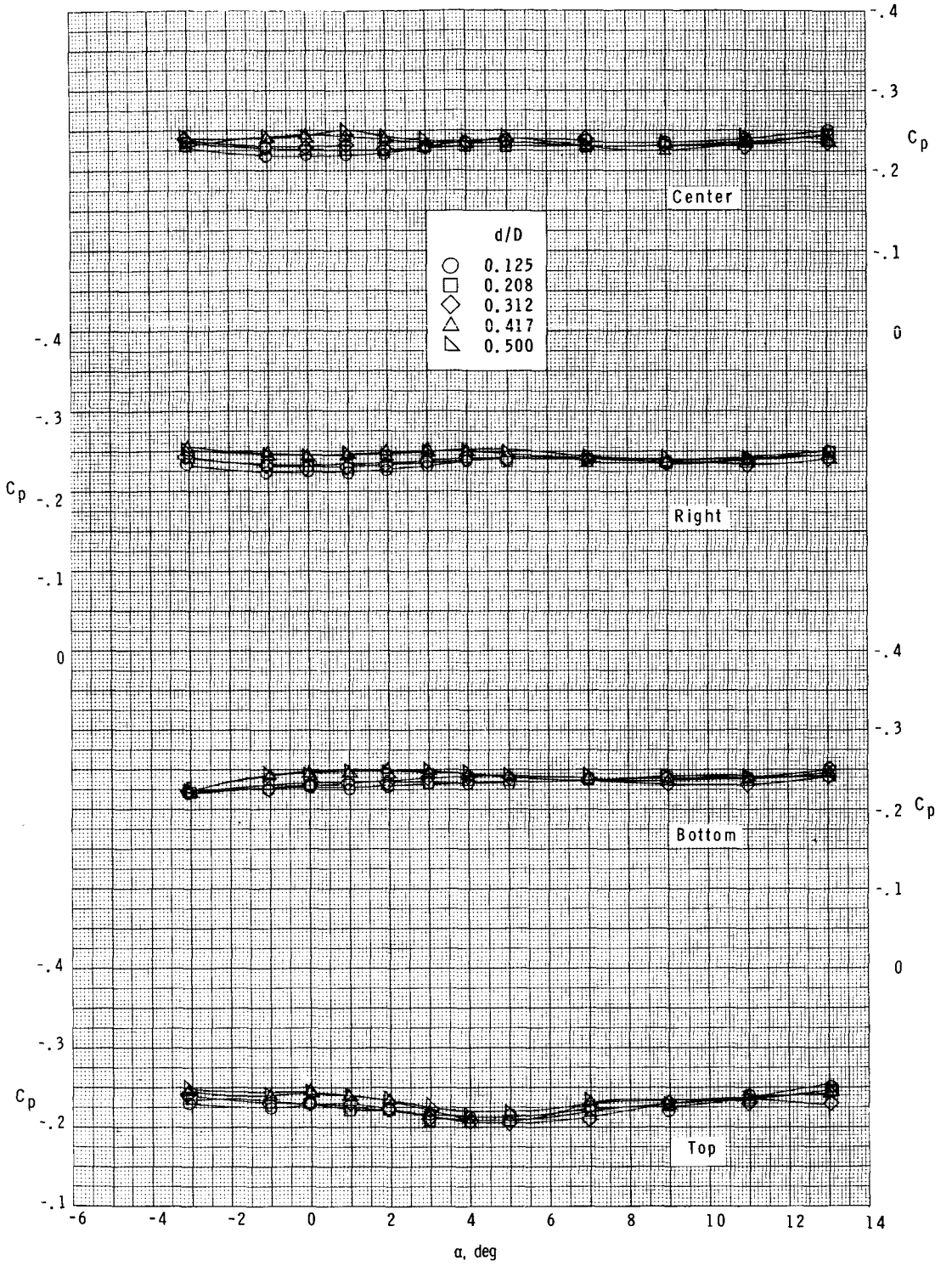

(b) $R = 2.60 \times 10^5$.

Figure 16.- Continued.

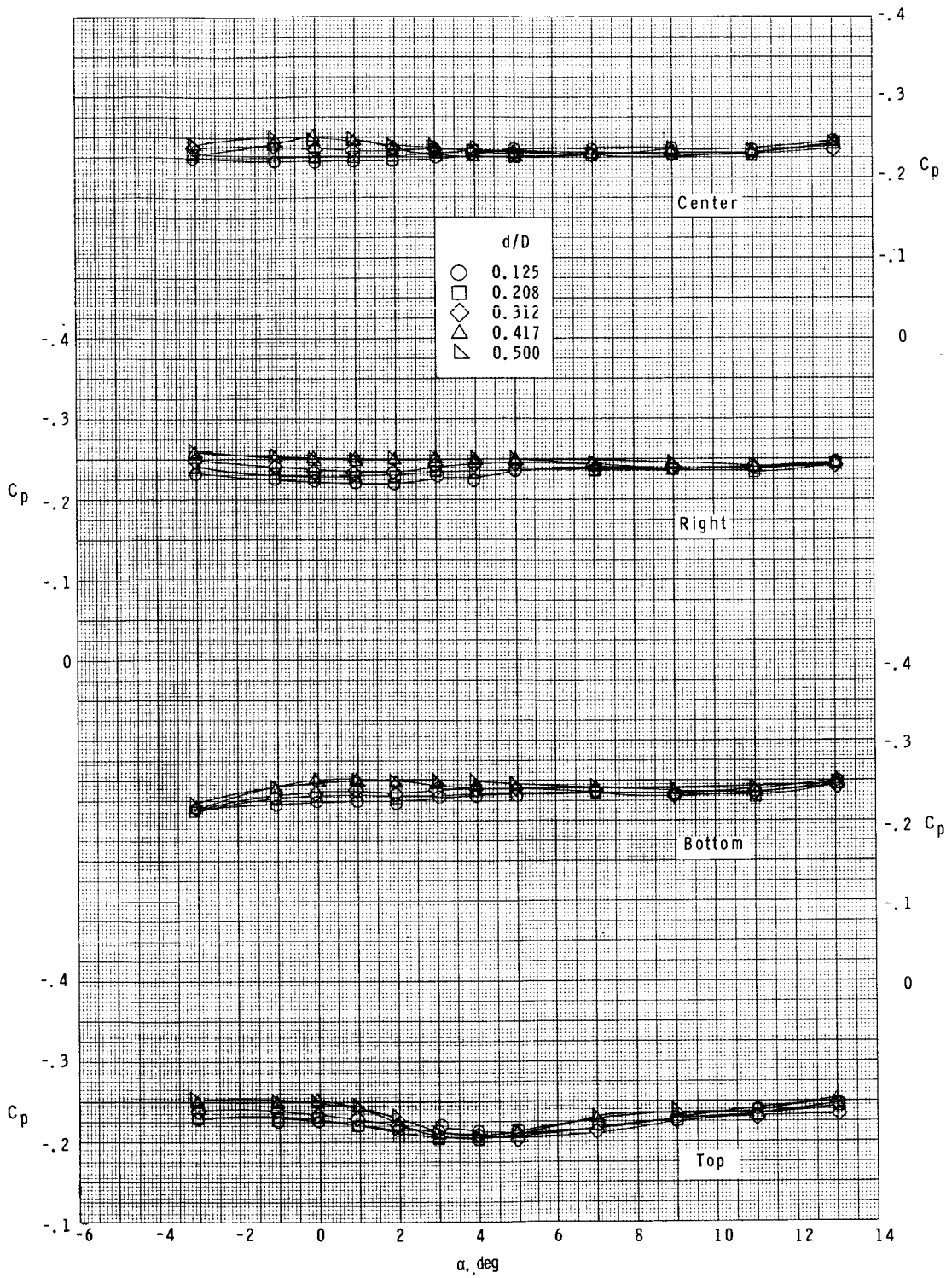

(c) $R = 3.47 \times 10^5$.

Figure 16.- Concluded.

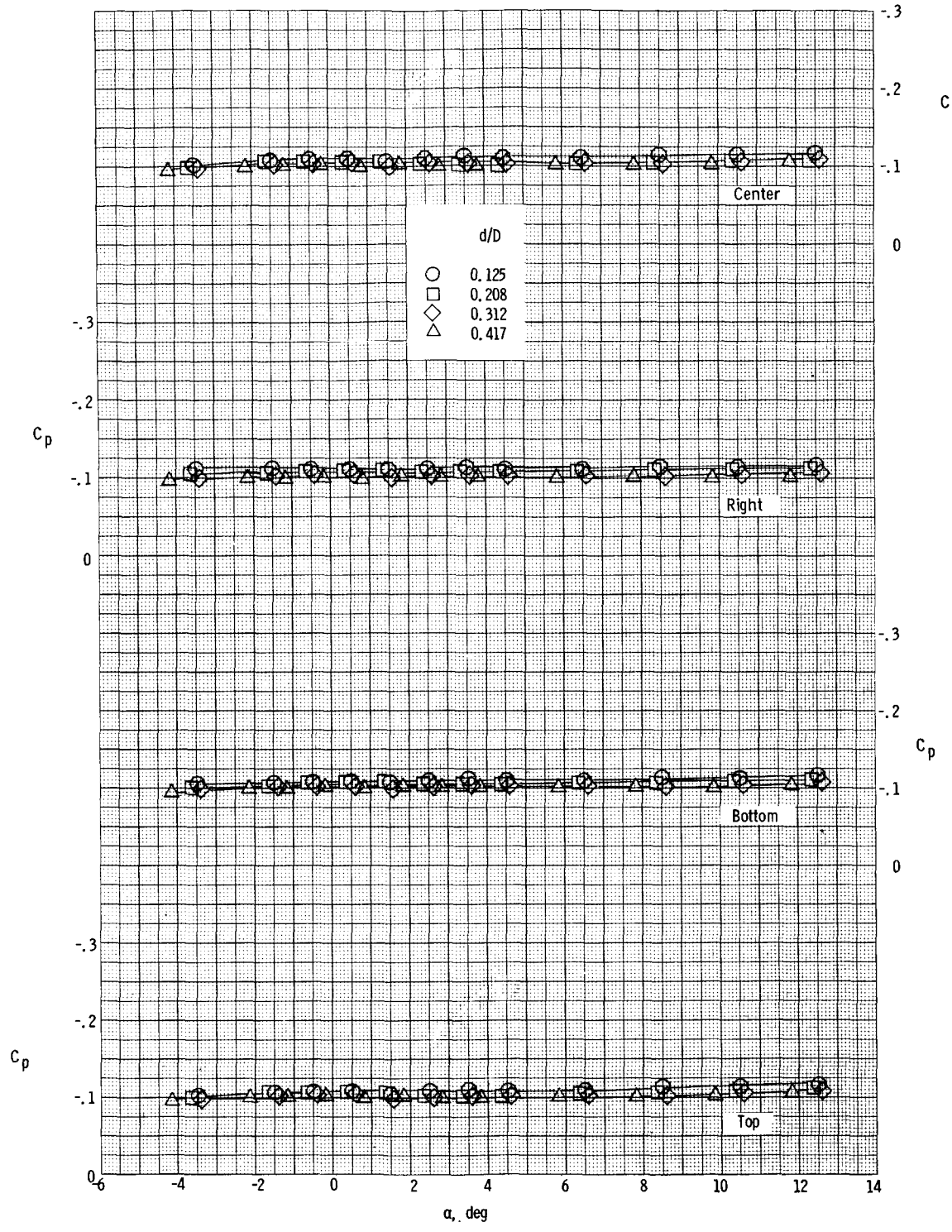

(a) $R = 1.61 \times 10^5$.

Figure 17.- Effect of sting diameter on the variation of base-pressure coefficient with angle of attack for three Reynolds numbers at $M = 2.94$.

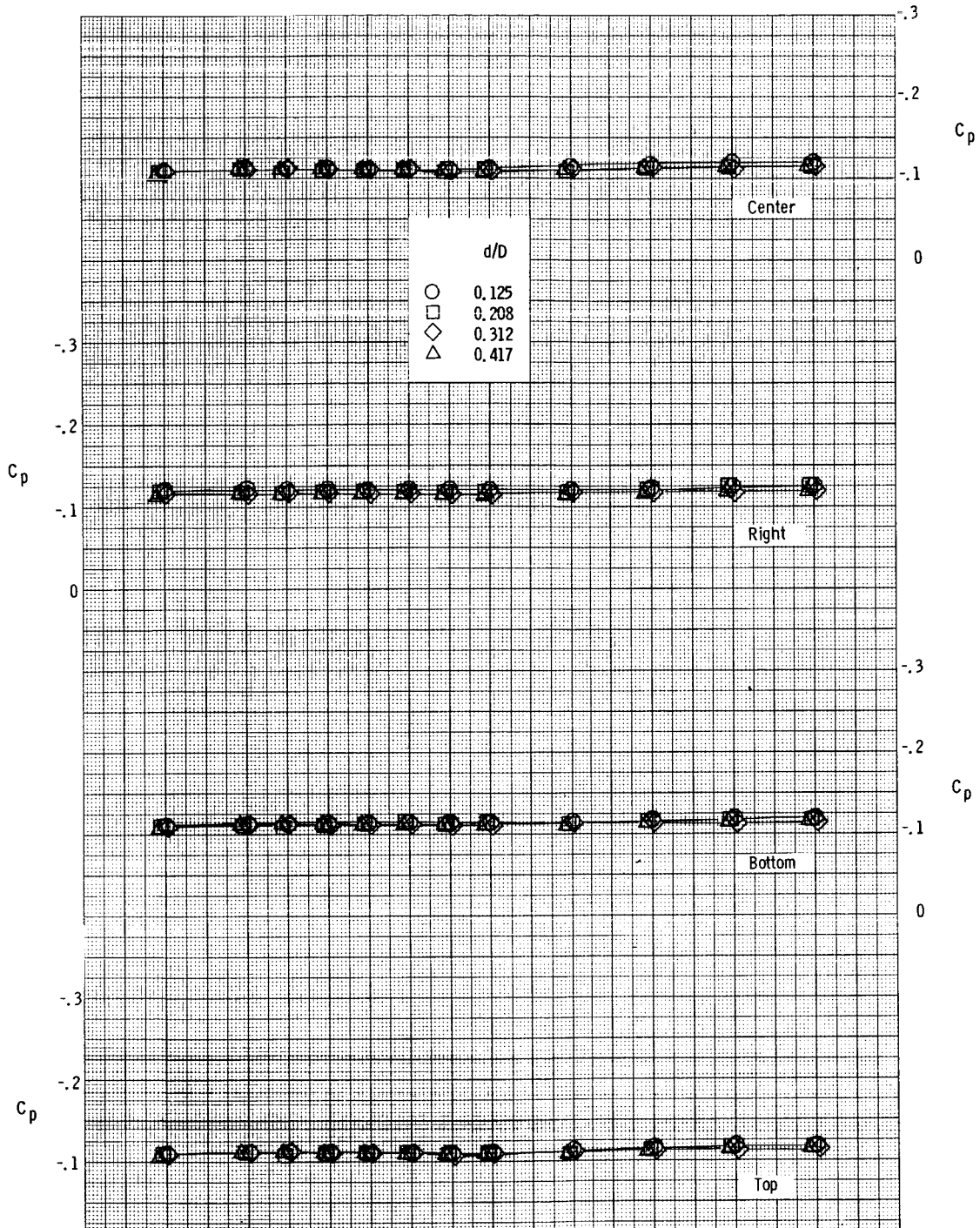

(b) $R = 2.68 \times 10^5$.

Figure 17.- Continued.

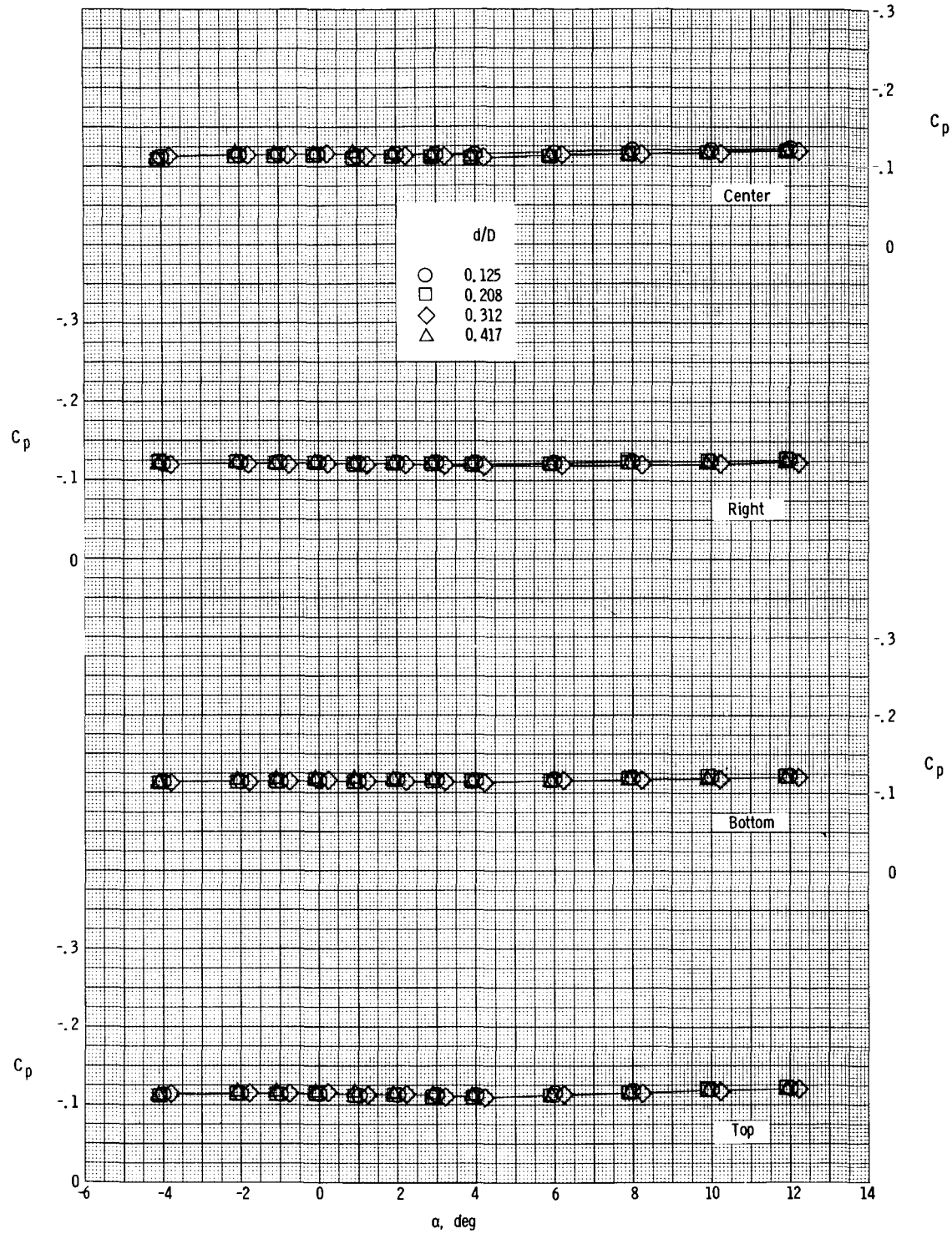

(c) $R = 3.76 \times 10^5$.

Figure 17.- Concluded.

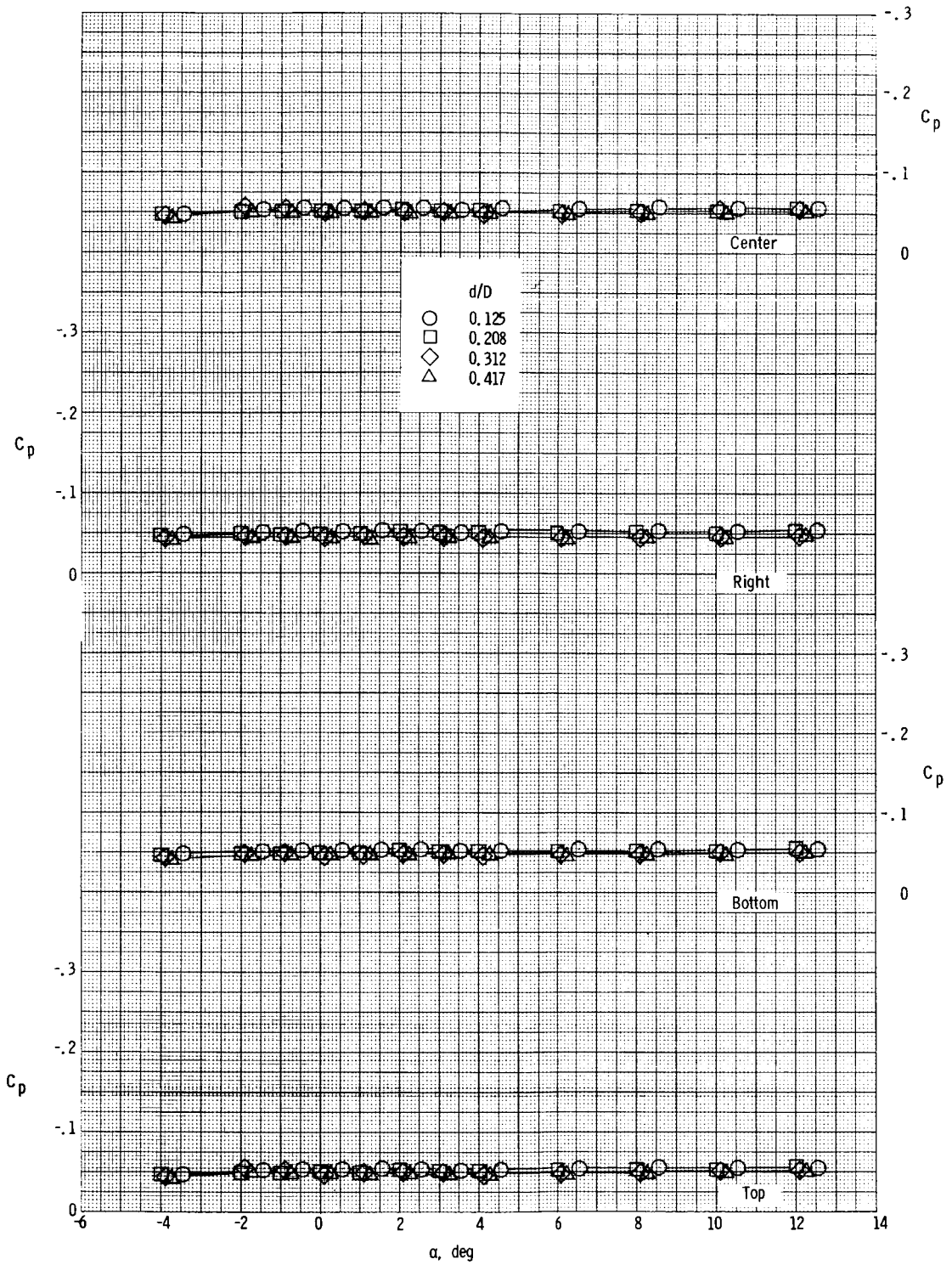

(a) $R = 2.63 \times 10^5$.

Figure 18.- Effect of sting diameter on the variation of base-pressure coefficient with angle of attack for two Reynolds numbers at M = 4.00.

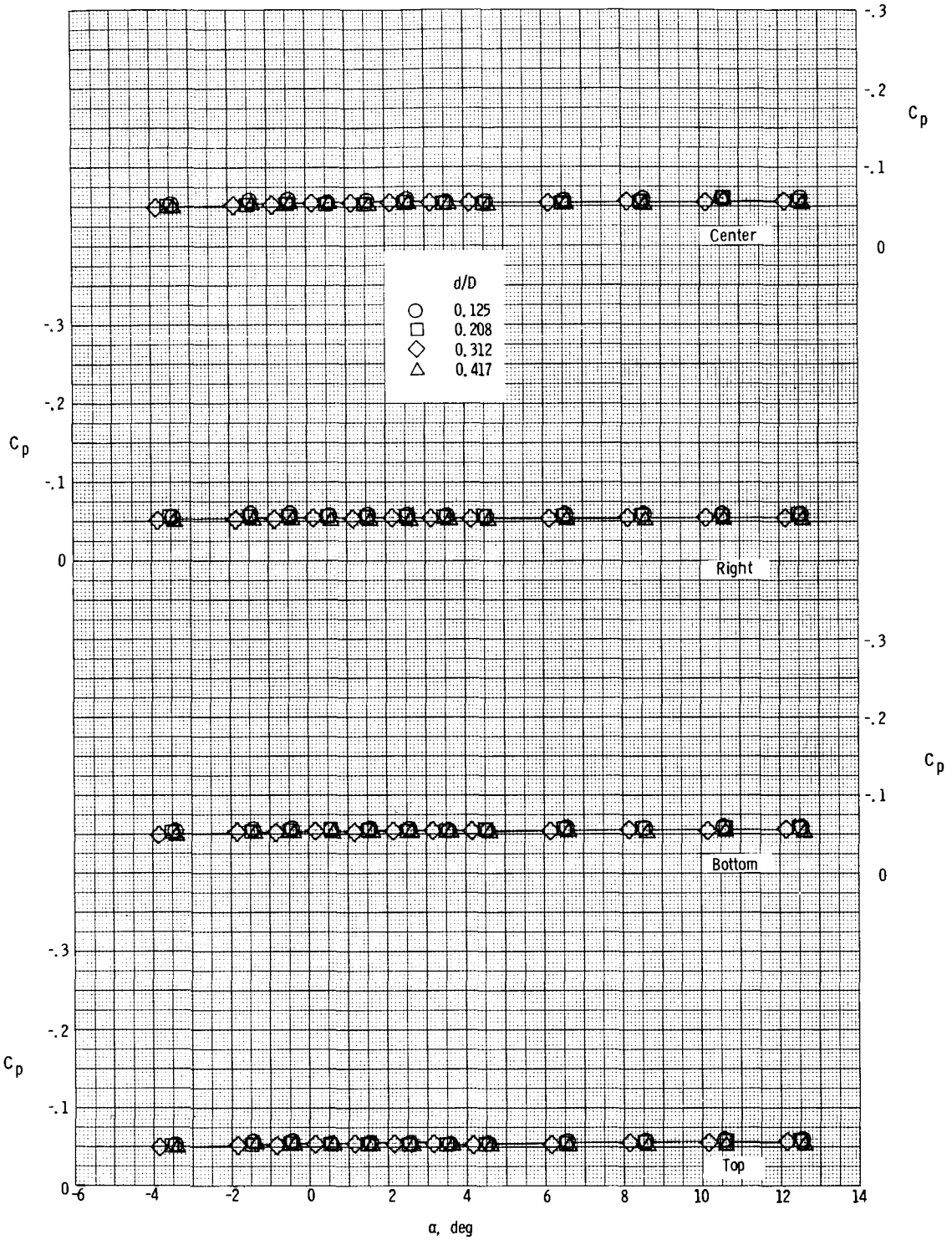

(b) $R = 3.80 \times 10^5$.

Figure 18.- Concluded.